MINOR AXIS FLEXURE AND COMBINED LOADING RESPONSE OF I-SHAPED STEEL MEMBERS

by

Muharrem Aktas

B.S. in Civil Engineering, Gazi University, 1996

M.S. in Civil Engineering, Gazi University, 1999

Submitted to the Graduate Faculty of

The School of Engineering in partial fulfillment

of the requirements for the degree of

Doctor of Philosophy

University of Pittsburgh

2004

UNIVERSITY OF PITTSBURGH

SCHOOL OF ENGINEERING

This dissertation was presented

by

Muharrem Aktas

It was defended on

November, 29 2004

and approved by

Morteza A.M. Torkamani, PhD, Associate Professor, Civil and Environmental Engineering

Jeen-Shang Lin, PhD, Associate Professor, Civil and Environmental Engineering

Julie M. Vandenbossche, PhD, Associate Professor, Civil and Environmental Engineering

Dr. Patrick Smolinski, PhD, Associate Professor, Mechanical Engineering

Dissertation Director: Dr. Christopher J. Earls, Associate Professor, Civil and Environmental Engineering

MINOR AXIS FLEXURE AND COMBINED LOADING RESPONSE OF

I-SHAPED STEEL MEMBERS

Muharrem Aktas, PhD

University of Pittsburgh, 2004

The present dissertation elucidates the problem of determining if a given I-shaped cross-section is properly proportioned to accommodate sufficient plastic hinge rotation capacity to facilitate the redistribution of moments in a structural system as needed to accommodate the formation of a collapse mechanism. It might be tempting to believe that application of the limiting flange plate slenderness value for the case of major axis flexure are applicable in this case; since the pervasive belief is that this approach ought to be conservative. However, the present research study indicates that this is not the case and thus more sophisticated analysis techniques are required to better understand this case.

Most current design specifications employed throughout the world prescribe the use of so-called interaction equations for the design of beam-columns. Most often these interaction equations are optimized for use with the members possessing I-shaped cross-sections that are bent about the major principal centroidal axis while simultaneously being subjected to compressive thrust. The current study then also focuses on the case wherein an I-shaped member is loaded in compression and simultaneously bent about the minor principal centroidal axis. It is shown that the current AISC interaction equations can be improved on in terms of their ability to predict failure in these types of members. Alterations to the existing AISC interaction equations are suggested for improving on strength predictions relative to this case.

Through these two research focuses, the present dissertation adds significantly to the state of knowledge surrounding the response of steel members possessing I-shaped cross-sections that are subjected to minor axis flexural effects; effects that are important to the robust and redundant design of structures in a system-wide sense.

Keywords: Interaction equation, weak axis, finite element modeling, steel I-section Minor axis flexure, compactness, ductility, plate buckling, moment redistribution

TABLE OF CONTENTS

LIST OF TABLES

LIST OF FIGURES

NOMENCLATURE

Symbol	Explanation
A_g	gross area
B_1	moment amplification factor
B_f	flange width
E	modulus of elasticity
K	effective length factor for prismatic member
L_b	unbraced length
L_e	member length
L_f	free length between the flange plates
L_s	specimen length
M_n	nominal flexural strength
M_{me}	second order elastic moment
M_p	plastic bending moment
M_u	required flexural strength
M_y	moment corresponding to onset of yielding
M_0	first order moment
P_e	Euler buckling load
P_n	nominal axial strength
P_u	required axial strength
R	rotation capacity
S	elastic section modulus

Z	elastic section modulus
b_f	flange outstand
b_w	web depth
c	plastic flow vector
f_c	flange camber
f_{ut}	ultimate tensile stress
f_y	yield stress
f_{yc}	compressive yield stress
f_{yt}	tensile yield stress
g	plastic potential factor
h	clear distance between flanges
k	plate buckling coefficient
t_f	flange thickness
t_w	web thickness
r_y	radius of gyration about the weak axis
$\dot{\varepsilon}^{p}$	incremental plastic strain
$\varepsilon_{\ln}^{pl}$	logarithmic plastic strain
ε_{nom}	engineering strain
σ_{nom}	engineering stress
σ_{true}	true stress
θ_p	plastic rotation
δ	mid-span deflection

ϕ	resistance factor
ϕ_b	resistance factor for flexure
ϕ_c	resistance factor for compression
λ	magnitude of the plastic strain
λ_p	limiting slenderness parameter for compact element
λ_c	column slenderness parameter

To my wonderful parents, Emine and Ziya Aktas

ACKNOWLEDGEMENTS

I want to dedicate this dissertation to the memory of my mother, Emine Aktas, who has passed away 2 months prior to my defense. I am really sorry for not being there when she needed me the most. I hope I made her as proud as she made me proud. I also would like to thank my father for his encouraging words when I needed the most. I also want to thank my parents for their love, and the sacrifice they made by not seeing me for 2 years.

I am deeply grateful to my advisor, Dr. Christopher J. Earls, for his continuous support, guidance and contributions that made this dissertation possible. He has always been available. I would like to thank him for his advice, flexibility, inspiration and motivation.

I would like to thank the members of my dissertation committee, Dr. Jeen-Shang Lin, Dr. Morteza Torkamani, Dr. Julie M. Vandenbossche and Dr. Patrick Smolinski for their constructive input and contribution.

My sincere thanks and appreciation go to my wife Betul Aktas, for her love, patience and continuous support. I also have to thank my little boy, Cihan, for the joy he brought to me and for reminding me of all the reasons why I had to complete my dissertation.

I thank my family, Filiz, Ishak, Hatice and Ismail, for their patience and support. Special and many thanks to my sister, Sumeyra, for her love and continued trust.

I would also like to thank Leslie for her help in every means which I can never forget. I feel lucky and happy for having great officemates, whom I will cherish for the rest of my life. I would like to thank Turkish community in Pittsburgh for their support when I needed it.

1.0 INTRODUCTION

In this research, I section flange compactness under minor axis bending and minor axis moment-thrust response behavior in steel I-shaped members are investigated by using nonlinear finite element methods.

The case of minor axis flexure in I-shaped cross-sections arises frequently in the consideration of bi-axial beam bending associated with perimeter spandrel members in exterior framing lines, as well as in the general case of a beam-column. In these instances, it may be desirable to employ cross-sections whose proportions are such that sufficient structural ductility is available in the member in order that system-wide moment redistribution may be achieved. Scenarios requiring this capacity to redistribute forces frequently arise in seismic design and other applications that require structural robustness against natural and man-made hazards.

The present study hopes to elucidate the problem of determining if a given I-shaped cross-section is properly proportioned to accommodate sufficient plastic hinge rotation capacity to facilitate the redistribution of moments in a structural system as needed to accommodate the formation of a collapse mechanism.

Many structural members, like beam columns, are subjected to some degree of both bending and axial load. There is no simple design procedure for beam columns because of the number of failure modes. Interaction equations are found to provide good results when compared

predicted and tested responses. The current AISC LRFD specification employs an interaction equation based approach for beam column analysis and design.

The present research has as a focus, the response of I-shaped steel members subjected to the simultaneous application of axial thrust and minor principal axis flexure. This response will be compared with the results of the current approach given in the LRFD specification.

The commonly used A992 steel grade is considered though out the present work. The study reported on herein involves the use of experimentally verified nonlinear finite element modeling strategies. While it has been shown that non-proportional loading can have an influence on important parameters governing beam-column response (especially when load reversals are at issue) (Hajjar 2003), the present study involves a research program wherein the traditional approach of proportional load application is used. This is the case since the great bulk of earlier research has focused on this case (Salmon and Johnson 1996), and this is the case at the heart of current specification equations used though out the world.

1.1 OVERVIEW OF COMPACTNESS

The strength or resistance of a beam in flexure is limited by some combination of local and overall buckling resistances. Figure 1 shows the general behavior of a wide flange beam (Yura, Galambos, and Ravindra 1978). Basically the behavior of the beam is divided in three response regimes: elastic, inelastic, and plastic ranges. In the elastic range, elastic buckling controls the behavior. In the inelastic range, some or all of the cross-section is yielded but only a small amount of inelastic deformations is available prior to failure. In the plastic range, the cross-

section reaches the plastic moment, M_p, and maintains this load level as the member tends to undergo large plastic deformations which allow for moment redistribution. In the current American steel design specifications, members are classified as, non-compact and compact as a means for characterizing their strength and deformation capacity. For sections permitted in plastic analysis, the specification requires a compact section (AISC, 1999). The specification defines a compact section as one that can develop a fully plastic stress distribution while exhibiting sufficient plastic hinge rotation capacity, prior to the onset of local buckling, to accommodate moment redistribution in the structural system (AISC, 1999).

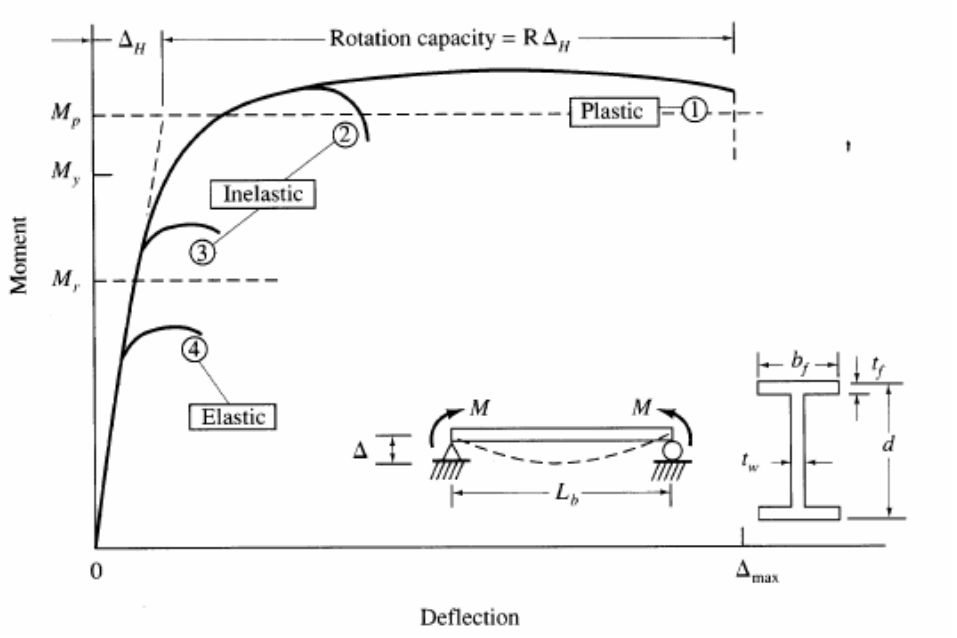

Figure 1 Beam behavior (Yura, Galambos, and Ravindra 1978)

1.2 MOMENT - ROTATION CURVES

Rotation capacity is a method of quantifying deformation capacity within a cross-section prior to instability eroding the cross-sectional capacity (Salmon & Johnson, 1995). There are a number of different definitions in the literature for rotation capacity.

According to Lay and Galambos (1965) rotation capacity, $R_h = \theta_h / \theta_p$, in which θ_p is the elastic rotation at the initial attainment of the plastic moment M_p. And θ_h is the plastic rotation at the point when moment drops below M_p , all on within the context of a normalized moment-rotation context.

Kemp (1985), proposed an alternative definition for rotation capacity as $R_{hm} = \theta_{hm} / \theta_p$ in which θ_{hm} is the plastic rotation up to the maximum moment on the moment rotation curve. He proposed this because of the practical difficulties associated with the accurately measuring the rotation correctly in the unloading range.

The definition for rotation capacity adopted in the present discussion is that presented by ASCE (1971): $R = \frac{\theta_2}{\theta_1} - 1$ where θ_2 is the rotation when the moment capacity drops below M_p on the unloading portion of the M - θ/θ_p plot, and θ_1 is the theoretical rotation at which the full plastic capacity is achieved based on elastic beam stiffness. This ductility response measure is described graphically in figure 2. It is currently assumed that $R = 3$ is an adequate level of structural ductility for the non-seismic design of steel building components (AISC 1999) and thus current compactness provisions are formulated with this measure in mind.

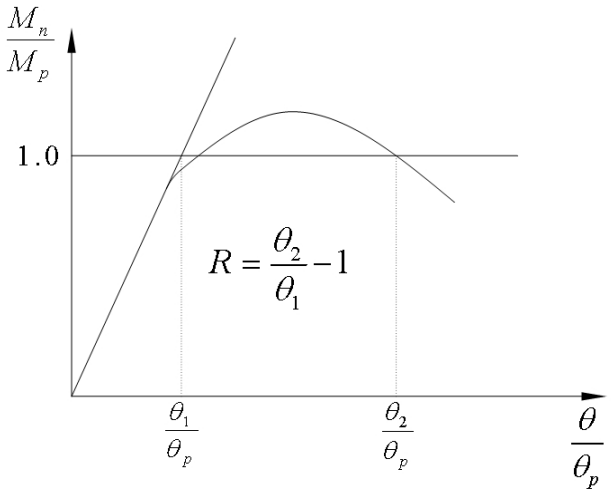

Figure 2 Definition of Rotation Capacity

1.3 OVERVIEW OF MOMENT AMPLIFICATION FACTOR

Structural members are usually subjected to the combination of bending and axial forces. When one of these effects is small enough to be neglected then the member can be designed as a column or as a beam. However; if there is a significant amount of both effects, then they both have to be considered. Such members are called beam-columns (Salmon & Johnson, 1995).

Including axial load brings a secondary bending moment which is equal to the axial compression force times the out-of-plane deflection measures with respect to the member longitudinal axis. First order methods don't take the displaced geometry into account and thus are unable to treat this important behavioral feature. Iterative numerical techniques, also known as second order methods of analysis, must be used to study the importance of these so-called "second order effects". However; such techniques are time consuming and not practical in

manual calculations. That is why in the AISC LRFD specification either a second order analysis or the moment amplification method is permitted (Segui, 2003). The latter of these two approaches is a simplification that is reasonable for hand calculations.

According to the moment amplification method, the first order moment is multiplied by the moment amplification factor to get the second order moment (i.e. the sum of the primary applied moment as well as the secondary moment due to the axial force acting through the out-of-plane defelction). The equation for amplification factor is developed as follows (Segui, 2003). For a simply supported beam with an initial crookedness is presented in figure 3.

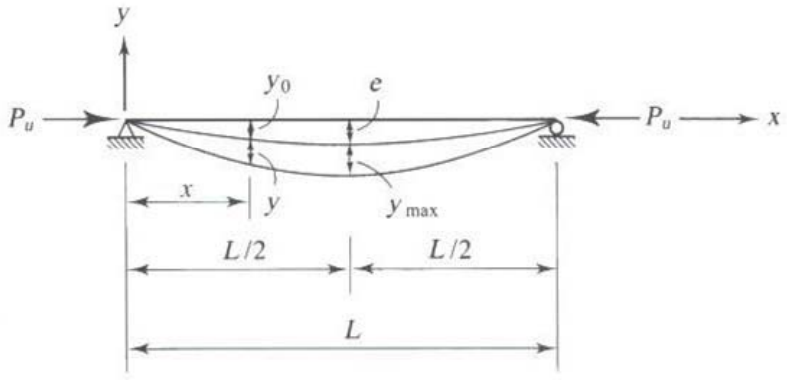

Figure 3 Simply supported beam with initial crookedness (Segui, 2003).

Initial out of straightness can be approximated by y_o where e is the maximum initial displacement at the midspan.

$$y_o = e \sin \frac{\pi x}{L} \tag{1}$$

The moment curvature can be expressed as

$$\frac{d^2y}{dx^2} = -\frac{M}{EI} \tag{2}$$

The moment at any location is going to be the moment caused by the axial force times the initial total deflection. Total deflection is the sum of the initial crookedness and the additional deflection y caused by the bending.

$$M = P_u(y_o + y) \tag{3}$$

When equation 3 is substituted back into the equation 2, equation 4 is obtained;

$$\frac{d^2y}{dx^2} + \frac{P_u}{EI}y = -\frac{P_u e}{EI}\sin\frac{\pi x}{L} \tag{4}$$

Equation 4 is an ordinary, non-homogeneous differential equation with two unknown integration constants that can be evaluated through the consideration of two boundary conditions which are; at $x = 0, \quad y = 0$ and at $x = L, \quad y = 0$. A function which satisfies these boundary conditions is

$$y = B\sin\frac{\pi x}{L} \tag{5}$$

Substituting equation back into the differential equation 4 leads to equation 6;

$$-\frac{\pi^2}{L^2}B\sin\frac{\pi x}{L} + \frac{P_u}{EI}B\sin\frac{\pi x}{L} = -\frac{P_u e}{EI}\sin\frac{\pi x}{L} \tag{6}$$

After solving for *B;*

$$B = \frac{-\frac{P_u e}{EI}}{\frac{P_u}{EI} - \frac{\pi^2}{L^2}} = \frac{-e}{1 - \frac{\pi^2 EI}{P_u L^2}} = \frac{e}{\frac{P_e}{P_u} - 1} \tag{7}$$

where $P_e = \frac{\pi^2 EI}{L^2}$ is the Euler buckling load. Thus

$$y = B \sin \frac{\pi x}{L} = \left[\frac{e}{\left(P_e / P_u \right) - 1} \right] \sin \frac{\pi x}{L} \tag{8}$$

Substituting equation 8 back into equation 3 gives;

$$M = P_u \left\{ e \sin \frac{\pi x}{L} + \left[\frac{e}{\left(P_e / P_u \right) - 1} \right] \sin \frac{\pi x}{L} \right\} \tag{9}$$

At $x = L/2$ the maximum moment occurs;

$$M_{\max} = P_u \left[e + \frac{e}{\left(P_e / P_u \right) - 1} \right] \tag{10}$$

Rearranging equation 10;

$$M_{\max} = P_u e \left[\frac{\left(P_e / P_u \right) - 1 + 1}{\left(P_e / P_u \right) - 1} \right] \tag{11}$$

$$M_{\max} = M_0 \left[\frac{1}{1-\left(P_u / P_e\right)} \right] \tag{12}$$

In this last equation M_0 is the first order moment. Then the moment amplification factor is (Segui, 2003);

$$\frac{1}{1-\left(P_u / P_e\right)} \tag{13}$$

1.4 BASIS FOR CURRENT CROSS-SECTIONAL COMPACTNESS LIMITS FOR UNSTIFFENED ELEMENTS

The goal of the US specifications in its prescription of so-called compactness criteria (AISC 1999) is to identify plate slenderness limits, λ_p, for cross-sectional plate components such that an overall flexural cross-section will be able to accommodate sufficient plastic hinge rotation to support system-wide moment redistribution as required for the development of a global collapse mechanism. In pursuit of this condition, compactness limits have historically been formulated to loosely accommodate strains approaching strain hardening values within an individual plate component prior to the attenuation of post-buckling strength due to effects of material nonlinearity.

As a point of departure for the work reported on herein, it is useful to consider the basis by which the current US Specification (AISC 1999) addresses plate compactness within the context of an unstiffened element; flanges in I-shaped cross-sections under uniform flexural compression. In this case, the question of how to address the uncertainty with regard to the nature of rotational edge restraint provided at the plate boundary associated with the flange-web

junction is addressed through consideration of the work carried out by Haaijer and Thurlimann (1957). Haaijer and Thurlimann discovered that unstiffened plates exhibit the onset of strain hardening at slenderness values, λ_c, of approximately 0.46 irrespective of whether the supported edge is fixed or pinned. In this discussion, slenderness is defined as

$$\lambda_c = \sqrt{\frac{F_y}{F_{cr}}} \tag{14}$$

where classical elastic plate buckling theory provides that

$$F_{cr} = k\frac{\pi^2 E}{12\left(1-\nu^2\right)\left(\frac{b}{t}\right)^2} \tag{15}$$

in which E and ν are the usual elastic material constants and b and t are the plate width and thickness quantities, respectively. The term k is the plate buckling coefficient which depends on the plate aspect ratio, edge support conditions, and stress distribution along the loaded edge. In the case of an I-shaped cross-sectional flange, the two extremes that k can assume are: 0.425 for the case of a supported edge that is pinned; and 1.277 for the case of a rotationally fixed supported edge. If the equation 15 is set to be equal to the yield stress, F_y, and if it is solved for the width-to-thickness ratio *(b/t)* equation 16 is obtained.

$$\frac{b}{t} = 162\sqrt{\frac{k}{F_y}} \tag{16}$$

As mentioned previously, Haaijer and Thurlimann have observed that unstiffened plate components under the action of a uniform edge compression achieve strain hardening response at slenderness values, λ_c, of 0.46 and thus equation 16 may be used to identify a plate slenderness limit for the attainment of strain hardening response as;

$$\frac{b}{t} = 162\lambda_c\sqrt{\frac{k}{F_y}} = 74.5\sqrt{\frac{k}{F_y}} \tag{17}$$

The only question remaining regards what value to assume for the plate buckling coefficient, k. It has been standard practice for AISC (1999) to employ elastic plate buckling coefficients as a guide in the development of actual design specification equations and as such it may be considered that the two extreme values for the present case of an I-section flange: 0.425 and 1.277 for the pinned and fixed cases, respectively, are bounding cases. If it is, somewhat arbitrarily, considered one third of the difference between these two values and add this result to the smaller of the two a k of 0.71 which can be applied to equation 17 is obtained so that a limiting plate slenderness value for the onset of strain-hardening is found as;

$$\frac{b}{t} = \frac{63}{\sqrt{F_y}} \approx \frac{65}{\sqrt{F_y}} = 0.38\sqrt{\frac{E}{F_y}} \tag{18}$$

It is noted that equation 18 represents the current compactness limit, λ_p, presented in the current AISC LRFD specification (1999) in Table B5.1 for the case of an I-section flange under the action of uniform flexural compression.

A similar approach to the foregoing when developing a compactness limit for the case of flanges in I-sections subjected to flexural compression due to minor axis bending may be applied; if it is assumed that Haaijer and Thurlimann's results concerning the invariance of λ_c with the degree of rotational restraint present at the supported edge in a uniformly compressed unstiffened element holds for the case of non-uniform compression. Non-uniform compression stresses would be expected along the loaded plate edge in flange outstands subjected to flexural compression (as depicted in figure 4).

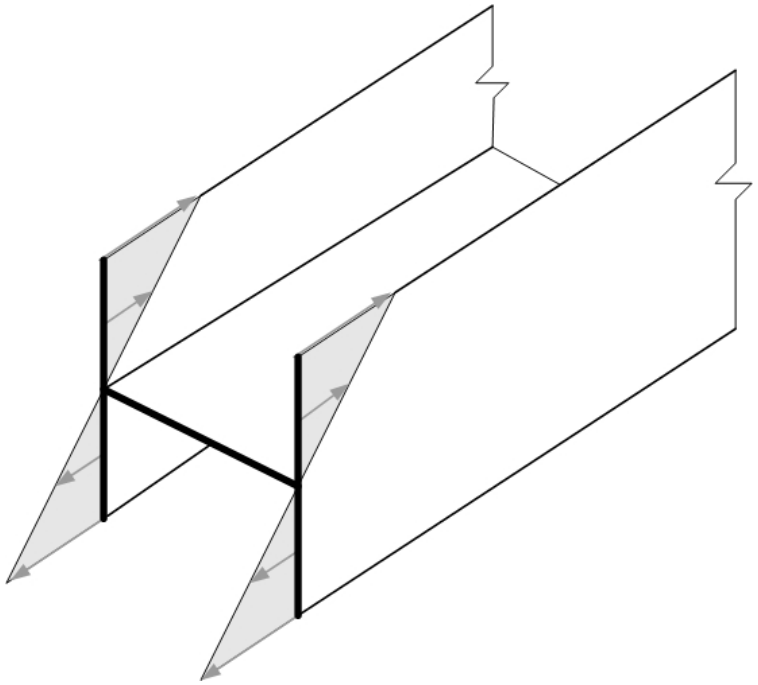

Figure 4 Minor axis flexural normal stress distribution

While Haaijer and Thurlimann did consider the case of non-uniform compressive stresses within a plate component, their investigation centered on the case of a stiffened element; consistent with the web of an I-shaped cross-section subjected to major axis flexure. Proceeding

with the assumption that the invariance in λ_c holds for the unstiffened case of a flange outstand in flexural compression due to minor axis flexure in an I-shaped cross-section, equation 17 may be reused as the basic requirement for the attainment of strain hardening in a non-uniformly compressed plate component. What is now left to do in the development of a compactness limit for flange outstands in non-uniform flexural compression is to identify a suitable plate buckling coefficient *k*. Guidance on the selection of an appropriate *k* value is obtained using the tabulated cases presented by Galambos (1998). It may be assumed that the flange outstand experiences compressive stress only (i.e. assuming that the neutral axis is at the flange-web junction). Two extreme values for *k* in this case may then be identified: 0.57 for a pinned supported edge and 1.61 for a rotationally restrained supported edge. Proceeding as in the case of an I-shaped beam flange outstand subjected to normal stress under major axis flexure, one third of the difference between the *k* values of these two extremes may be added to the smaller of the two to arrive at $k = 0.92$. We may then employ this value in equation 17 to arrive at a limiting plate slenderness value of

$$\frac{b}{t} = \frac{71}{\sqrt{F_y}} \approx 0.42\sqrt{\frac{E}{F_y}} \tag{19}$$

The limits obtained from equation 19 can be compared with results obtained from a finite element parametric study considering flange outstands having various parametric combinations of: cross-sectional aspect ratio (B_f / d); unbraced length-to-cross-sectional depth ratio (L_b / B_f); web slenderness ratio, (h / t_w); flange slenderness ratio, $(B_f / 2t_f)$, and steel yield strength.

1.5 BASIS FOR CURRENT INTERACTION EQUATIONS FOR MEMBERS UNDER AXIAL LOAD AND BENDING

When considering the strength of a steel member under the combined effects of axial load and flexure, two general approaches have historically been used (Galambos 1998): design charts and tables of safe moment-thrust combinations; and so-called "interaction" expressions that are in principal based on the formulaic representation:

$$f\left(\frac{P_{required}}{P_{provided}}, \left[\frac{M_{required}}{M_{provided}}\right]_{X,Y}\right) \leq 1.0 \tag{20}$$

Where P denote axial load, and M denotes moments about the X-axis (major principal centroidal axis or strong-axis) and the Y-axis (minor principal centroidal axis or weak-axis). It has been the latter approach, the interaction equation method, that has emerged as the dominant approach for design within the context of modern building specifications though out the world (Galambos 1998). As an initial approach in the formulation of a reasonable base-line form of an interaction expression, equation 20 may be restated in the commonly accepted form serving as the point of departure for essentially all specifications that employ the interaction approach.

$$\frac{P}{P_u} + \frac{M}{M_u} \leq 1.0 \tag{21}$$

In equation 21, P_u denotes the pure column strength of the member being considered (i.e. its axial capacity in the absence of moment) and M_u denotes the capacity of the same member under pure bending (i.e. its flexural capacity in the absence of axial loading). The quantities P and M denote the respective failure loads acting in combination on the member in question. The capacity of a given member may be obtained from experimental testing, but frequently such an approach is cumbersome due to the fact that an extremely large potential design space must be explored which involves such variables as: member cross-sectional proportions, moment-thrust ratios, unbraced length, etc. In practice, it has been commonplace to employ numerical means for the identification of failure in members loaded by a combination of axial force and moment. Chen and Lui (1987) provide a helpful overview to one technique wherein raw cross-sectional capacity is treated through the consideration of a fiber analysis. A fiber analysis is a means by which a zero-length member of given cross-sectional geometry is studied by assigning a finite number of uniaxial fibers to fixed coordinates within the cross-section and assigned idealized stress-strain response histories as would be consistent with coupon testing in a universal testing machine. With this type of idealization, moment and axial force can be varied (in the presence of initial residual stresses) until an unstable combination of loading is achieved – a failure point on the interaction line / surface. This technique can be extended to the consideration of members of finite lengths wherein inelastic global instability limit states may also be treated (Kanchanalai 1977). In addition to inelastic cross-sectional strength and member stability issues, the amplification of the primary applied moment as a result of so-called “second-order effects” (due to the axial force of the member acting over a moment arm emanating from the lateral deflection induced by the primary moment) can trace its familiar form in specifications to an earlier edition of the SSRC Guide (Johnston 1976) wherein equation 21, above, is modified as:

$$\frac{P}{P_u} + \frac{M_0}{M_u\left(1 - P/Pe\right)} \leq 1.0 \tag{22}$$

where M_o is the first-order or primary moment applied directly to the member, and P_e is the axial elastic critical load for the member when buckling in the plane of primary moment is enforced. The additional denominator term appearing in equation 22 as compared with equation 21 represents a consideration of member level second order effects.

While the general underlying approach of most international specifications is rooted in the form of equation 21, certain subtle differences do present themselves in side-by-side comparisons of their form. Since the topic of the present study is restricted to minor axis flexure, the equations presented will be only those germane to that context and then in a format utilizing a uniform notation so as to facilitate direct comparison. The Canadian specification (CSA 2002) employs an interaction equation of the form:

$$\frac{P_u}{\phi P_n} + \frac{0.85M_u}{\phi M_n} \leq 1.0 \tag{23}$$

while the Eurocode 3 (ECS 2002) equation appears as

$$\frac{P_u}{\phi P_n} + \frac{M_u}{\phi M_n} \leq 1.0 \tag{24}$$

In the case of the US specification (AISC 1999), a two-part interaction equation format is used:

For $\frac{P_u}{\phi_c P_n} < 0.2$

$$\frac{1}{2}\frac{P_u}{\phi_c P_n}+\frac{M_u}{\phi_b M_n}\le 1.0 \qquad (25)$$

and for $\frac{P_u}{\phi_c P_n}\ge 0.2$

$$\frac{P_u}{\phi P_n}+\frac{8}{9}\frac{M_u}{\phi_b M_n}\le 1.0 \qquad (26)$$

While it is instructive to note the interaction equation formats for the various specifications, it is pointed out that individual member capacity predictions will vary from specification to specification as a results of these and other differences related to the calculation of axial capacity as well as the determination of compactness in cross-section (i.e. the ability of the cross-section to form a plastic hinge and maintain structural ductility).

The foregoing interaction equations have been developed with the intention of optimizing their predictive capabilities within the context of the major-axis (e.g. strong-axis) flexural case. It has been noted by others (Galambos, 2001) that the presence of mono-symmetry in an I-shaped cross-section can have a pronounced impact on the economy of design emanating from a use of interaction equations such as the foregoing. Other investigators (Alduri and Madugula, 1992) have noted the importance of considering the pronounced effect that deviations from the ideal I-shaped cross-sectional case can have on the accuracy on interactions equations of the type presented in equations 25 and 26. Other researchers (Liew et al 1991) have pointed to the fact that equations of such as 25 and 26 may be less than robust in their ability to treat the case of an I-shaped beam-column within the context of minor-axis flexure (e.g. weak-axis flexure in the presence of axial compression).

1.6 SCOPE

This dissertation contains mainly three parts;

1. Verification of finite element modeling techniques using full-scale experimental testing results obtained in the open literature.
2. Parametric study results carried out using the verified nonlinear finite element modeling approach and focusing on the fundamental behavior of I-sections subjected to minor axis flexure and combined minor axis flexure and axial compressive thrust.
3. Discussion of the results.

In section 2 non linear finite element analysis is discussed in a general sense with the source of nonlinearities being called out explicitly. In the same section, the commercial finite element software package ABAQUS is discussed briefly, including the S4R shell elements and von Mises metal plasticity with isotropic hardening. Also nonlinear finite element solution algorithms are briefly discussed in this same section of the dissertation.

In section 3 details of the modeling techniques used in the verification process are explained; both for pure minor axis bending case and for the combined loading case. Geometry of the test specimens with the proper imperfection geometry and their material model are discussed in depth in this section. Also, figures comparing the numerical finite element results with the results of the full-scale experimental tests are presented.

In section 4, compactness of I-shaped beams under minor axis bending is discussed throug the consideration of results obtained from a parametric study.

A similar parametric study and its concomitant results are used in section 5 to understand the interaction of axial force and minor axis bending response for I –shaped beams.

Concluding remarks are given is section 6 for both cases.

2.0 NON LINEAR FINITE ELEMENT ANALYSIS

Nonlinear finite element modeling is at the heart of the research work reported on in the current study. Given the reliance of the present work on this analytical method, it is important to clearly state the modeling approached used, software packages employed, and any assumptions made during the construction of the finite element analogs for the I-shaped cross-sections under investigation. In addition, verification of the modeling techniques against full-scale experimental testing can be of great value.

The commercial multipurpose finite element software package ABAQUS version 6.3 is employed in this research. All modeling reported herein considers both nonlinear geometric and material influences. The incremental solution strategy chosen for this work is the modified Riks-Wempner method (ABAQUS, 2003).

Material nonlinearity is modeled using ABAQUS standard metal plasticity material model which is based on an incremental plasticity formulation employing associated flow assumptions in conjunction with a von Mises failure surface whose evolution in stress-space is governed by a simple isotropic hardening rule.

The I-shaped cross-sections considered in the current research employ shell finite elements positioned along the middle surfaces on the cross-sectional constituent plate

components. The S4R nonlinear, finite strain, shell element from the ABAQUS element library is employed in this research. The following sub-sections endeavor to meet the above requirements and lead to a clear understanding of the approach, and subsequent limitations, of the present work.

2.1 SOURCE OF NONLINEARITIES IN STRUCTURAL RESPONSE

For structural analysis there are three sources of nonlinearities in analysis. The corresponding nonlinear effects are identified by the terms material, geometric and boundary conditions. All modeling reported herein considers both nonlinear geometric and material influences.

Material Nonlinearity: The stress-strain curve of steel is linear elastic until some significant point called the yielding point. After the attainment of the yield point, the stress strain curve becomes non linear and the strains become partially irrecoverable. In other words when the material behavior does not fit the elastic model $(\sigma = E\varepsilon)$ there is a phenomenon of material nonlinearity. Effects due to the constitutive equations (stress-strain relations) that are non linear, are referred to as material nonlinearities.

Geometrical nonlinearity: In elementary structural theory the effect of deformations are neglected when writing the equations of equilibrium and motion. In other words the behavior is described with respect to the undeformed configuration. Real structures are in equilibrium in their deformed configuration, not their undeformed configuration, as implied by elementary structural theory. Especially when there is large deflection small strain case, geometric nonlinearity must be taken into account. Ignoring the effects of geometric nonlinearity makes the

governing kinematic relationships linear and thus it is impossible to capture phenomena such as bifurcation buckling.

2.2 NON LINEAR FINITE ELEMENT SOLUTION ALGORITHM

The objective of the nonlinear finite element analysis is to trace the non linear load-displacement path in multi-dimensional configuration space. In a non linear analysis, solving a single system of linear equations directly does not give the equilibrium condition related to physical system response. The loading must be defined as a function of time and nonlinear response obtained by incrementing time (in the case of a static analysis, time is a dummy variable associated with incremental loading of the structural system). In ABAQUS this simulation is achieved by breaking the total time into a number of time increments. ABAQUS then calculate the approximate equilibrium configuration at the end of each time increment via intermediate iterations carried out within each increment. Several solution algorithms are proposed and applied to trace the equilibrium path. Newton's method is the basic method, and many other algorithms are developed by modifying this method. However, Newton's method fails around the critical points; meaning it is unable to negotiate solution features at the interface between stable and unstable equilibrium conditions. One solution method for tracing the nonlinear equilibrium path that is used in ABAQUS in such instances is Riks-Wempner method.

The advantage of the Riks-Wempner method is its ability to trace behavior beyond a critical point. In other words, this technique permits limit points on the equilibrium path to be negotiated. The ability to accurately negotiate such limit points is a prerequisite for any compactness study since unloading response is at the heart of the currently accepted measure for flexural ductility: rotation capacity, R. The Riks-Wempner method is also sometimes referred to

as the arc length method. In arc-length methods, the solution is constrained to lie either in a plane normal to the tangent of the equilibrium path at the beginning of the increment or on a sphere with radius equal to the length of the tangent. This method allows tracing snap-through as well as snap-back behavior (Ramm and Stegmuller, 1982). The algorithm for Riks method can be found in depth in the literature (Riks, 1972), (Riks, 1979) and (Crisfield, 1986).

2.3 VON MISES METAL PLASTICITY MODEL IN ABAQUS

A yield criterion is a law which defines the limit of elastic behavior under any possible combination of stress at a point in a given material. ABAQUS permits several different type of yield criteria, but the von Mises yield criterion is selected in this research because of its ability to accurately predict yielding in body centered cubic crystalline based metals such as steel (ABAQUS, 2001).

When developing the mathematical model for a yield criterion some assumptions may be made. First, material may be assumed to be isotropic. Second, Bauschinger effect may be neglected. Third, uniform hydrostatic tension or compression does not have an effect on yielding (Chakrabarty, 1987). A geometrical representation of the yield criterion in principal stress space and for biaxial stress space is shown in figure 5 and 6, respectively. The yielding only depends on the deviatoric stress vector *OP*. The elastic state of stress is defined as being any point inside the cylinder, and yielding is defined as any state of stress that permits the stress point to lie on the surface of the cylinder.

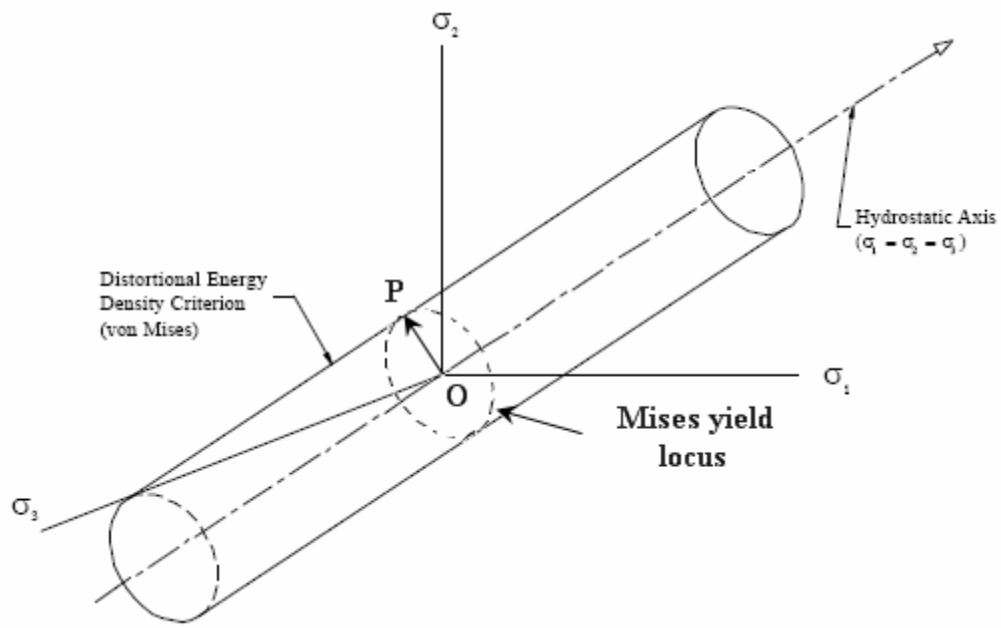

Figure 5 Yield surface in principal stress space

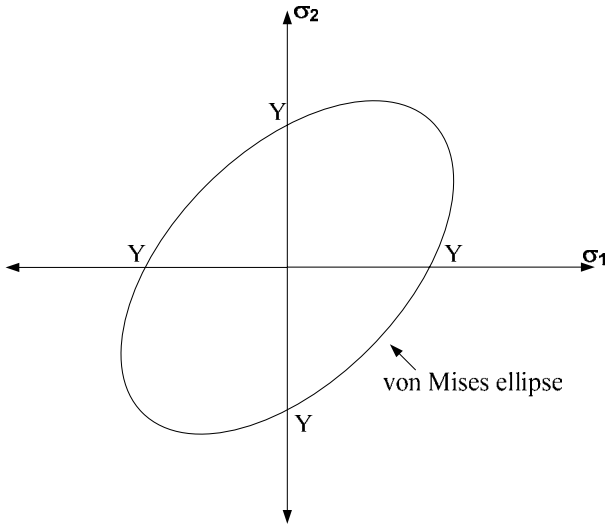

Figure 6 Yield surface for biaxial stress state ($\sigma_3 = 0 \quad and \quad Y = \sigma_Y$)

According to the von Mises criterion yielding will occur when the distortional strain energy density of the structure reaches the distortional strain energy density at yield in uniaxial tension or compression (Boresi, 2002). The total strain energy density U_o can be defined with two components.

$$U = U_V + U_D \tag{27}$$

where U_V is the strain energy density associated with pure volume change. This can be neglected because it is known that hydrostatic pressure does not have effect on yielding. U_D is the distortional strain energy density and is defined in the principal stress state as

$$U_D = \frac{(\sigma_1 - \sigma_2)^2 + (\sigma_2 - \sigma_3)^2 + (\sigma_3 - \sigma_1)^2}{12G} \tag{28}$$

where G is the shear modulus. When uniaxial stress state stress values are known to be

$$\sigma_1 = \sigma \quad and \quad \sigma_2 = \sigma_3 = 0 \tag{29}$$

(as in the case of a uniaxial coupon test) then the distortional strain energy at yield will have the form (Boresi, 2002).

$$U_{DY} = \frac{\sigma_Y^{\,2}}{6G} \tag{30}$$

2.4 EVOLUTION OF FAILURE SURFACE - ISOTROPIC HARDENING

Plastic deformations may continue after initial yield is reached, and this behavior may be accompanied by changes in the yield surface. The relationship for the post yield behavior of the material is known as the flow rule. When the material is loaded beyond a certain point the stress state reaches the yield surface making yield function zero at that point.

If the material is non hardening (i.e. perfectly plastic material) the yield surface does not change thus the stress point always lies on a surface formed by the locus of points corresponding to a constant yield stress. In other words incremental loading will either tend to reduce the value of the yield function below zero, which is also known as unloading, or incremental loading will tend to increase the value of yielding function above zero, which is not physically possible. In this case the stress point moves on the yield surface as the structure deforms plastically. If the material is strain hardening, yield surface evolves as the plastic deformation develops. In this case the yield surface expands or moves with the stress point still on the yield surface. To account for such changes the yield function must be generalized to define the subsequent yield surface configurations beyond the initial one. However, what will be the direction of the plastic flow must be answered (Deierlein, Haijjer, Konvinde, 2001).

The incremental plastic strain can be written in the form of plastic flow vector, c, and the magnitude of the plastic strain, λ.

$$\dot{\varepsilon}^{p} = \lambda c \tag{31}$$

c will be defined as a function of stress state such as plastic potential function g.

$$c = \frac{\partial g}{\partial \sigma} \tag{32}$$

In order to catch the real behavior of the material through analytical means, an appropriate plastic potential function should be picked. A plastic potential function can be chosen as the direction to cause maximum dissipation of plastic work. Knowing that plastic work is the irrecoverable part of the work done during a loading-unloading cycle gives the equation

$$dW^p = \sigma^t . \dot{\varepsilon}^p \tag{33}$$

$$dW^p = \sigma^t . \lambda c \tag{34}$$

After differentiating and setting equal to zero the following equation is obtained.

$$\dot{\sigma}^t . c = 0 \tag{35}$$

According to this equation for maximum plastic dissipation, the direction of plastic strain vector must be located perpendicular to the incremental stress vector. Having known that the stress state is on the yield surface the incremental stress vector must be tangent to the yield surface which makes *c* normal to the yield surface (figure 7). Also the new plastic potential surface is now the yield surface. This choice of the flow rule, where the plastic straining is perpendicular to the yield surface is called associative flow rule (Deierlein, Haijjer, Konvinde, 2001).

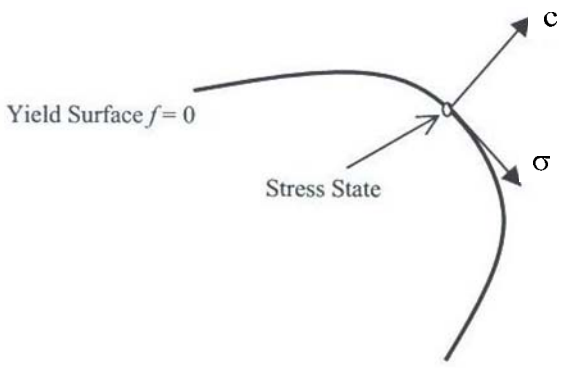

Figure 7 Normality of plastic strain

Getting the maximum dissipation of plastic work by the associative flow rule is only valid for elastic-perfectly plastic materials. This flow rule may not give maximum plastic dissipation for many types of hardening material. However, it is very popular and widely used in the literature for its capability of capturing true behavior for a large variety of materials (Deierlein, Haijjer, Konvinde, 2001). Associated flow models give good results with the materials whose plastic flow is formed by dislocation motion when there are no sudden changes in the direction of the plastic strain rate at a point (ABAQUS, 2001).

After reaching the yield point, many materials show an increase in stress with the increase in strain. Also after unloading and reloading the same material is seen to have increased its yield point. This response of the material is called the hardening response. Increase in the yield point also means increase in the yield surface. If the yield surface changes its size uniformly in all directions, such that the yield stress increases (or decreases) in all stress directions as plastic straining occurs, then the response is called isotropic hardening (ABAQUS, 2001) (figure 8).

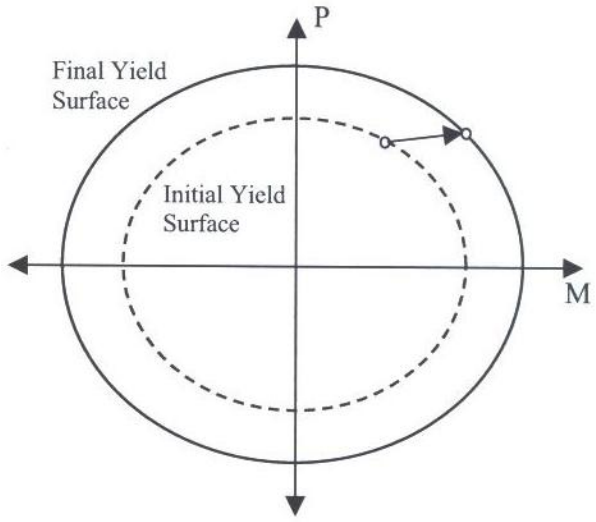

Figure 8 Description of isotropic hardening (Deierlein, Haijjer, Konvinde, 2001).

Meaning that in the case of the von Mises yield surface, isotropic hardening is manifested through an evolution of the cylindrical yield surface in the three dimensional principal stress space such that on planes oriented orthogonally with the hydrostatic stress generator of the surface the circular outline of the von Mises surface appears as a cylinder whose circumference increases, as the stress point continues to impinge on the yield surface during plastic flow, while the location of the center of the circle remains unchanged. In this research, isotropic hardening and the associated flow rule are adopted and used in conjunction with the ABAQUS software system.

2.5 S4R SHELL ELEMENT

The ABAQUS shell element library includes general purpose shell elements and specially formulated shell elements for thick and thin shell problems. In this study the S4R general purpose shell element is used to model the actual three dimensional geometry of the beam. This element is selected for use in the parametric study based on its satisfactory performance in the verification work described in the papers by Thomas and Earls and Greco and Earls (2003a,b).

In the S4R there are four nodes possessing 6 degrees of freedom per node. The general purpose shell elements give accurate solutions to most applications. S4R allows transverse shear deformation to be considered in a fashion that is consistent with Mindlin-Reissner theory. Also, it employs the discrete Kirchhoff techniques to provide satisfactory results as the shell thickness decreases (ABAQUS, 2001)

Finite membrane strains are taken into account in the S4R formulation and thus the element admits changes in thickness as a function of membrane strain. Poisson's ratio of the section defines whether the shell thickness changes as a function of the membrane strain or not. Setting the Poisson's ratio to zero will keep the shell thickness constant and will allow the elements fit for small strain large rotation analysis (ABAQUS ,2001).

S4R formulation is based on a first order shear deformation theory. In other words the shell employs linear displacement and rotation interpolation in the context of Mindlin-Reissner theory, but the shear deformations are then obtained directly from a consideration of the nodal deformations. This approach is made to be consistent with the assumption that cross-sections remain plain but not normal to the Gauss surface of the shell.

ABAQUS uses a lower order quadrature rule, called reduced integration, to calculate the S4R element stiffness. A single integration point is used in this particular element. Reduced

integration has two main advantages: it significantly reduces running time by using fewer sampling points; and with fewer sampling points, some of the more complicated displacement modes offer less resistance to deformation. This increases the accuracy of finite element analysis (Cook, 1989). Sometimes using reduced integration yields element stiffness matrices that display one or more false zero energy mode, which may also be the cause of an unstable, or very inaccurate solution (Bathe, 1982). However; ABAQUS overcomes this problem by using hourglass control. Hourglass control assigns an artificial (and usually quite small) stiffness to the so-called drilling degree of freedom on the shell. This stiffness value depends on the factors usually given as a small fraction of typical shear modulus for material (ABAQUS, 2001).

3.0 VERIFICATION OF NUMERICAL MODELING

Experimental testing is the best way to investigate the inelastic post buckling response of I-beams. However, it is expensive and time consuming to perform the large series of tests needed to investigate the response of I-beams having many reasonable dimensions. The other choice is to use a numerical experimental series with the help of a computer to perform the required parametric studies. Such numerical experiments rely on accurate computer models of the I-beams. The nonlinear finite element program, ABAQUS, is employed in this research. In non linear finite element analysis techniques, assumptions related to the type of stress strain curve, boundary conditions, initial imperfection etc. may impact on the quality of the numerical results.

As it is that the nonlinear finite element modeling technique is the primary vehicle for the research program reported on herein, it is clearly of great importance to establish the accuracy of the modeling strategies employed in this study. As part of the current work, a careful search of the experimental literature is undertaken in order that an appropriate research program might be identified for use as a test case for the current verification study. Once a verified model has been constructed, reliable data can be produced by doing parametric studies using the finite element models. However, accuracy of the computer modeling depends on how well the real material's physical and mechanical properties are defined.

The most appropriate study found in the literature is centered on some work reported on at the University of Sydney (Rasmussen and Chick 1995). This experimental research program

focuses on the study of I-shaped members possessing slender cross-sectional profiles subjected to combined loading applied in a proportional fashion. As part of this Australian research, the extreme case of pure minor axis bending as well as the cases where the interaction of minor axis bending with axial loading are considered and thus valuable experimental results are contained in this work; vis-à-vis a verification study related to the present research.

3.1 SOURCE OF MODELING UNCERTAINTIES

There are some uncertainties in both physical testing as well as finite element modeling. For the test specimens, stress strain properties, yield strength values of the material, and the plate geometry may be different through the section and along the beam length. Also mis-measured and reported initial geometric imperfections and residual stresses, unreported material properties, such as stress strain properties of material loaded in compression, do have important affects on the results of numerical models. Tension properties of the material are reported for the test specimen studied in this research. However, because of the Bauschinger affects, the tension behavior does not represent the compression behavior. In addition, as deformations become large, support and restraint conditions become critical and variability in these values can change the result dramatically.

In finite element modeling the analyst must define the information listed below:

- Initial geometry of the specimen with imperfections
- Boundary conditions
- Mesh density

- Element type
- Material model with material stress-strain properties
- Numerical solution procedure with convergence tolerances

3.2 DESCRIPTION OF EXPERIMENTAL TESTING PROGRAM FROM THE LITERATURE FOR I BEAM UNDER MINOR AXIS BENDING.

Rasmussen and Chick (1995) conducted a series of experimental tests under minor axis bending and axial force. Only two of these tests were performed under pure bending. In this research these two test specimens are used to validate the finite element modeling strategies for the investigation of I-section flange compactness under minor axis bending, alone.

3.2.1 Geometry of the test specimen

Rasmussen and Chick had tested a series of thin walled I-beams in combined compression and minor axis bending. Rasmussen and Chick (1995) focus on a single I-shaped cross-section whose nominal dimensions appear in figure 8. Using this single cross-section, three distinct study cases are considered through the variation of the member unbraced length. Specifically, short (L_b = 800mm), medium (L_b = 3500mm), and long (L_b = 5800mm) members are treated in their work. As a focus of the current verification efforts, only the short and long cases are considered because they are the only tests performed under minor axis bending. The cross-section used in

the experimental test was a slender I-section fabricated from high strength steel with $F_y = 350\ MPa$.

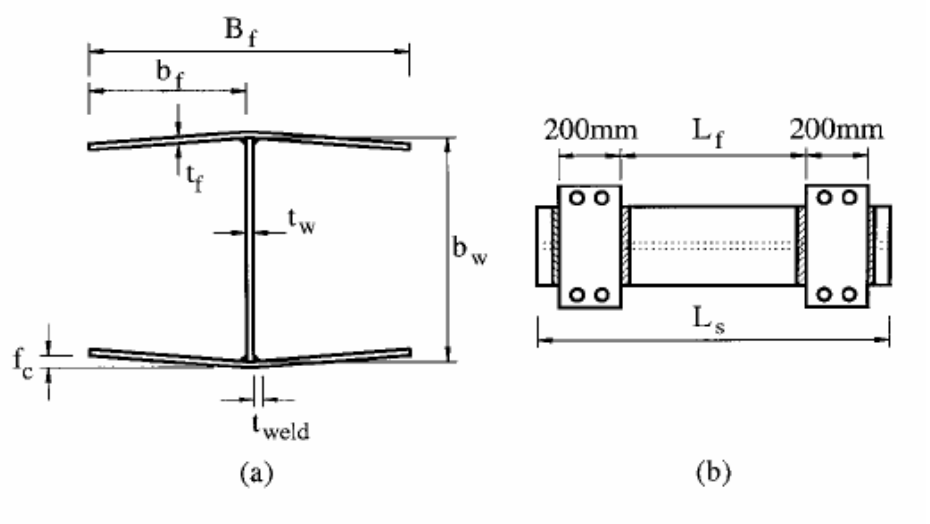

Figure 9 Nomenclature (Rasmussen, 1995)

Table 1 presents the measured cross-sectional dimensions.

Table 1 Specimen dimensions

Specimen	L_s	L_f	t_f	t_w	b_w	B_f	f_c
	(mm)						
800-6	795.5	327	5.01	5.04	240	239	6
5800-5	5798	5175	4.98	5.02	241	240.5	5

3.2.2 Material Model

The behavior in the strain-hardening region is generally based on the nominal stress and engineering strain; which are calculated without considering the change in area of the cross-section. However, the change in the cross-sectional area of the specimen may be an important parameter when large deformations occur. In these cases the strain hardening range should be characterized using the true stress, obtained by dividing the load by the current area of the specimen. Nominal stress and strain data for uniaxial test for isotropic material can be converted into true stress and logarithmic plastic strain by using the following equations;

$$\sigma_{true} = \sigma_{nom}\left(1+\varepsilon_{nom}\right) \tag{36}$$

$$\varepsilon_{\ln}^{pl} = \ln\left(1+\varepsilon_{nom}\right) - \frac{\sigma_{true}}{E} \tag{37}$$

Rasmussen and Chick presented stress-strain properties of material loaded in tension in their report. Residual stresses are not included in this research since it is known to have no influence over the observed strength of hot-rolled structural members.

Experimentally determined mechanical response values from coupon testing appear in table 2, in engineering units. These are converted to an idealized multilinear true stress and logarithmic strain format (see figure 10, table 3 and table 4) prior to importation into the finite element software package, ABAQUS.

Table 2 Material properties

Specimen	*Plate Number*	*E (GPa)*	f_{yc} *(MPa)*	f_{yt} *(MPa)*	f_{ut} *(MPa)*
800-6	7	198	446	420	498
5800-5	4	200	466	431	509

Table 3 Stress- Strain values for Test Specimen 800-6

σ_{nom}	ε_{nom}	σ_{true}	$\varepsilon_{\ln}^{pl}$
420	0.0021	420.89	0
420	0.0167	427	0.014376
490.9	0.0577	519.22	0.053465
522.72	0.125	588.06	0.114813
522.72	0.2019	628.27	0.1807497

Table 4 Stress-Strain values for Test Specimen 5800-5.

σ_{nom}	ε_{nom}	σ_{true}	$\varepsilon_{\ln}^{pl}$
431	0.0022	431.93	0
431	0.0231	440.95	0.0206099
510	0.0615	541.38	0.0570123
526.67	0.0885	573.26	0.081899
526.67	0.1462	603.64	0.1333936

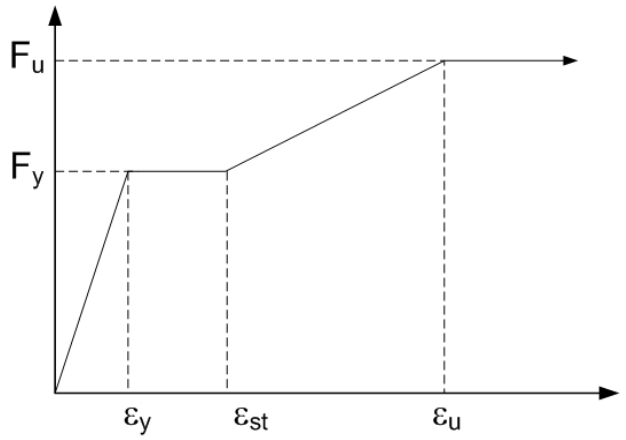

Figure 10 Representative Idealized Material Model used in Finite Element Modeling

3.2.3 Geometric Imperfections

Since the verification test case considered in this part of the study involves minor principal axis flexure of an I-shaped beam under the action of pure moment, bifurcation related response must be considered as a possible factor governing overall response. When applying the finite element method to bifurcation-type stability problems, it is oftentimes advisable to incorporate a reasonable imperfection field into the finite element model. The incorporation of the imperfection field is used to perturb the model from the condition of perfect geometry; failure to do this may result in the model artificially persisting in the perfect state throughout the loading history. The potential proximity of the finite element displacement solution to an initial perfect geometry arises since such a configuration is a mathematically admissible equilibrium state (even post bifurcation). However this configuration is meaningless physically since the slightest loading disturbance, or geometric imperfection, would render such an equilibrium state inaccessible to practical cases. As a means of guarding against any potentially physically aberrant response, a reasonable displacement-based imperfection field should be incorporated

into finite element models whose response has the potential of being governed by bifurcation buckling. In such cases, it is not imperative that the precise governing buckling mode be used as an initial imperfection adopted at the start of the nonlinear solution. Rather, any imperfection field used need only possess elements of the dominant features that are contained in the governing mode.

In the present verification study, it is observed from linearized eigenvalue buckling analyses, carried out with ABAQUS, that the governing mode of instability in minor axis I-shaped members in pure bending involves localized buckling within the flange. The perfect geometry was seeded with sinusoidal a varying imperfection given by equation

$$w_o = A\, y \sin(\frac{\pi x}{L}) \tag{38}$$

The magnitude of imperfections for the flanges was taken as the maximum allowable fabrication imperfection permitted by the American Welding Society (AWS D1.1:2000); this is schematically illustrated in figure 11.

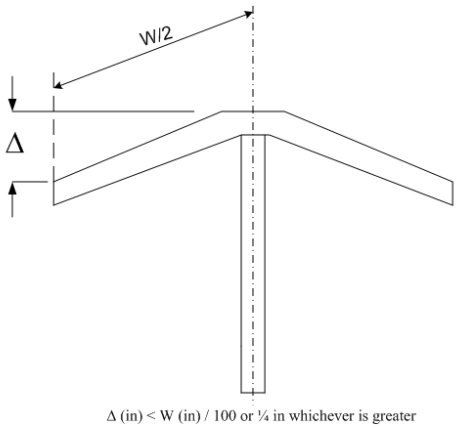

Figure 11 Measurement of flange warpage and tilt.

Two types of constantly imposed imperfections were investigated, sinusoidal varying imperfection possessing a half wavelength of $B_f / 2$ that is phase shifted by 180 degrees between opposite flange tips and the same field without phase shift (figure 12 and figure 13). Effects of phase shift and imperfection sensitivity are only searched in specimen 800-6 and in 5800-5.

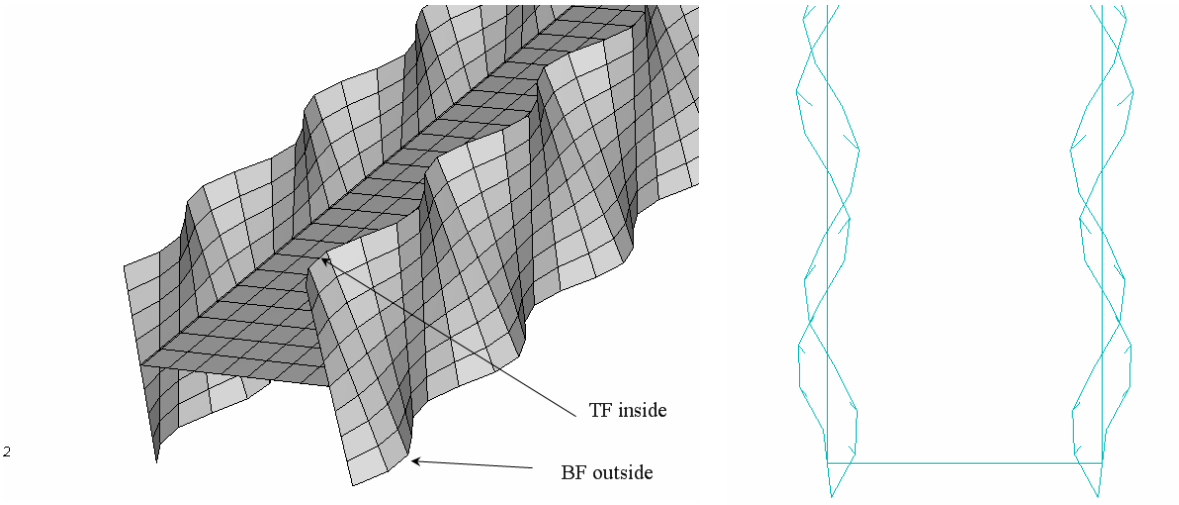

Figure 12 Imperfection with phase shift.

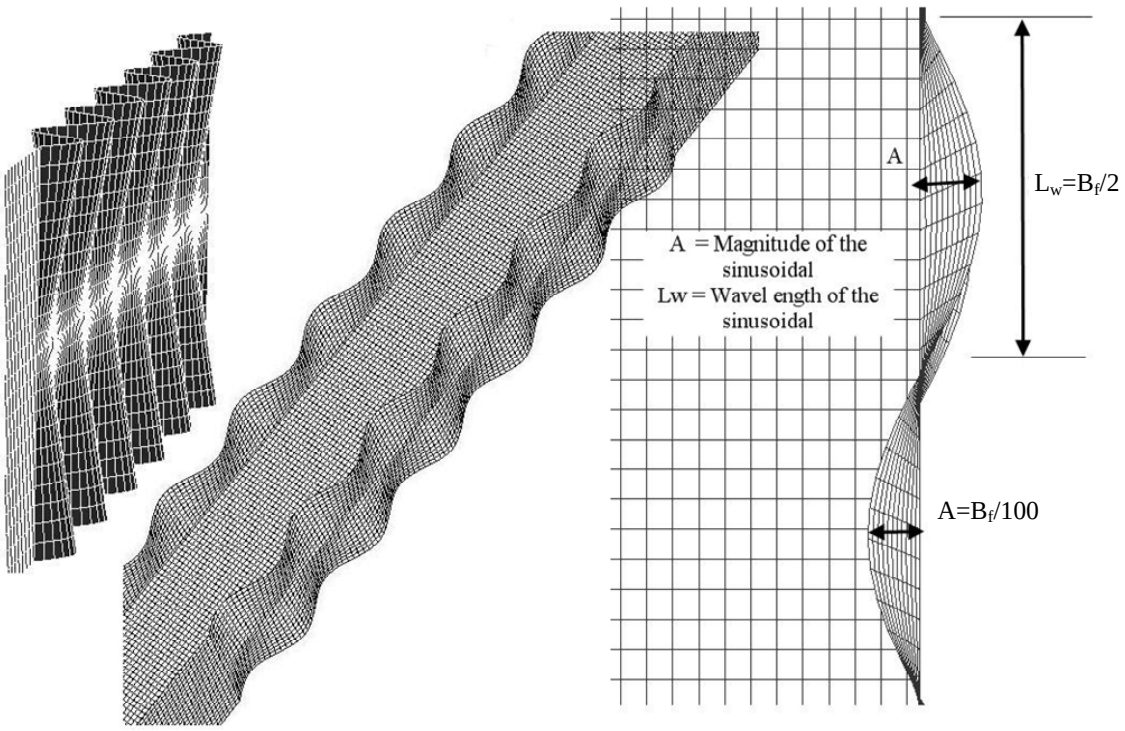

Figure 13 Sinusoidal imperfection without phase shift.

The results showed that existence of the phase shift in the imperfection does not have affect on the moment rotation curve. These results can be seen in figure 14.

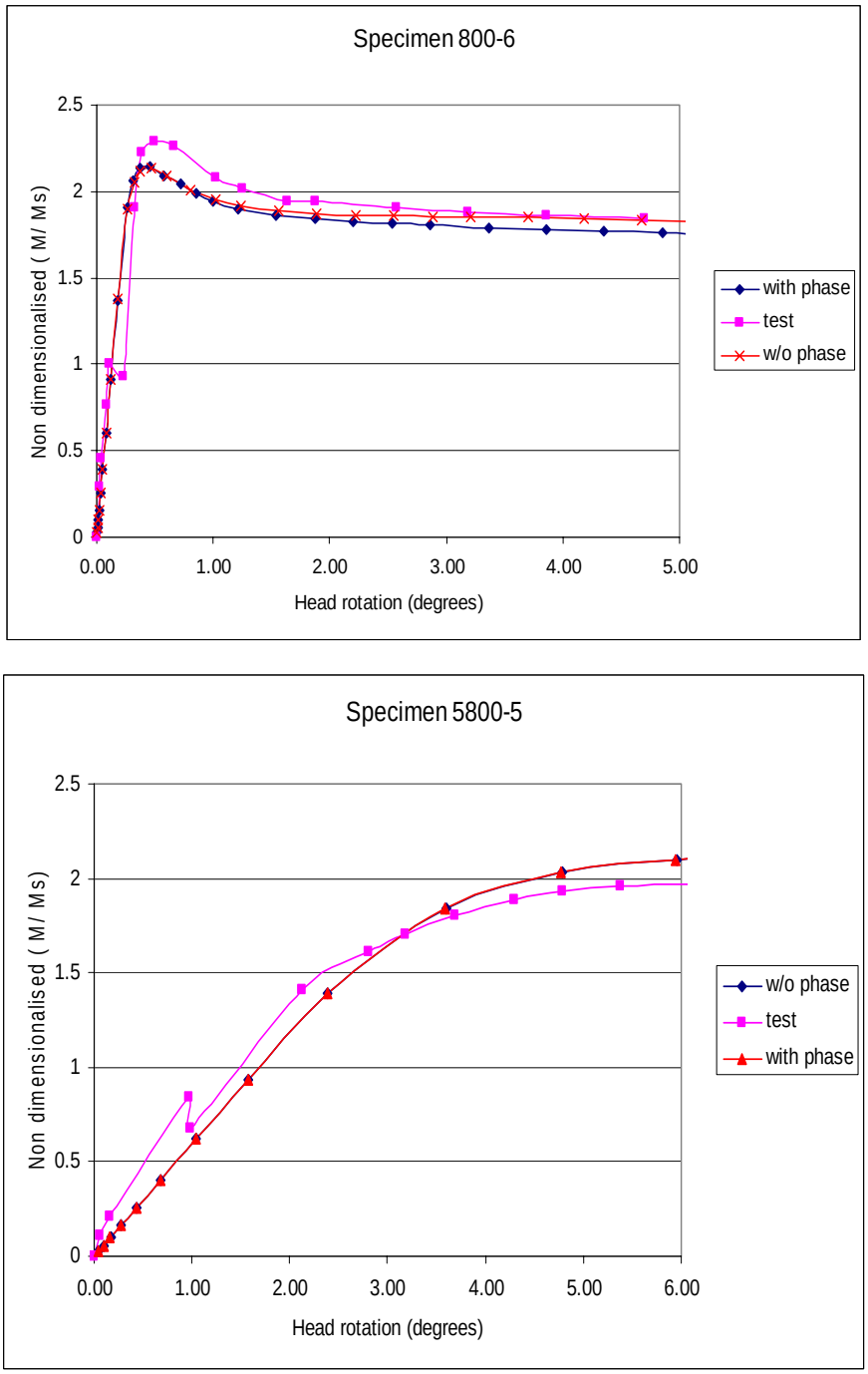

Figure 14 Comparison of imperfections with and without phase shift

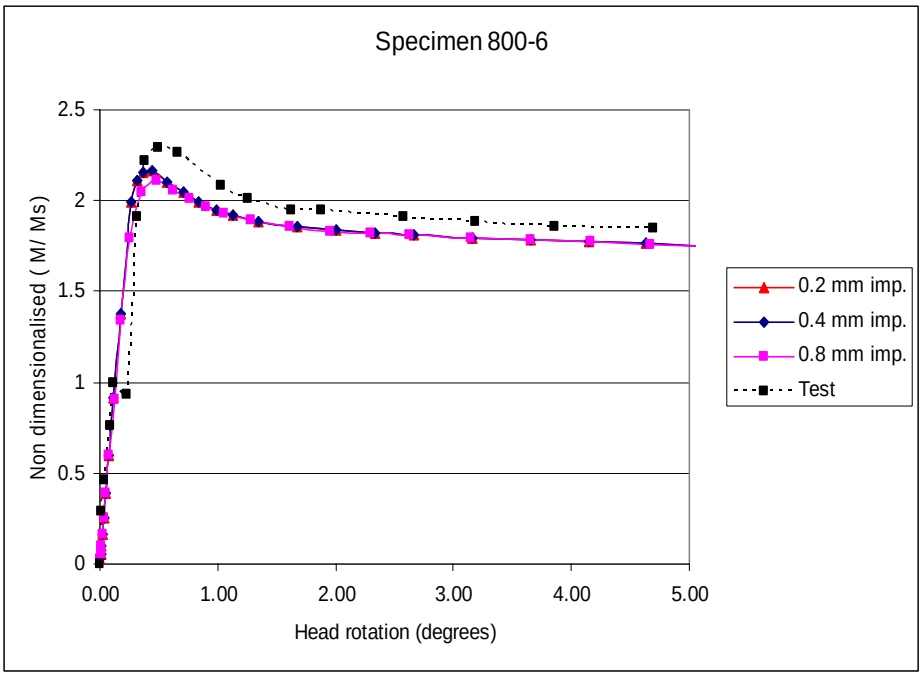

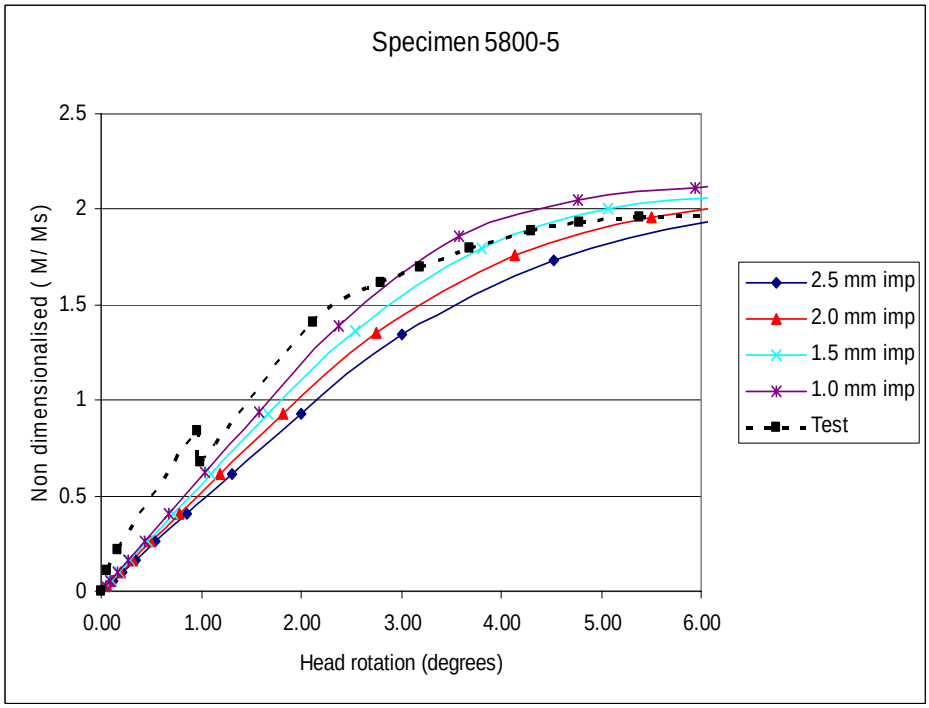

Figure 15 Imperfection sensitivity results

Also the magnitude of the peak imperfection deflection amplitude is varied to see if the model is sensitive to the imperfections or not. The result of the studies for the given test specimen under different imperfection magnitudes is given in figure 15. Variation of imperfection of the test specimens at the flange tips and overall along the beam is given in figure 16.

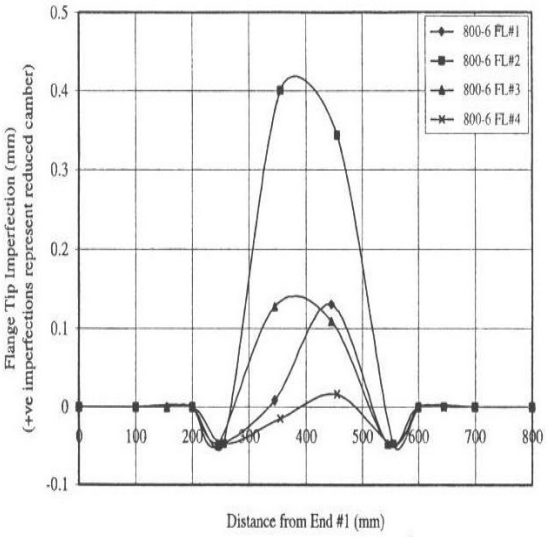

Figure 33: Specimen 800-6 Flange Geometric Imperfections

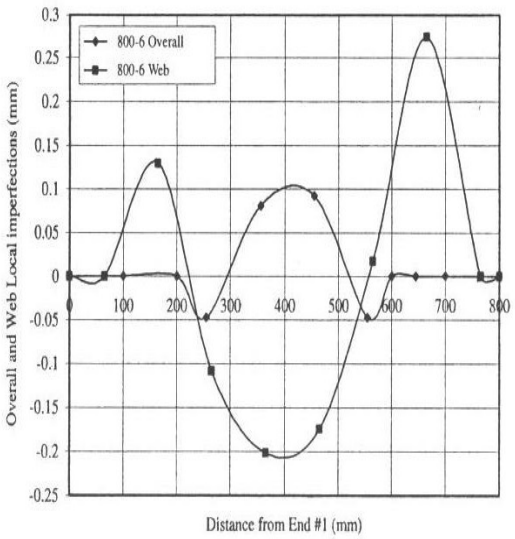

Figure 34: Specimen 800-6 Web and Overall Geometric Imperfections

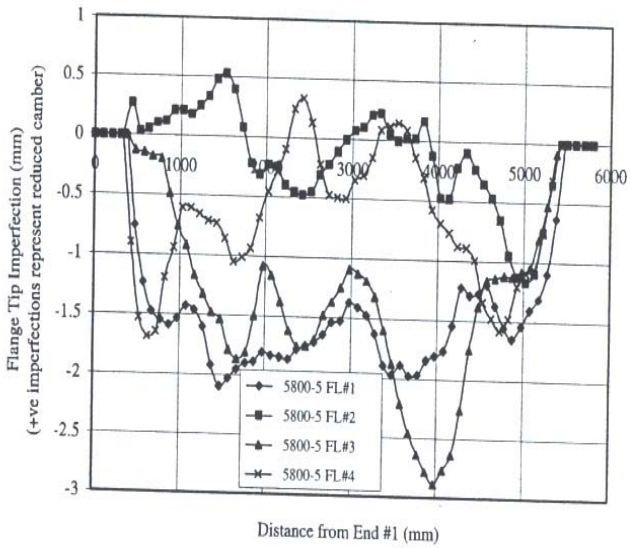

Figure 53: Specimen 5800-5 Flange Geometric Imperfections

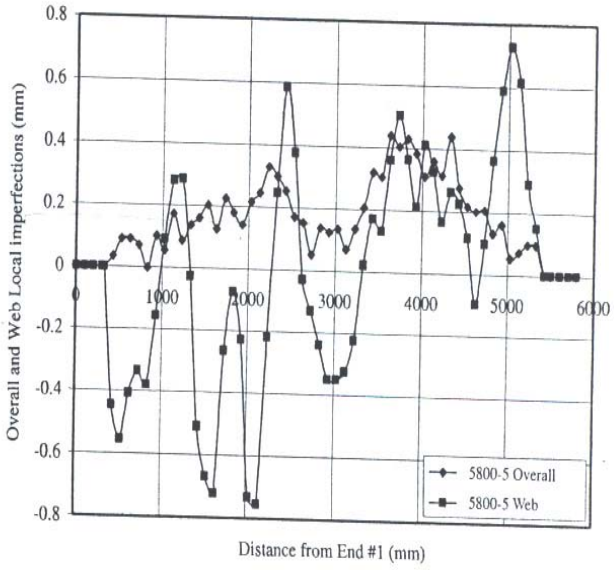

Figure 54: Specimen 5800-5 Web and Overall Geometric Imperfections

Figure 16 Imperfection of the test specimen (Rasmussen, 1995)

Based on these results, the wavelength and the magnitude for sinusoidal type geometry are taken as $0.5xB_f$ and $B_f / 100$, respectively. These values are used throughout the remainder of this work.

3.2.4 Finite element model for searching the I-section flange compactness under minor axis bending

Finite element mesh: In this research, the results of a parametric study are carried out using the same verified nonlinear finite element modeling approach discussed in the earlier sections. The same sinusoidally varying localized imperfection field of intensity $B_f / 100$ is used in this portion of the work. As a means of creating a constant moment region of investigation for this study, a three segment beam, acted on by two equally spaced concentrated transverse loads applied to the third points, is used to create a central constant moment region possessing precisely the moment profile required by current specification writing bodies as the foundation case for provisions (figure 17).

These forces are applied at the flange-web junctions of the cross-section. While there is also moment gradient loading being applied at both rigid end segments, these end segments are not of interest in this research; that is why they are modeled as being approximately rigid through the use of and elastic modulus that is one order of magnitude higher than that of middle segment. Imperfections were applied only on the flanges. In addition, the rigid segments were not seeded with imperfections, and mesh densities used throughout the entire length of the beam were constant and uniform.

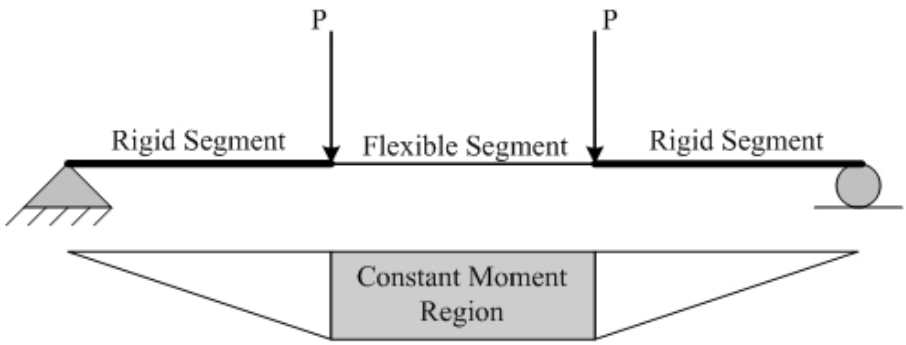

Figure 17 Loading of the model

Boundary Conditions: The model is a simple supported beam. However; restraint against out of plane translation is applied at the flange tips at the flexible-rigid transition interfaces. A schematic depiction of the loading, geometry, and boundary conditions used in this work appears in figure 18.

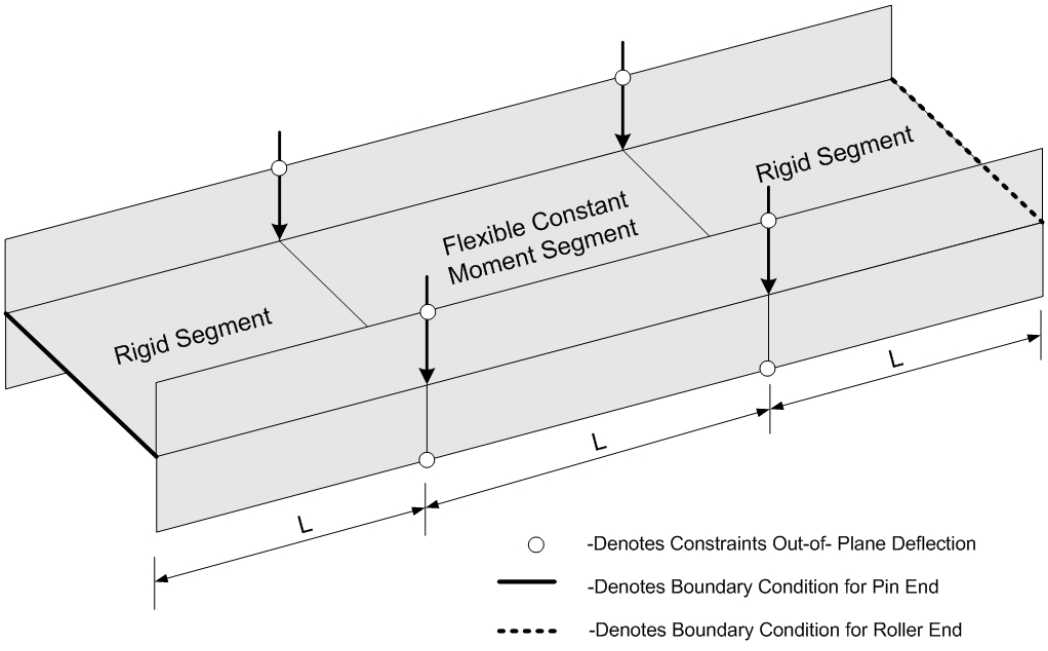

Figure 18 Boundary conditions and loading for the model

3.2.5 Verification Results for the I-section flange compactness under minor axis bending

Employing the above specializations, the two constant moment minor axis flexural cases are reproduced in the computer in order that suitable structural response results can be generated and compared with the results from the experimental program of Rasmussen and Chick (1995). Plots comparing normalized moment and absolute rotation appear in figures 19–20. Based on these results, it appears that the present modeling techniques are sufficiently robust to undertake the outlined parametric study.

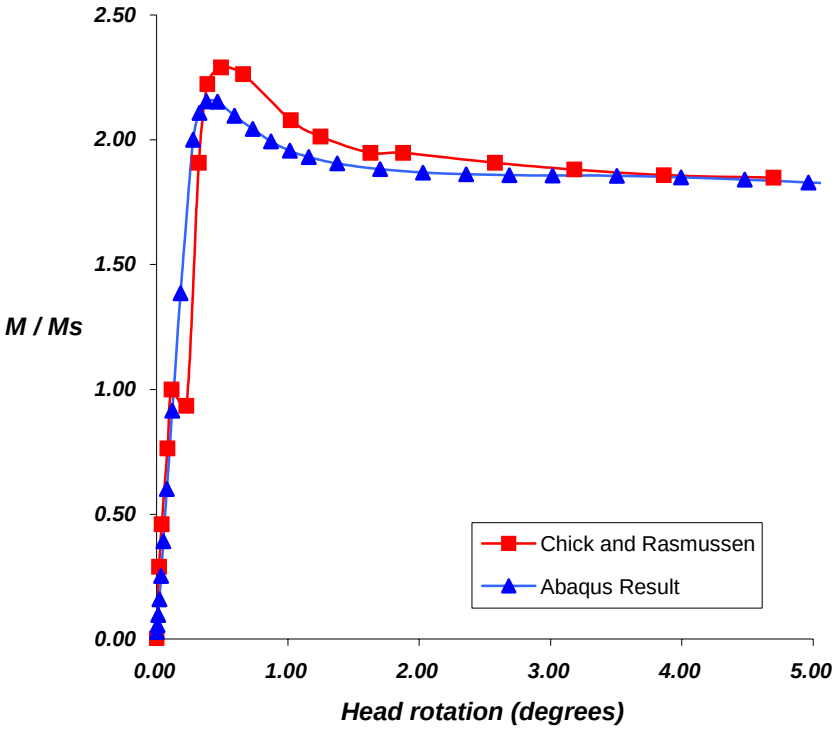

Figure 19 Comparison of test result with FEA for 800-6

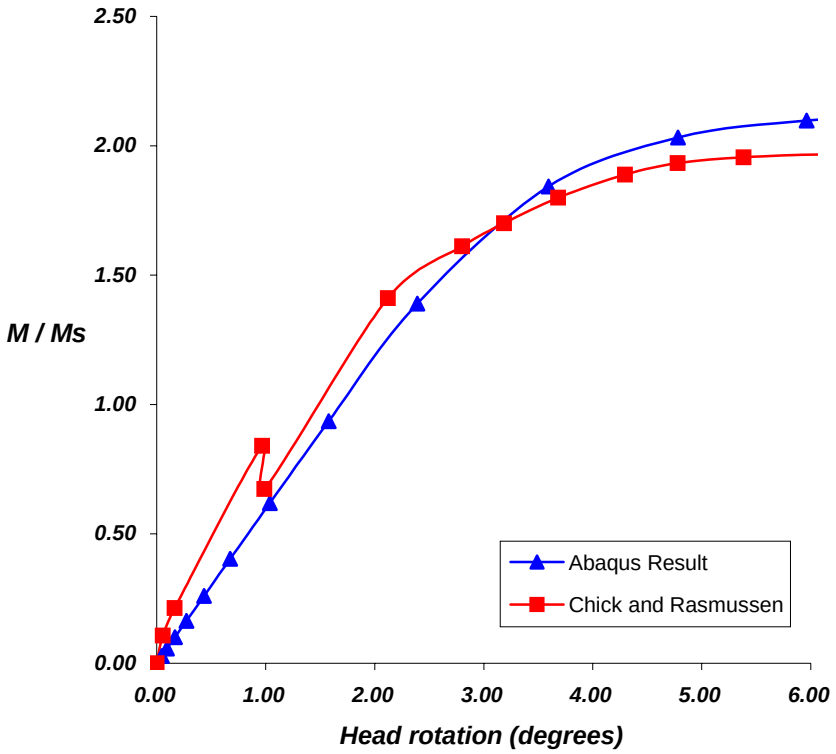

Figure 20 Comparison of test result with FEA for 800-6

As mentioned earlier, unreported data from test can interfere with proper modeling. For instance only uniaxial tension behavior is reported in the test report. Because of Bauschinger effect $f_{yc} \neq f_{yt}$ (see table 2), it is anticipated that the reported mechanical response properties in the report of Rasmussen and Chick is inadequate for comparability between the experimental testing and any subsequent finite element analogs. However the model of the test specimen only considers the uniaxial tension material behavior which does not necessarily represent the actual behavior of the specimen. Furthermore, residual stresses are not taken into account in the finite element modeling. This may also play a role in any observed lack of agreement between the experimental tests and the finite element analogs since residual stresses may have a significant

impact on light gauge metal structural members, such as those being considered in the verification study (as opposed to the heavier hot-rolled sections at the heart of the current research's parametric study discussed later).

In order to compare the physical results of the tests the deflected shape of the models are compared with that reported by Chick and Rasmussen (1995). In the report Chick and Rasmussen (Rasmussen, 1995) it is stated that: "The 800-Series specimen formed two local buckle half-wavelengths in the compression flange outstands which grew in amplitude until the end of the test. The tension flange outstands remained flat while yielding in tension as the test progressed."

In figure 21 an ABAQUS deformation plot shows that the characteristic behavior of the model matches with that stated in the test report.

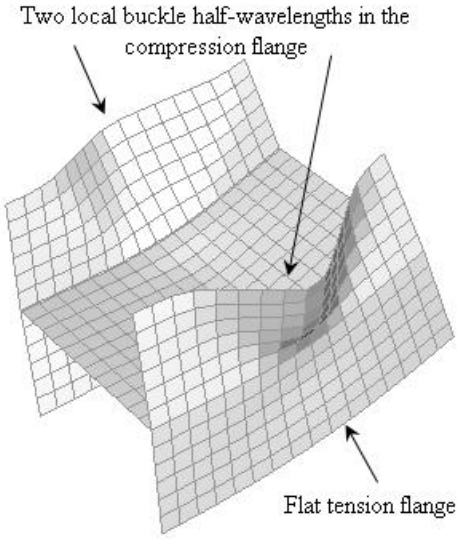

Figure 21 Deformed shape of the numerical model for test specimen 800-6.

In the report Chick and Rasmussen (Rasmussen, 1995) states;

“The 5800-Series specimen formed local buckles of consistent amplitude and wavelength over the entire length of the compression flange outstands. These deformations changed in amplitude from when they were first apparent. Failure eventually occurred at one quarter of the length from one end of the specimen where yield lines formed in the compression flange outstands.”

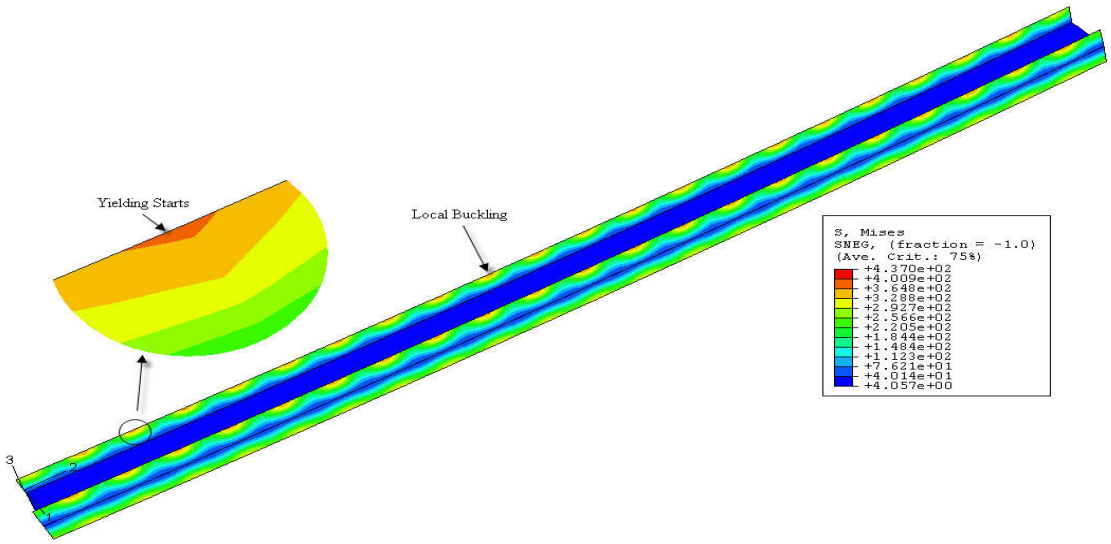

Figure 22 Deformed shape of the numerical model for test specimen 5800-5.

Again in this model ABAQUS deformation plot (figure 22) shows good agreement with the statement made in the test report.

3.3 DESCRIPTION OF EXPERIMENTAL TESTING PROGRAM FOR I-SHAPED BEAMS UNDER MINOR AXIS MOMENT – THRUST

Beams with 3500 mm and 5800 mm lengths from the research of Ramussen and Chick (1995) are used to validate the finite modeling strategies for the investigation of interaction between axial loading and minor axis bending. Since a detailed description of modeling is mentioned in previous section, only the differences between the two modeling approaches will be reported in this section. Total of seven tests are verified for this part of the research.

3.3.1 Geometry of the test specimen

The measured cross-sectional dimensions, in addition to the ultimate forces applied to the models, are tabulated in table 5.

Table 5 Measured specimen lengths and applied loads

Specimen	t_f(mm)	t_w(mm)	b_w (mm)	B_f (mm)	f_c (mm)	M (kNm)	P(kN)
3500-2	5.02	4.95	240.50	240.00	4.50	5.53	653
3500-3	4.97	4.98	240.00	239.50	6.50	9.57	553
3500-4	4.96	5.00	240.00	239.00	6.00	13.2	427
3500-5	5.01	5.00	240.50	239.50	4.50	39.63	65
5800-2	4.91	5.01	240.00	240.00	4.50	1.79	430
5800-3	4.99	5.01	241.00	240.00	5.00	7.26	318
5800-4	5.07	5.05	241.00	240.00	5.50	18.21	181

3.3.2 Material model

Uniaxial tension test results carried out under quasi-static conditions are adjusted to be static values according to the paper of Galambos and Ravindra (1978). In that paper stress levels are decreased by 4 ksi because of the difference between the dynamic test loading and the actual static loading. Static yield stress is independent of testing procedure and the behavior of testing machine. Static yield stress is defined as the stress level when the strain rate is zero or when the testing speed is zero (Galambos, 1998). In figure 23 difference between static and dynamic loading can be seen. For example; uniaxial tension test results for plate 2 is given in figure 24 and the amount of deduction calculated is also shown on figure 24.

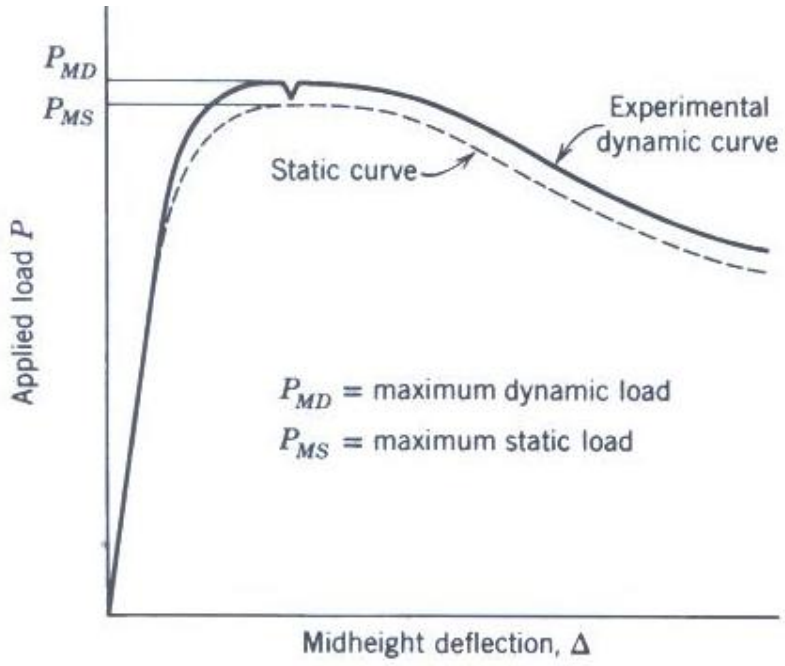

Figure 23 Difference between dynamic loading and static loading (Galambos,1998).

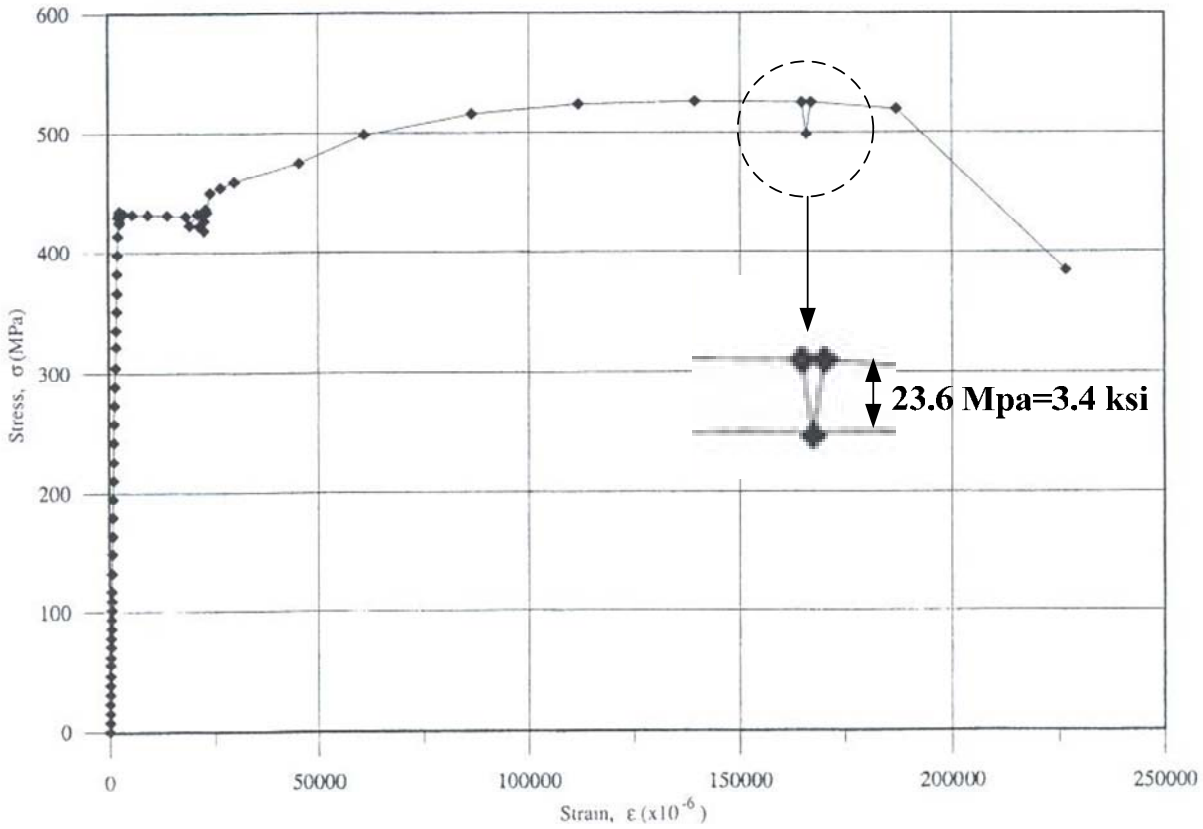

Figure 24 Stress strain plot for plate 2.

The reported mechanical response values from coupon testing appear in table 6 in engineering units; these are subsequently adjusted to be static values and then converted to an idealized multilinear true stress and logarithmic strain format (see figure 10, table 7,8,9,10 and 11) prior to importation into the finite element software package, ABAQUS.

Table 6 Mechanical properties

Specimen	*Plate*	*E (GPa)*	f_{yc} *(MPa)*	f_{yt} *(MPa)*	f_{ut} *(MPa)*
3500-2	6	204	457	431	503
3500-3	2	198	450	435	498
3500-4	3	200	453	436	506
3500-5	4	200	466	431	509
5800-2	1	199	451	435	502
5800-3	2	198	450	435	498
5800-4	1	199	451	435	502

Table 7 Stress- Strain values for Plate 1

σ_{nom}	ε_{nom}	σ_{true}	$\varepsilon_{\ln}^{pl}$
435.5	0.002188	408.874	0
435.5	0.014904	414.4099	0.012567
503	0.063462	507.3492	0.05884
525	0.10875	554.5098	0.100305
525	0.186635	595.404	0.167991

Table 8 Stress -Strain values for Plate 2

σ_{nom}	ε_{nom}	σ_{true}	$\varepsilon_{\ln}^{pl}$
435	0.002197	408.3766	0
435	0.018269	415.3681	0.015867
499.3333	0.061538	502.4825	0.057042
523.3333	0.111731	554.2267	0.10298
523.3333	0.186731	593.4767	0.168066

Table 9 Stress -Strain values for Plate 3

σ_{nom}	ε_{nom}	σ_{true}	$\varepsilon_{\ln}^{pl}$
436	0.00218	409.3715	0
436	0.011538	413.4517	0.009267
506.6667	0.065385	512.2158	0.060637
526.6667	0.105769	554.7928	0.097629
526.6667	0.186538	597.3312	0.167916

Table 10 Stress -Strain values for Plate 4

σ_{nom}	ε_{nom}	σ_{true}	$\varepsilon_{\ln}^{pl}$
431	0.002155	404.3498	0
431	0.013077	409.0571	0.010809
510	0.061538	513.8056	0.057012
526	0.088462	544.9517	0.081903
526	0.146154	575.2979	0.133397

Table 11 Stress -Strain values for Plate 6

σ_{nom}	ε_{nom}	σ_{true}	$\varepsilon_{\ln}^{pl}$
431	0.002113	404.3315	0
431	0.009615	407.5652	0.007436
483.3333	0.046154	478.062	0.042642
520	0.1	544.421	0.092506
520	0.176923	584.421	0.159903

3.3.3 Geometric imperfections

In the finite element analogs of the experimental test specimens, a reasonable displacement-based imperfection field is incorporated into the finite element models in the form of sinusoidally varying imperfection possessing a half wavelength of $B_f / 2$, that is phase shifted by 180 degrees between opposite flange tips (see figure 12) as well as a maximum displacement amplitude equal to 0.2 times the flange thickness.

3.3.4 Finite element model for I-Shaped Beams under minor axis moment - thrust

Finite element mesh: The I-shaped cross-sections are built-up using S4R shell finite elements from ABAQUS element library positioned along the middle surfaces of the cross-sectional constituent plate components (figure 25).

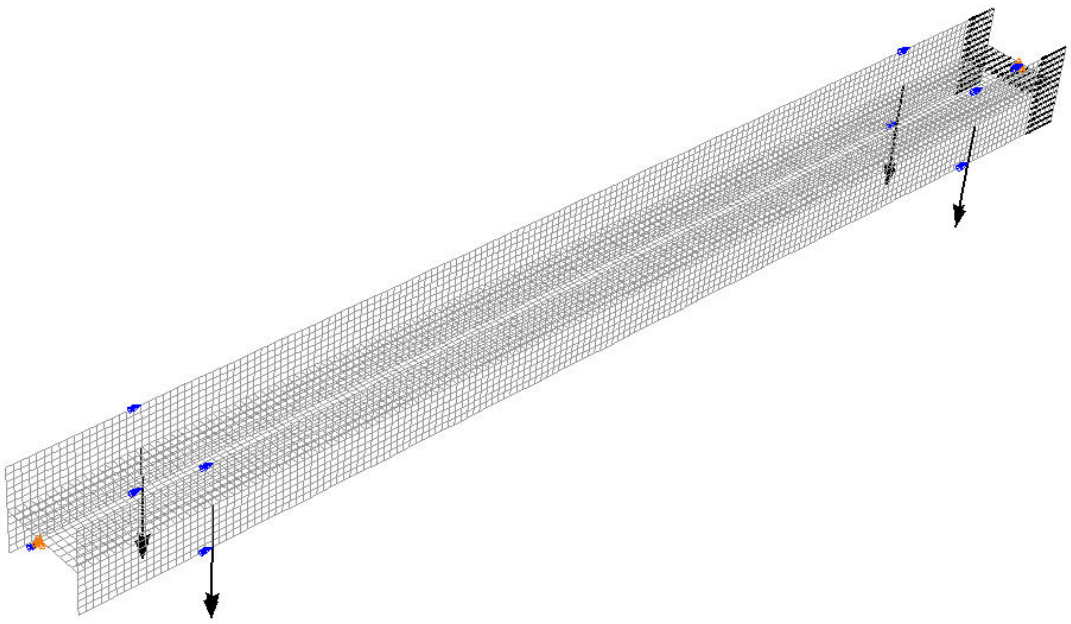

Figure 25. Representative Shell Finite Element Mesh

A constant moment loading is achieved by applying four concentrated forces perpendicular to the beam longitudinal axis. Axial loads are applied at the nodes at the roller end of the simply supported beam. The two end segments adjacent to the constant moment region, are made to behave rigidly.

Boundary Conditions: The model is a simple supported beam. However; restraint against torsion is applied at the flange tips at the flexible-rigid transition interfaces. A schematic depiction of the loading, geometry, and boundary conditions used in this work appears in figure 26. At the end of the I-shaped member, along the plate edges, rigid beam elements from the ABAQUS element library are employed to assist with maintaining ideal kinematics at points associated with the imposition of boundary conditions.

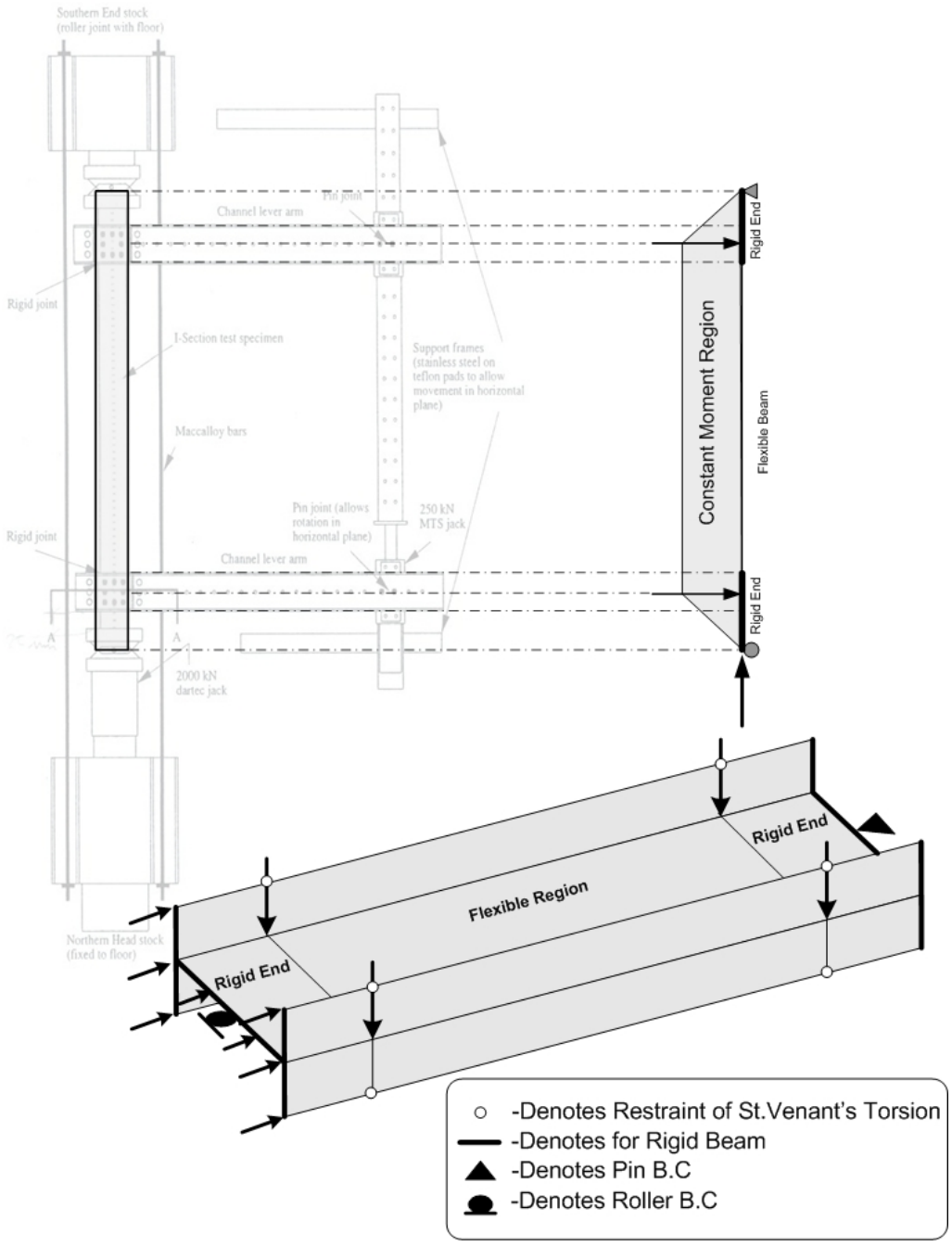

Figure 26 Test rig and finite element modeling

3.3.5 Verification of Test Results for I-Shaped Beams under minor axis moment - thrust

Results from seven of the experimental specimens reported on from the research program of Rasmussen and Chick (1995) are compared with equivalent finite element models. Plots comparing these interaction responses appear in figures 27 and 28. In these figures, the maximum inelastic moment at the mid-span versus the axial load are plotted. The maximum moment is calculated as the sum of the end moment and the moment produced by the eccentricity of the axial force; $M = M_{end} + P\delta$ where δ is the mid-span deflection (i.e. the sum of the primary and secondary moments). Based on these results, it appears that the present modeling techniques are sufficiently robust to undertake the desired parametric study.

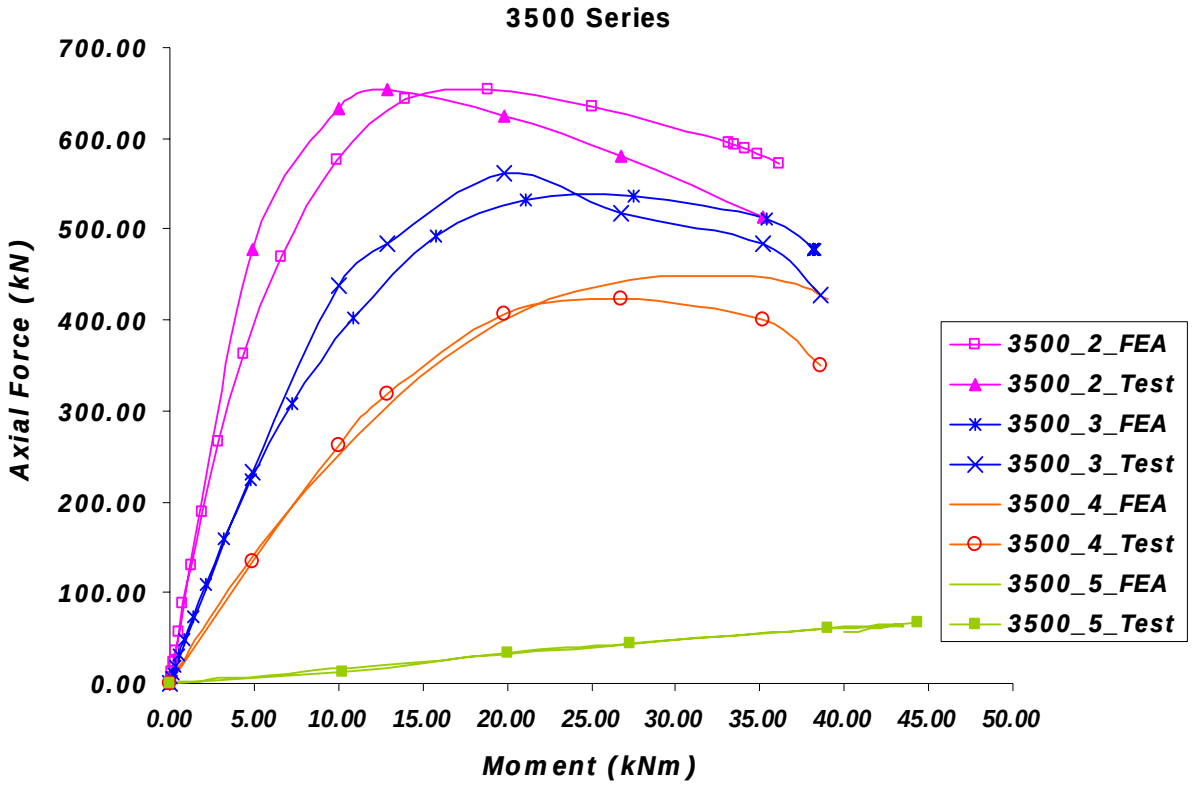

Figure 27 Comparison of results for 3500 series

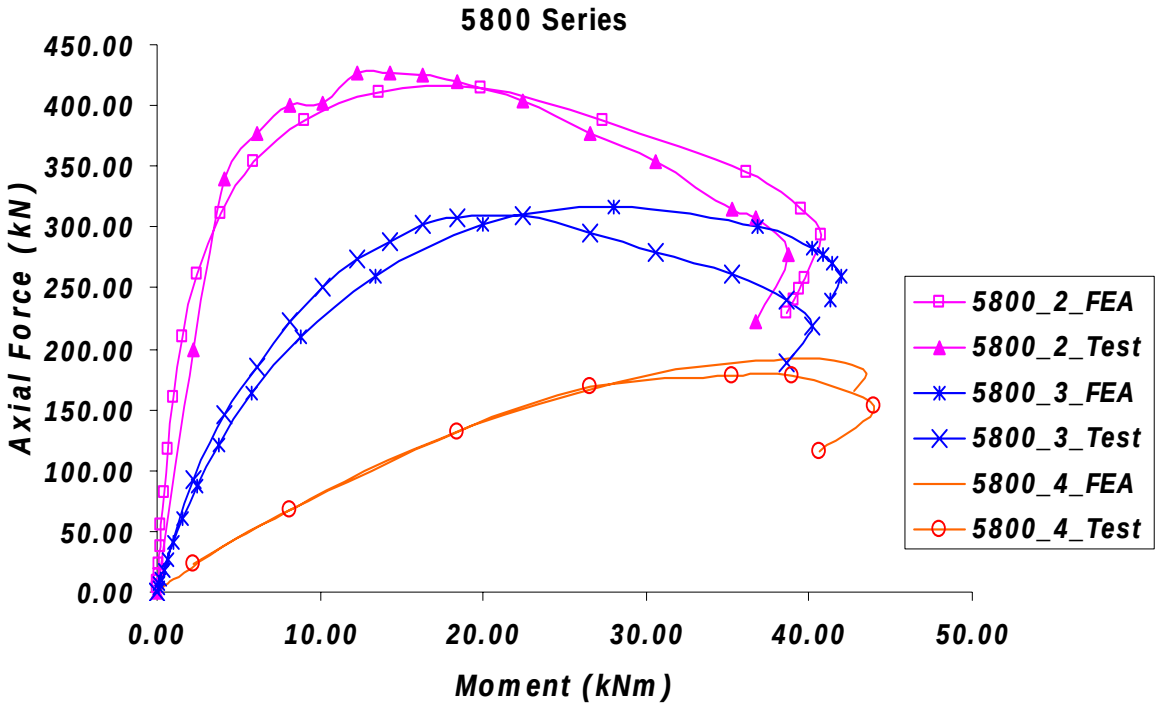

Figure 28 Comparison of results for 5800 series

Rasmussen and Chick (1995) also reported the maximum axial force and corresponding second order moment values at the end points. It is noted that the format of these test results allows foran easy comparison with the design interaction curve in AISC-LRFD since it is defined is terms of ultimate axial load (P_u) versus second order elastic moment (M_{meu}). In order to compare the experimental results with design interaction equations, end moment must be converted to second order moments. This can be done by using the following equation;

$$M_{meu} = B_1 \times M_{endu} \tag{39}$$

$$B_1 = \frac{1}{1 - \frac{P_u}{P_e}} \tag{40}$$

where Euler buckling load is $P_e = \frac{\pi^2 EI}{L^2}$; a value enforced to be the flexural buckling load about the minor principal axis in this context, and M_{endu} is the first order end moment coinciding with the controlling value of P_u. Furthermore, M_{endu} from the ABAQUS results is converted into M_{meu} and compared with the corresponding values given by Rasmussen. Comparison of these values can be seen in table 12.

Table 12 Comparison of ultimate axial load and second order elastic moments

	P_u (kN)		M_{meu} (kNm)	
Specimen	*FEA*	*Test*	*FEA*	*Test*
3500-2	654.00	653.00	9.82	9.80
3500-3	536.28	553.00	14.75	15.60
3500-4	449.12	427.00	20.11	18.80
3500-5	63.97	65.00	40.79	41.50
5800-2	414.51	430.00	5.99	7.30
5800-3	317.29	318.00	16.02	16.20
5800-4	191.85	181.00	28.78	26.30

Based on results from figure 27 and 28, as well as the failure loads presented in table 12, it appears that the present modeling techniques are sufficiently robust to undertake the current research work investigating combined loading response of I-shaped steel cross-sections bent about the minor-axis in the presence of axial compressive loading.

4.0 I-SHAPED BEAMS UNDER MINOR AXIS BENDING

4.1 PARAMETRIC STUDY

Rotation capacity for wide-flange beams under major axis bending is studied by various researchers. Kemp (1985) examined the ratio of $b_f / t_f, d / t_w, L / r_y, L / t_f$ and found their influences on plastic flexural ductility or rotation capacity of wide flange beams. He also reported that strain hardening properties of the steel is an important factor in affecting the observed flexural ductility. Based on the studies of Roik and Kuhlman (1987), the L / b_f ratio was also found to be an important parameter in determining the rotation capacity. However, it is pointed out that in the case of major axis flexure, the occurrence of lateral-torsional buckling is an important factor in the manifestation of overall beam rotation capacity (a situation consistent with the observed sensitivity on L / b_f) . This is not the case for an I-beam in minor axis bending since the cross-section cannot experience this overall mode of buckling.

The present parametric investigation considers the variation of five physical quantities: cross-sectional aspect ratio (B_f / d) unbraced length-to-cross-sectional depth ratio (L_b / b_f) ; web slenderness ratio, (h / t_w) flange slenderness ratio, $(B_f / 2t_f)$, and steel yield strength. The individual parameters are varied within the context of five groupings of a series of given quantities as defined in table 13.

Parametric studies are constructed for each different h/t_w ratio. For each h/t_w ratio, L_b/b_f ratio is varied from two to nine. Also B_f/d is varied from 0.4 to 0.9 for each L_b/b_f ratio. When arriving at individual plate slenderness limits for compact flange response, the ratio $B_f/2t_f$ is varied for a fixed combination of the other four parameters until compact response is achieved. A schematic depiction of this approach can be seen in figure 29. For each h/t_w group there will be at least 96 finite element model runs.

Table 13 Parametric Study Naming Convention

	h/t_w=60	h/t_w=90	h/t_w=120
f_y=50	Group 1	Group 2	Group 3
f_y=60	Group 4	NA	NA
f_y=70	Group 5	NA	NA

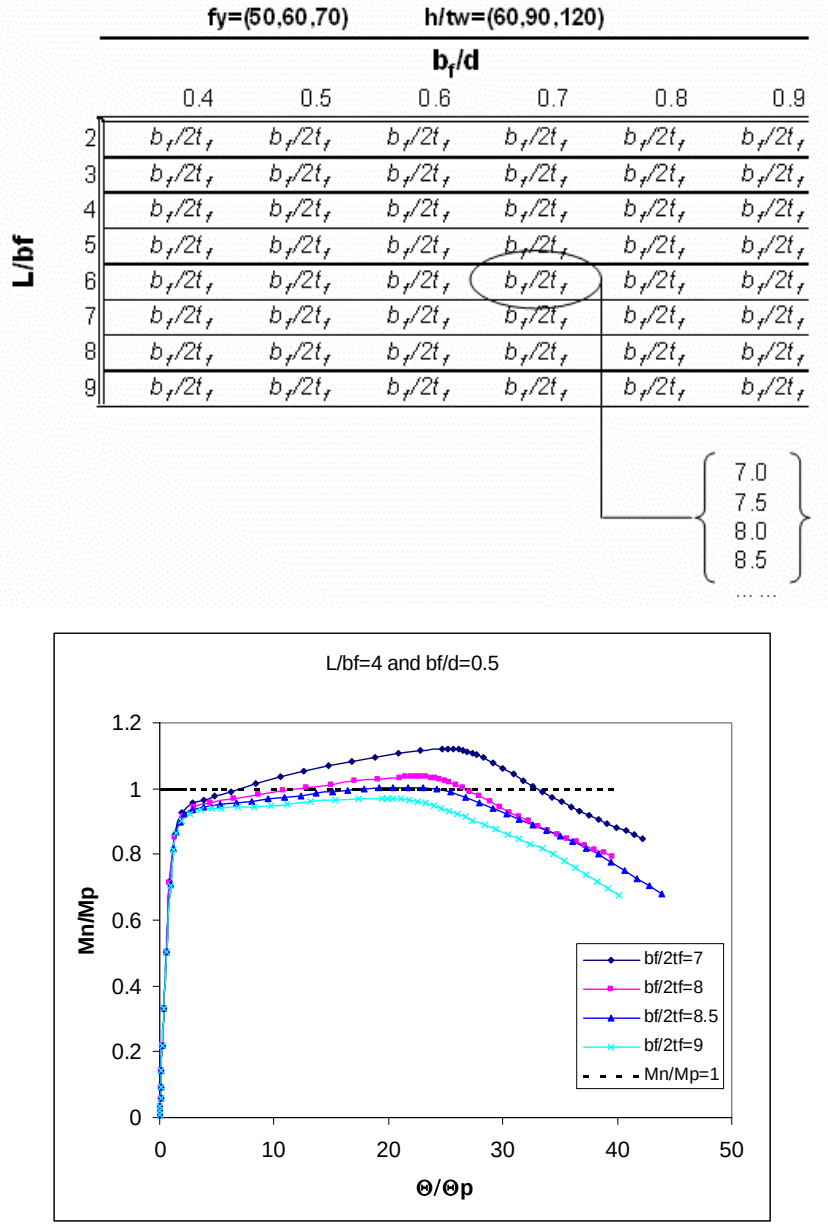

Figure 29 Depiction of Approach Taken in Arriving at compactness Results (note: b_f refers to the complete flange width in this figure)

In order to see the effects of material strength 50 ksi, 60 ksi and 70 ksi steel are used in the parametric study. The true stress and logarithmic plastic strain values for these steels are given in table 14.

Table 14 True stress and logarithmic strain values for parametric study models

50 ksi σ_{true}	50 ksi ε_{ln}^{pl}	60 ksi σ_{true}	60 ksi ε_{ln}^{pl}	70 ksi σ_{true}	70 ksi ε_{ln}^{pl}
50	0	60	0	70	0
51.345	0.0092	61.345	0.0092	81.345	0.0092
75	0.0557	78	0.0557	88	0.0557
80	0.09	89	0.09	99	0.09

4.2 GENERAL BEHAVIOR

As expected, the results showed no evidence of lateral torsional buckling. The only instability phenomenon was the local buckling of compression portion of the flanges. A typical deflected shape, with von-Mises stresses, can be seen in figure 30.

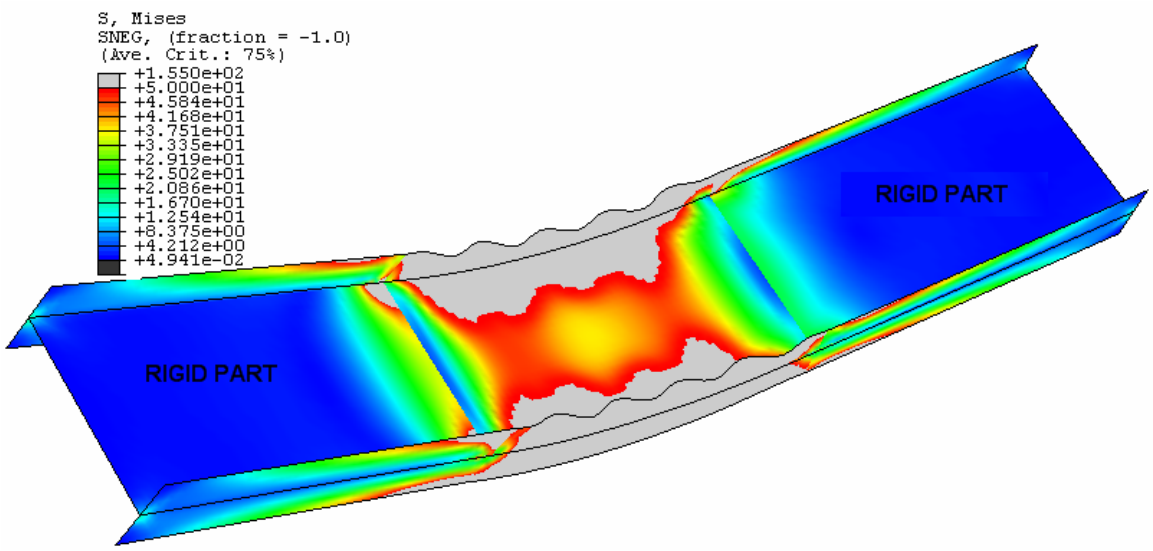

Figure 30 Typical deflected shape and stress distribution

When a given beam reaches its plastic moment capacity, flanges both in the compression and tension regions (i.e. above and below the neutral axis) are yielded. However, for some cases the web did not yield, or just started to yield, as the section reached its plastic moment capacity. It is not surprising that the web failed to yield in most instances since itsw location corresponds to the theoretical neutral axis position of the cross-section. The stress distribution for $L/B_f=2$ of group 2 is given in figure 31. For each B_f/d ratio, there are two plots which represent the state of stress at incipient plastic moment and at the attainment of ultimate moment. The numbers under each figure show the increment number, and the lower number is for the state of plastic moment. For each finite element model shown below, the left figure is at M_p and the right figure is at M_u.

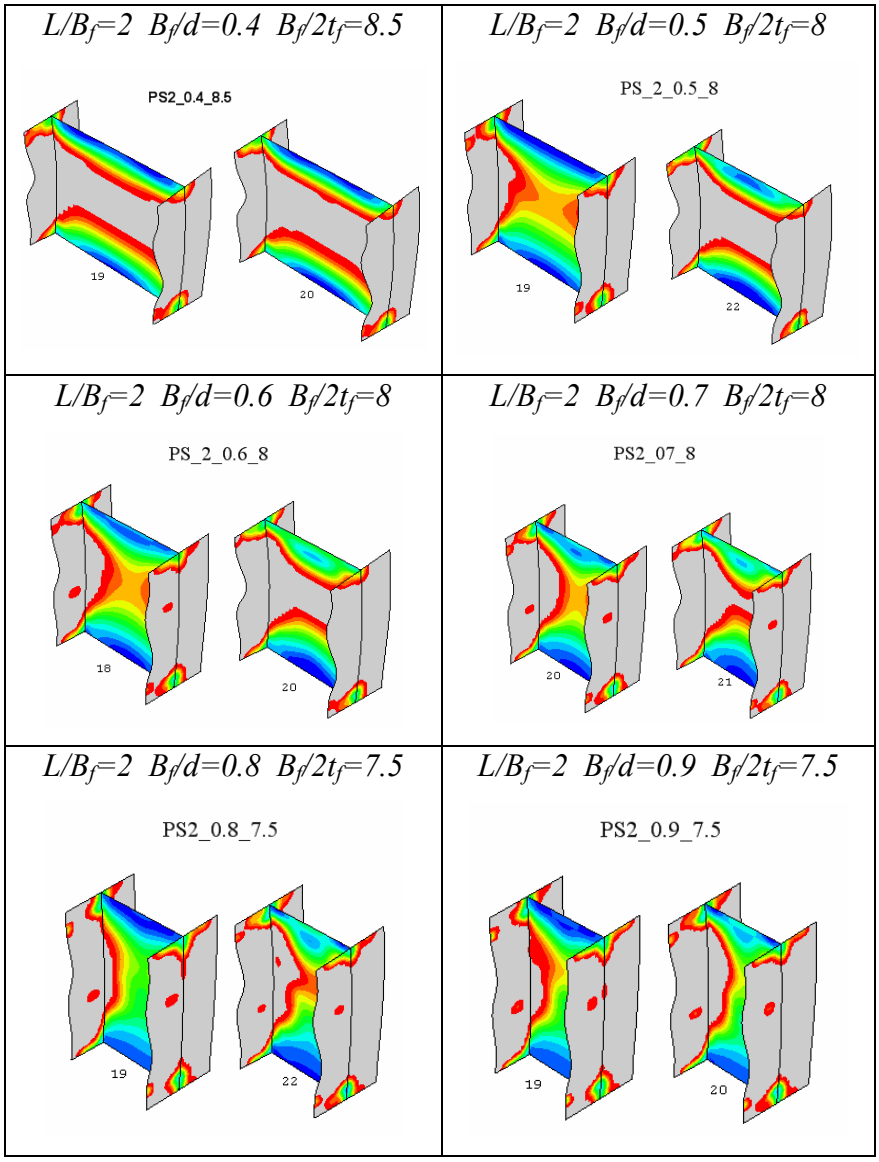

Figure 31 von Mises stress distribution for $L/B_f = 2$ at M_p and at M_u

In order to see the affect of L/B_f in web yielding behavior, same plots are given for $L/B_f = 9$ of group 2 in figure 32.

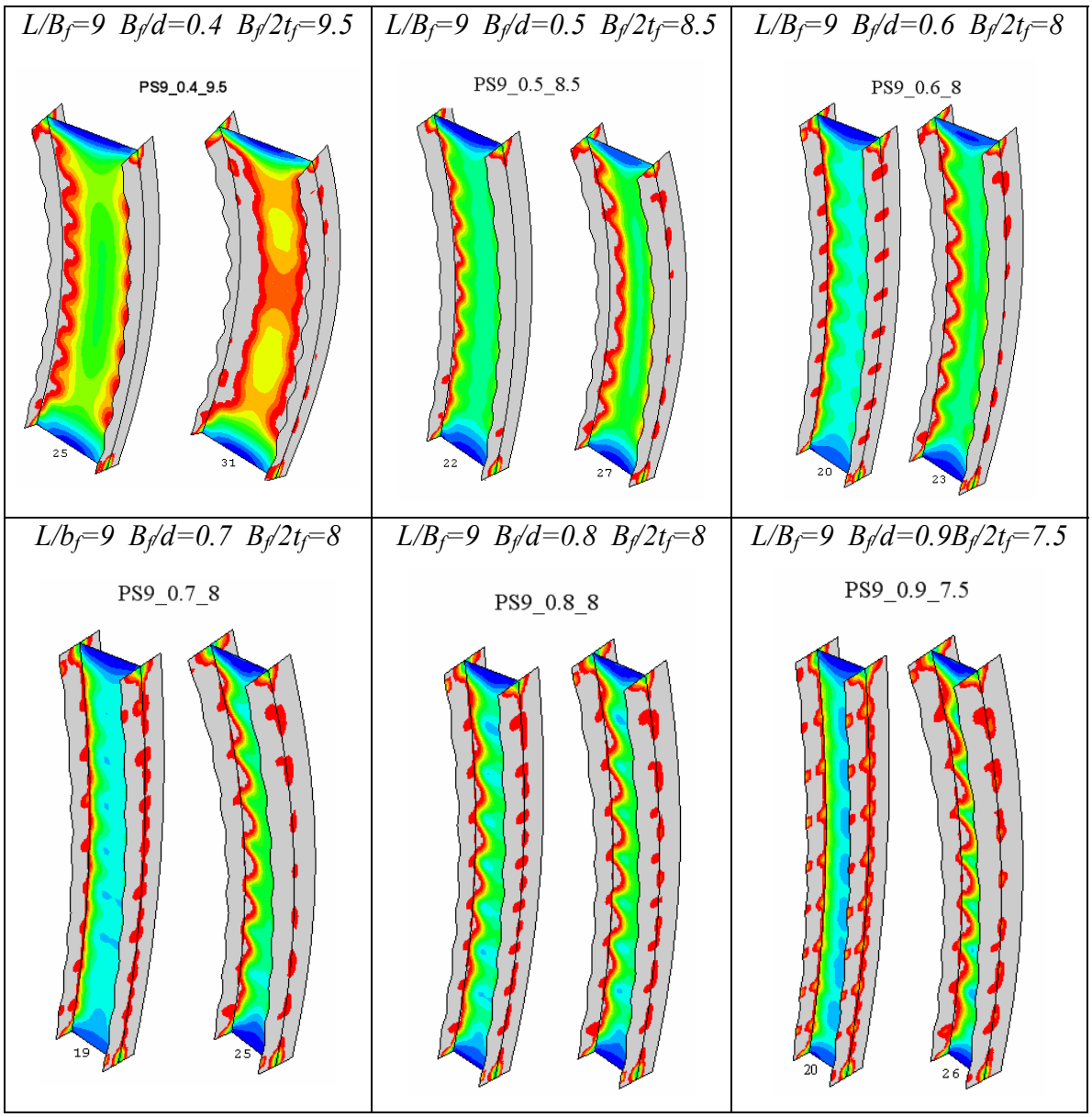

Figure 32 von Mises stress distribution for $L/B_f = 9$ at M_p and at M_u

From figure 31 and figure 32 it can be said that for higher B_f/d ratio there is a limited amount of web yielding at plastic moment state. Also as the L/b_f ratio gets higher the tendency for web yielding to occur at M_p decreases.

4.3 MOMENT ROTATION CURVES

Moment rotation curves for each parametric combination displayed a significant sensitivity related to when there was rotation capacity to be measured and when there was none at all. For example, this can be seen in moment rotation curve for $L/B_f=4$, $B_f/d=0.5$ and $h/t_w=90$ (group 2) (see figure 29). For $B_f/2t_f=8.5$ the rotation capacity is 24.24 which is much greater than three: the minimum rotation capacity mentioned in AISC (1999) manual. However for $B_f/2t_f=9$ there is no rotation capacity at all. The delineation between small finite rotation capacity values and very large rotation capacities is referred to as the critical rotation capacity herein. It has been found that the critical moment rotation values vary from 32.71 to 5.34; sometimes slight changes in slenderness yield enormous improvements in structural ductility and other times such changes result in only small, incremental improvements.

More than 40 discrete parametric data points are obtained from an analysis space of more than 480 individual runs. The 40 discrete parametric points for the flange slenderness values where the critical rotation capacities are found are presented in tables 15,16,17,18, and 19.

The corresponding critical rotation capacities, calculated at these parametric points, are tabulated in tables 20,21,22,23 and 24. In addition, for the group 2 parametric points, some representative trend lines are plotted in figure 33. In figures 34 and 35 moment rotation curves for the case of $L/B_f=2$ and $L/B_f=9$, from group 2, is presented.

Table 15 Critical $B_f/2t_f$ ratio values for Group 1

f_y=50 h/t_w=60

L/B_f	**B_f/d**					
	0.4	0.5	0.6	0.7	0.8	0.9
2	*9.5*	*8.5*	*8.5*	*8*	*8*	*8*
3	*9.5*	*8.5*	*8.5*	*8*	*8*	*8*
4	*10*	*9*	*8.5*	*8.5*	*8*	*8*
5	*na*	*na*	*9*	*8.5*	*8*	*8*
6	*11.5*	*10*	*9*	*8.5*	*8.5*	*8.5*
7	*na*	*10*	*9*	*9*	*8.5*	*8.5*
8	*na*	*10*	*9.5*	*9*	*8.5*	*8.5*
9	*na*	*10.5*	*9.5*	*9*	*8.5*	*8.5*

Table 16 Critical $B_f/2t_f$ ratio values for Group 2

f_y=50 h/t_w=90

L/B_f	**B_f/d**					
	0.4	0.5	0.6	0.7	0.8	0.9
2	*8.5*	*8*	*8*	*8*	*7.5*	*7.5*
3	*8.5*	*8*	*8*	*8*	*7.5*	*7.5*
4	*9*	*8.5*	*8*	*8*	*7.5*	*7.5*
5	*9*	*8.5*	*8*	*8*	*8*	*7.5*
6	*9*	*8.5*	*8*	*8*	*8*	*7.5*
7	*9*	*8.5*	*8*	*8*	*8*	*7.5*
8	*9.5*	*8.5*	*8*	*8*	*8*	*7.5*
9	*9.5*	*8.5*	*8*	*8*	*8*	*7.5*

Table 17 Critical $B_f/2t_f$ ratio values for Group 3

	f_y=50 h/t_w=120					
	B_f/d					
L/B_f	0.4	0.5	0.6	0.7	0.8	0.9
2	*8.5*	*8*	*8*	*7.5*	*7*	*6.5*
3	*na*	*8*	*na*	*7.5*	*na*	*6.5*
4	*8.5*	*8*	*8*	*7.5*	*7*	*6.5*
5	*8.5*	*8*	*8*	*7.5*	*7*	*7*
6	*8.5*	*8*	*8*	*na*	*7*	*7*
7	*8.5*	*8*	*8*	*8*	*7*	*7*
8	*8.5*	*8*	*8*	*8*	*na*	*Na*
9	*8.5*	*8.5*	*8*	*8*	*7.5*	*7*

Table 18 Critical $B_f/2t_f$ ratio values for Group 4

	f_y=60 h/t_w=60					
	B_f/d					
L/B_f	0.4	0.5	0.6	0.7	0.8	0.9
2	*8*	*7.5*	*7.5*	*7.5*	*7.5*	*7.5*
3	*8*	*7.5*	*7.5*	*7.5*	*7.5*	*7.5*
4	*8.5*	*8*	*7.5*	*7.5*	*7.5*	*7.5*
5	*9*	*8*	*8*	*7.5*	*7.5*	*7.5*
6	*10*	*8.5*	*8*	*8*	*7.5*	*7.5*
7	*10*	*9*	*8.5*	*8*	*7.5*	*7.5*
8	*na*	*9*	*8.5*	*8*	*8*	*7.5*
9	*na*	*9*	*8.5*	*8.5*	*8*	*8*

Table 19 Critical $B_f/2t_f$ ratio values for Group 5

f_y=70 h/t_w=60

L/B_f	**B_f/d** 0.4	0.5	0.6	0.7	0.8	0.9
2	*7.5*	*7*	*7*	*7*	*7*	*7*
3	*7.5*	*7*	*7*	*7*	*7*	*7*
4	*7.5*	*7.5*	*7*	*7*	*7*	*7*
5	*8*	*7.5*	*7.5*	*7*	*7*	*7*
6	*8.5*	*8*	*7.5*	*7.5*	*7*	*7*
7	*9*	*8*	*8*	*7.5*	*7.5*	*7.5*
8	*9*	*8.5*	*8*	*7.5*	*7.5*	*7.5*
9	*9*	*na*	*8*	*7.5*	*7.5*	*7.5*

Table 20 Critical rotation capacity values for Group 1

f_y=50 h/t_w=60

L/B_f	**B_f/d** 0.4	0.5	0.6	0.7	0.8	0.9
2	*29.78*	*28.16*	*20.92*	*19.93*	*19.37*	*15.84*
3	*25.61*	*24.58*	*18.36*	*18.13*	*16.67*	*13.34*
4	*32.71*	*21.99*	*19.61*	*15.92*	*15.85*	*14.58*
5	*na*	*na*	*16.83*	*16.21*	*16.19*	*14.45*
6	*30.15*	*20.67*	*18.92*	*17.38*	*14.39*	*11.94*
7	*na*	*21.69*	*18.46*	*13.66*	*13.42*	*11.15*
8	*na*	*21.71*	*14.20*	*13.10*	*12.24*	*10.93*
9	*na*	*18.76*	*15.99*	*12.72*	*11.32*	*9.87*

Table 21 Critical rotation capacity values for Group 2

	f_y=50 h/t_w=90					
	B_f/d					
L/B_f	0.4	0.5	0.6	0.7	0.8	0.9
2	*23.64*	*20.69*	*15.90*	*10.72*	*13.20*	*10.05*
3	*24.52*	*21.91*	*16.25*	*12.73*	*13.98*	*11.24*
4	*21.98*	*19.37*	*18.16*	*15.87*	*15.55*	*12.33*
5	*20.12*	*16.27*	*16.67*	*13.93*	*12.08*	*13.06*
6	*18.49*	*13.54*	*13.97*	*12.09*	*10.67*	*12.71*
7	*17.53*	*14.04*	*12.78*	*10.13*	*9.39*	*10.71*
8	*15.29*	*11.11*	*10.47*	*8.75*	*7.60*	*9.22*
9	*16.10*	*11.38*	*9.38*	*8.59*	*7.34*	*8.22*

Table 22 Critical rotation capacity values for Group 3

	f_y=50 h/t_w=120					
	B_f/d					
L/B_f	0.4	0.5	0.6	0.7	0.8	0.9
2	*18.49*	*16.48*	*10.28*	*9.41*	*9.61*	*9.09*
3	*na*	*13.08*	*na*	*9.03*	*na*	*8.68*
4	*15.35*	*14.25*	*11.33*	*10.03*	*7.34*	*8.32*
5	*15.53*	*13.93*	*10.69*	*10.21*	*8.44*	*5.34*
6	*14.11*	*13.65*	*10.67*	*na*	*7.34*	*5.97*
7	*12.51*	*11.75*	*10.36*	*7.41*	*8.52*	*5.86*
8	*11.03*	*10.32*	*9.44*	*8.11*	*na*	*na*
9	*10.38*	*8.74*	*8.57*	*7.35*	*7.70*	*6.08*

Table 23 Critical rotation capacity values for Group 4

f_y=60 h/t_w=60

L/B_f	B_f/d 0.4	0.5	0.6	0.7	0.8	0.9
2	*21.06*	*22.56*	*18.65*	*15.56*	*13.11*	*9.68*
3	*19.94*	*17.96*	*14.70*	*13.17*	*11.58*	*9.10*
4	*19.86*	*16.20*	*15.97*	*13.89*	*12.83*	*11.32*
5	*19.19*	*15.74*	*12.99*	*13.80*	*12.09*	*10.75*
6	*19.22*	*14.94*	*12.49*	*11.39*	*12.45*	*11.17*
7	*22.73*	*14.19*	*12.43*	*11.94*	*11.91*	*10.47*
8	*na*	*15.46*	*12.84*	*11.34*	*9.53*	*9.80*
9	*na*	*15.37*	*12.49*	*9.32*	*9.06*	*7.55*

Table 24 Critical rotation capacity values for Group 5

f_y=70 h/t_w=60

L/B_f	B_f/d 0.4	0.5	0.6	0.7	0.8	0.9
2	*15.38*	*16.82*	*12.91*	*11.02*	*9.86*	*9.19*
3	*15.09*	*13.53*	*11.92*	*10.78*	*9.89*	*8.26*
4	*18.57*	*13.20*	*13.72*	*11.48*	*10.34*	*9.48*
5	*14.94*	*11.69*	*9.90*	*11.57*	*10.46*	*9.68*
6	*14.48*	*12.22*	*10.67*	*9.45*	*10.11*	*9.34*
7	*15.42*	*13.66*	*11.16*	*9.60*	*8.53*	*7.28*
8	*17.27*	*13.20*	*10.65*	*9.52*	*8.21*	*7.08*
9	*17.79*	*na*	*9.75*	*9.12*	*7.72*	*6.68*

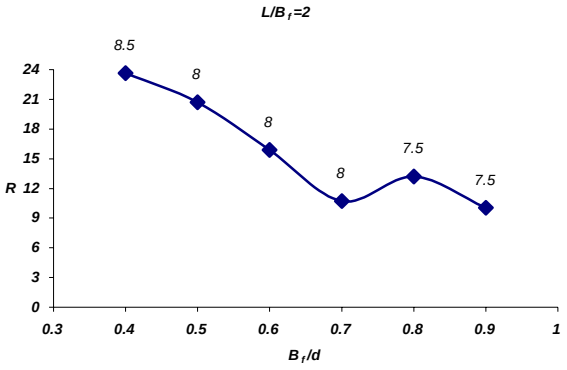
L/B f =2
8.5
8
8
8
7.5
7.5
R
24
21
18
15
12
9
6
3
0
0.3
0.4
0.5
0.6
0.7
0.8
0.9
1
B f /d

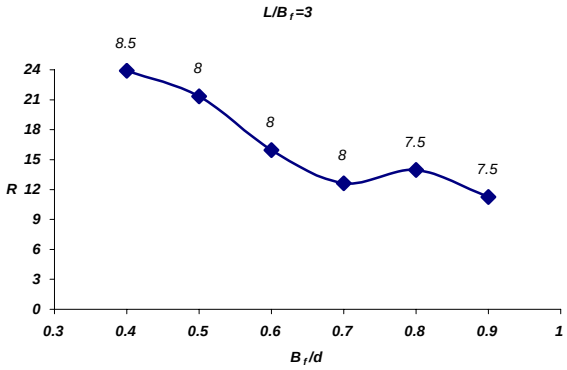
L/B f =3
8.5
8
8
8
7.5
7.5
R
24
21
18
15
12
9
6
3
0
0.3
0.4
0.5
0.6
0.7
0.8
0.9
1
B f /d

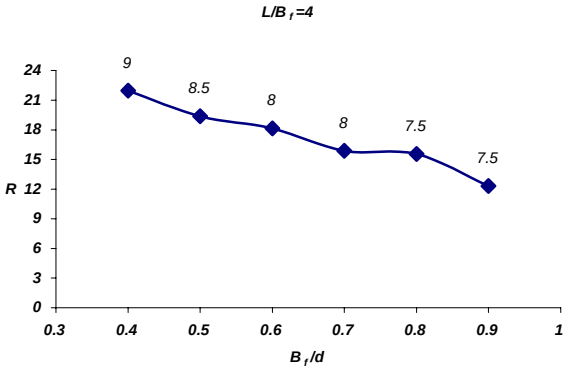
L/B f =4
9
8.5
8
8
7.5
7.5
R
24
21
18
15
12
9
6
3
0
0.3
0.4
0.5
0.6
0.7
0.8
0.9
1
B f /d

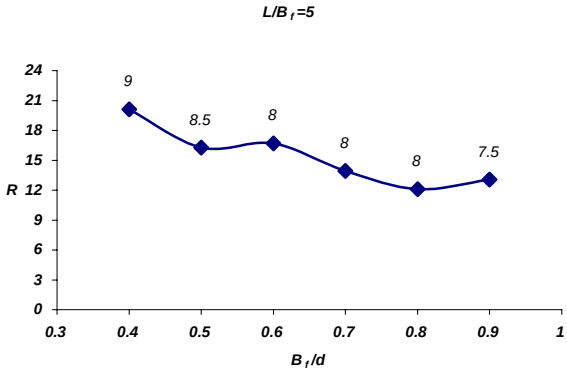
L/B f =5
9
8.5
8
8
8
7.5
R
24
21
18
15
12
9
6
3
0
0.3
0.4
0.5
0.6
0.7
0.8
0.9
1
B f /d

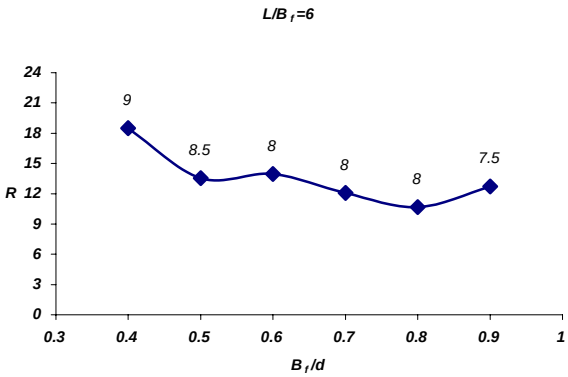
L/B f =6
9
8.5
8
8
8
7.5
R
24
21
18
15
12
9
6
3
0
0.3
0.4
0.5
0.6
0.7
0.8
0.9
1
B f /d

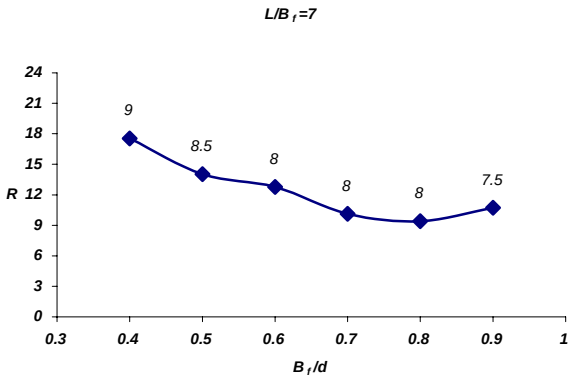
L/B f =7
9
8.5
8
8
8
7.5
R
24
21
18
15
12
9
6
3
0
0.3
0.4
0.5
0.6
0.7
0.8
0.9
1
B f /d

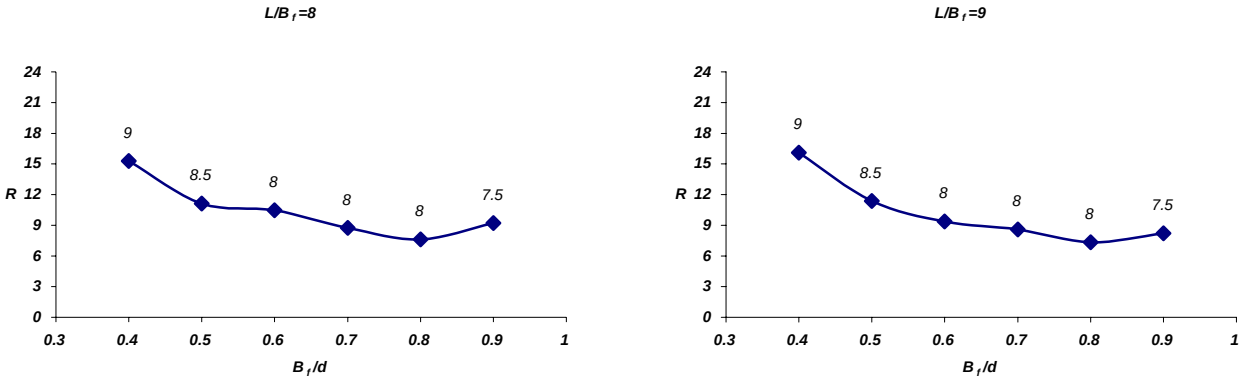

Figure 33 $B_f/2t_f$ values for varying B_f/d values for group 2

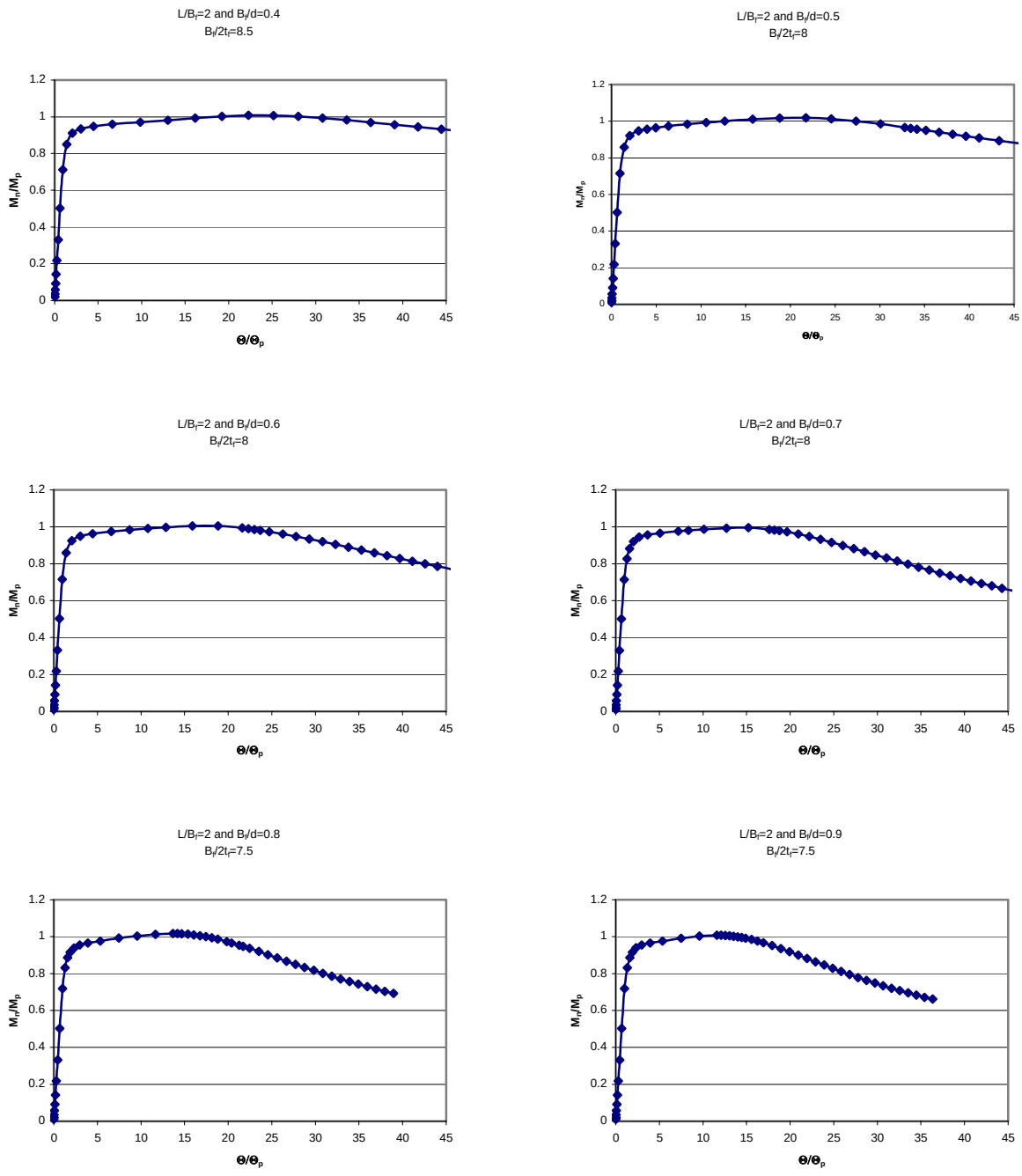

Figure 34 Moment-rotation curves for $L/B_f=2$ of group 2

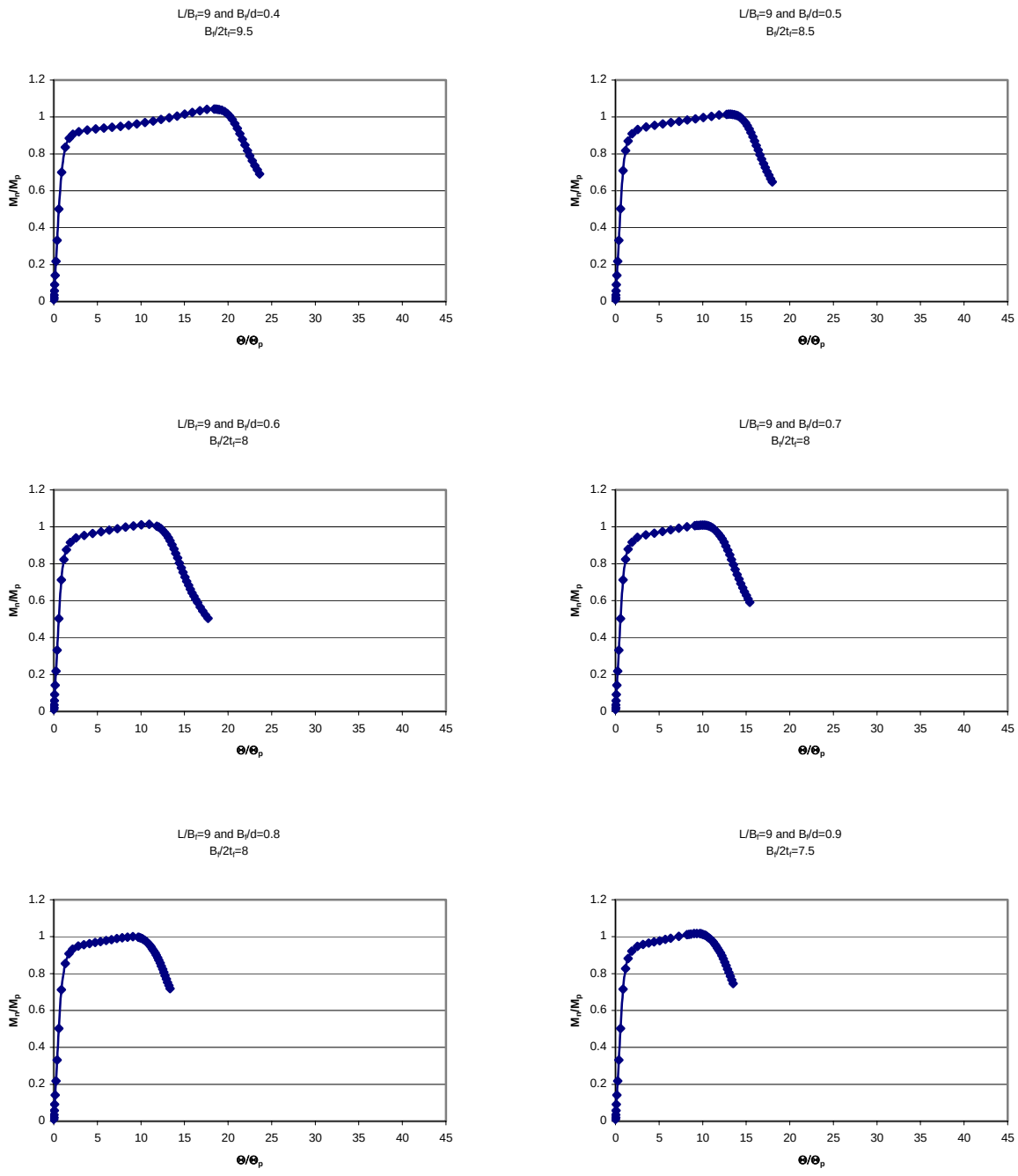

Figure 35 Moment-rotation curves for *L/B*$_f$*=9* of group 2

4.4 DISCUSSION OF RESULTS

As the parameters of the study are varied, certain trends in behavior become clear. The current section endeavors to describe the observed differences as well as to describe possible mechanisms that may explain the observed response and thus lend additional insight into the problem of minor axis compactness.

One discussion point that conspicuously presents itself is related to the applicability of exiting specification recommendations, for major axis flexural flange compactness, to the case of minor axis flexure. While it is commonly believed that the foregoing practice is conservative (based on so-called "common sense"), this may not actually be the case. Based on the results presented herein for the three steel grades considered, it appears to be un-conservative to apply the major axis provisions to the case of minor axis flexure. For the case of steel with a minimum specified yield stress of 345MPa, the US specification requires that for compactness, the ratio $B_f / 2t_f$ may not exceed 9.2. However, the results presented herein clearly indicate that the maximum permissible plate ratio $B_f / 2t_f$ may be as low as 6.5 (depending on web slenderness ratio, h / t_w, and cross-sectional aspect ratio, B_f / d). Similar results hold for the cases with steel having yield stresses of 414MPa and 483MPa.

4.4.1 Effect of steel yield strength on flange compactness limit

Based on the compactness results gleaned from the finite element modeling results obtained using steel possessing yield strengths of 345MPa, 414MPa, and 483MPa, certain trends in cross-sectional compactness arise. As the yield strength increases from 345MPa to 483MPa, the maximum permissible cross-sectional plate slenderness ratio decreases by as much as 25%.

Meaning that as steel strength increases, a significantly more strict compactness limit must be enforced, as compared with cross-sections made from lower strength steels. It is noted that this sensitivity to yield stress is somewhat greater than what the US specification predicts (15% decrease in maximum permissible limiting plate slenderness resulting from the noted 138MPa steel strength increase – all other parameters held constant). However, it is noted that in cases where the cross-section possesses a large cross-sectional aspect ratio, B_f / d, (approximately 0.9) the diminution of the maximum permissible flange slenderness resulting from the increasing steel strength is much more consistent with current specification predictions; although overall magnitude of the slenderness limit predicted by the specifications is still un-conservative.

4.4.2 Effect of web slenderness on flange compactness limit

A clear parameter influencing the maximum permissible flange slenderness limit is web slenderness, h / t_w. Using the web compactness limit from the US specification (in conjunction with a steel yield strength of 345MPa), for the case of major axis flexure, results in a web slenderness limit of 90. As part of the current research effort, a variation of +/- 30% (i.e. h / t_w = 60, 90, and 120) is considered in the following discussion. As web slenderness, h / t_w, increases, the maximum permissible flange slenderness required for compact behavior decreases (in some cases by as much as 25% as h / t_w increases by 100%).

4.4.3 Effect of Cross-sectional aspect ratio on flange compactness limit

It is interesting to note that the ratio of cross-sectional flange width to cross-sectional depth ratio, B_f / d (aspect ration), has a pronounced influence on the limiting flange slenderness required for

compact response. In general, as the aspect ratio increases (from 0.4 to 0.9), decreases as large as 25% are observed to occur in the limiting flange slenderness. This would indicate that, as an isolated parameter, cross-sectional aspect ratio is at least as important as web slenderness in affecting limiting flange slenderness requirements for compact response in minor axis flexure. However, it is pointed out that as the span-to-depth ratio approaches 7, the fluctuation in flange compactness as a function of cross-sectional aspect ratio all but disappears.

4.4.4 Effect of span-to-flange width ratio on flange compactness limit

In the present research, a series of different span-to-depth ratios, $L_b / B_{f,}$ are considered; ranging from 2 to 9. Based on the author's experience in modeling, beams whose span-to-flange width ratio is greater than or equal to 7 tend to behave well; vis-à-vis Bernoulli-Euler beam theory. Those beams whose span-to-flange width ratios are less than 7 tend to exhibit significant effects of internal shear. This fact is pointed out since it is noted that as the span-to-flange width ratio increases, in the test population considered in the current research, increases in concomitant flange slenderness limits accompany this growth; increasing by as much as 17% in the most extreme instance (all other parameters held constant).

4.4.5 Effect of web-restraint on flange compactness limit

Based on the foregoing, it seems that the major factors influencing minor axis flange compactness are web slenderness and cross-sectional aspect ratio. However, a closer examination of the results hints at a mechanical basis for this: the effect of web-restraint on the inelastic flange buckling. In arriving at this conjecture, it is observed that at low span-to-flange

width ratios, the reduction in the flange compactness limit, as a function of cross-sectional aspect ratio, is greatest. In addition, at high span-to-flange width ratios, the flange slenderness limit for compactness is quite steady across different cross-sectional aspect ratios, and this steadiness occurs in conjunction with the largest observed permissible values for the flange slenderness.

One may use the foregoing, in conjunction with the observation that flange compactness limits are somewhat insensitive to changes in span-to-flange width ratio, to shed light on an obvious limitation in the modeling: the presence of rigid ends in the model. It might have been surmised that the rigid ends would provide an artificially high restraint against local buckling and thus improve structural ductility; allowing for more liberal flange compactness limits. Such a restraining effect ought to be most pronounced as the span lengths decrease and the rigid ends subsequently move closer together. In actuality, the opposite trend is observed and the most liberal minor axis flange compactness limits occur at the larger span-to-flange width ratios for the beam in question. So the question remains; if some restraint of the flanges is leading to increases in compactness limits then where is the restraint coming from? The hypothesis is that the restraint is coming from the web. Based on the research results, it is noted that as the web slenderness increases, it is easier for the flange to buckle locally. This may be ascribed to the reduced flexural rigidity in the web as its slenderness is increased. It is further pointed out that this web restraint effect appears to be more pronounced in cases wherein the member in minor axis flexure is permitted to act like a beam (i.e. when span-to-flange width ratios are greater than or equal to 7). At lower span-to-flange width ratios, the effects of shear complicate the observed response and thus make it difficult to find a mechanistic basis for observed differences in flange compactness.

4.4.6 Comparison with Equation 19

The approach taken in deriving equation 19 in section 1.4 is philosophically consistent with what the US Specification (AISC 1999) has done for the case of flange outstands subjected to compression due to major axis flexure. Applying the one third difference between the plate buckling coefficients, that is subsequently added to the lower bound value, produces a plate slenderness limit, for compactness in 345 MPa flanges, of 10.2; a value far in excess of what is observed to be a safe limit from the current finite element modeling results. A more appropriate use of an equation 19 approach might be to preserve the plate buckling coefficient associated with the pinned supported plate edge (0.57) wherein a more reasonable value of 7.9 is arrived at for an appropriate ceiling for a flange slenderness limit, $B_f / 2t_f$, as required for compact cross-sectional response for use in conjunction with 345 MPa steel. Limiting flange slenderness values of 7.3 and 6.7 are also obtained from this approach in the case of steel with yield strengths of 414MPa and 483MPa, respectively. While it is that such an approach may be on the conservative side for the parametric space explored, the method is flawed in a phenomenological sense since it tacitly denies the relevance of edge restraint which has clearly been shown to be of importance to this problem. However, as a simple and easily understood means for prescribing minor axis flange compactness limits, it may be of some use.

5.0 I-SHAPED STEEL CROSS-SECTIONS BENT ABOUT THE MINOR-AXIS IN THE PRESENCE OF AXIAL COMPRESSIVE LOADING

5.1 PARAMETRIC STUDY

The present parametric investigation for interaction equations considers variations in weak-axis slenderness, L_b / r_y; cross-sectional proportions such as: flange slenderness, b_f / t_f, and web slenderness, h / t_w. In the case of weak-axis slenderness, L_b / r_y ratios of 40, 50, and 100 are considered. In all of the sections considered, the webs and flanges are compact (in a strong-axis sense), but the flange of the W12x72 (US customary designation) case considered is very close to the compactness limit prescribed by AISC (1999). A total of three cross-sections taken from AISC Manual (AISC 1999) are used in developing the computer models (table 25). For each cross-section, the weak-axis slenderness ratio, L_b / r_y is changed as mentioned above. The same sinusoidally varying localized imperfection field (that is described earlier) is employed in the parametric study, a peak displacement amplitude equal to $B_f /100$ is adopted, as per the maximum allowable fabrication imperfection permitted by AWS (2000).

Table 25 Cross-sections used in the parametric study

Cross Section	b_f/t_f	h/t_w	b_f/d
W12x72	9.00	22.60	0.98
W12x96	6.80	17.70	0.96
W14x132	7.10	17.70	1.00

Loading for the current parametric study is achieved using the configuration displayed in figure 36. For each cross-section and for the various weak axis slenderness values, L_b / r_y considered, a parameter, α, is changed from 0.005 to 0.8, to achieve the various fractions of moment and axial force; which subsequently grow at the same rate within the given proportionality ratio being considered. For each run P_u (ultimate axial load) and the corresponding M_u (ultimate moment) are plotted to define the interaction curve for the given member. For example for cross-section W12x26 with $L_b / r_y = 40$, α values and corresponding *P* and *M* plots are given in figure 37.

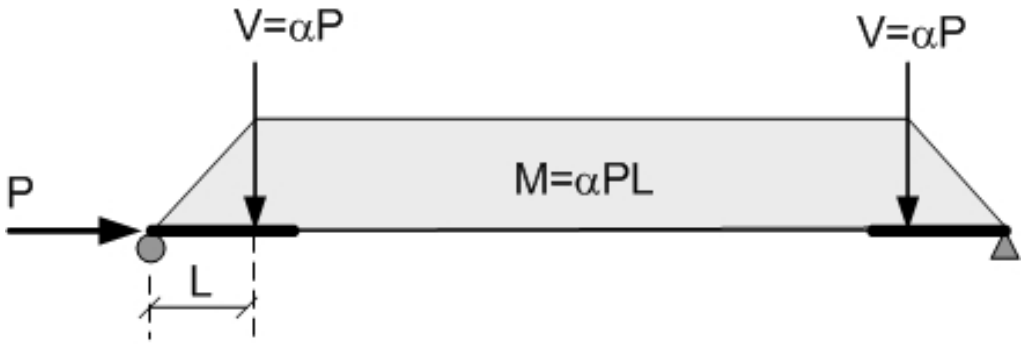

Figure 36 Schematic description of loading for the parametric study.

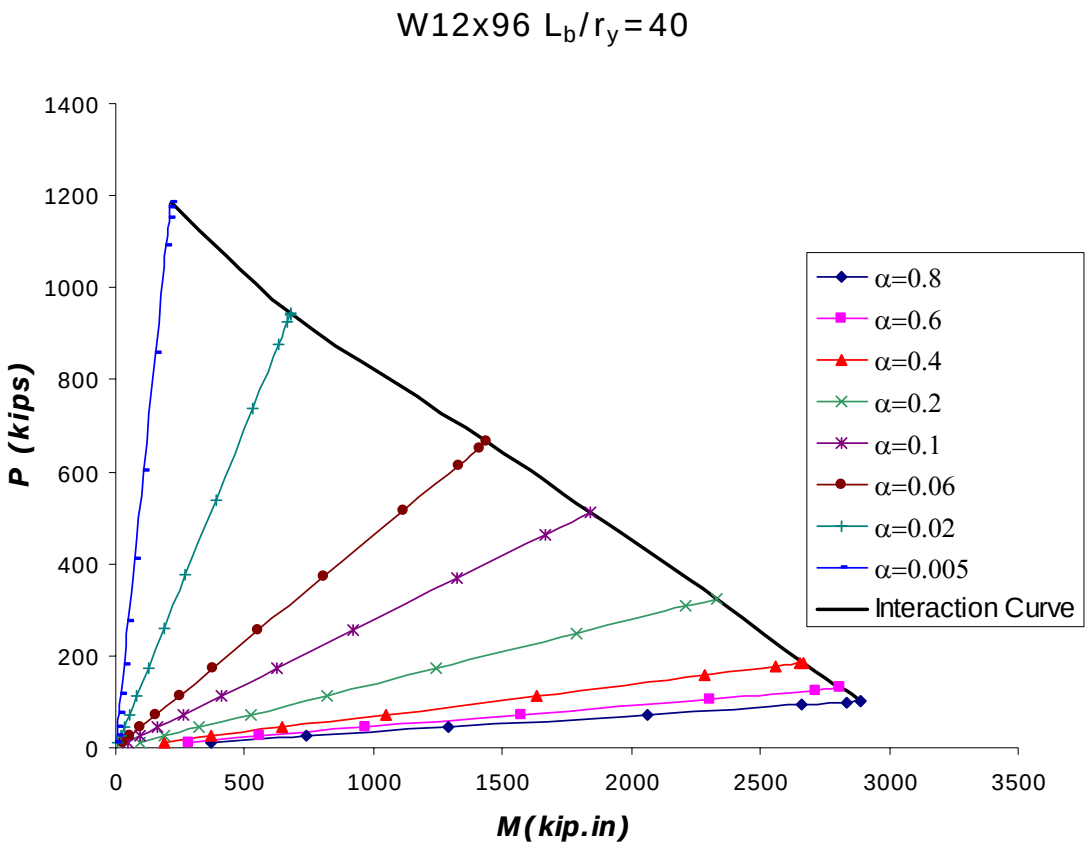

Figure 37 Representative interaction curve for a given cross-section

In order to include the second order effects due to the beam column behavior , additional moment resulting from P_u is calculated as $P_u \times \delta$ where δ is the difference between the midspan deflection and the deflection at the intersection of rigid and flexible beam ($\Delta_2 - \Delta_1$) (figure 38). This additional moment is added to the primary moment observed from FEA.

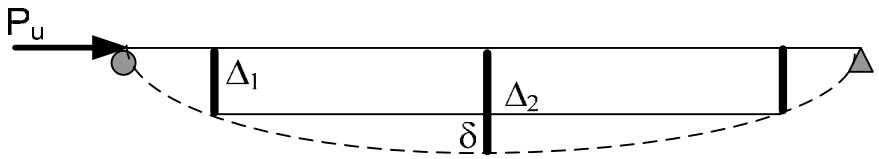

Figure 38 Calculation of additional moment

5.2 GENERAL BEHAVIOR

Formation of local buckles were observed along the flange outstands; the deflected shape of the beam, as obtained from FEA, is presented in figure 39. Increasing the load makes the local buckles at the compression flanges more distinct. The tension flange outstands fail by yielding in tension. As the numerical test progresses, the tension flange straightened from its initial local buckled configuration. See figure 40 and figure 41.

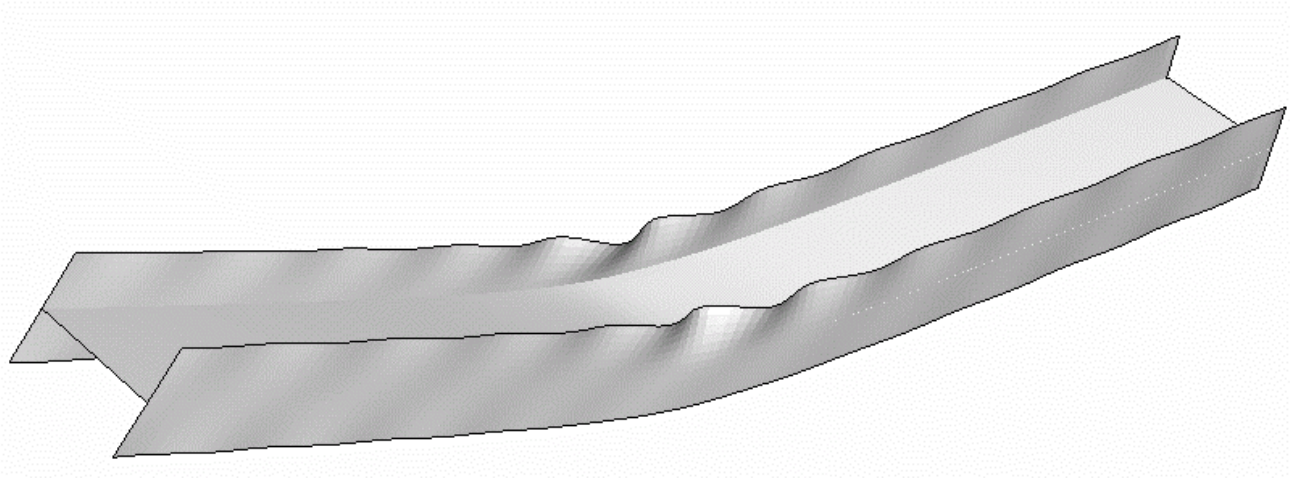

Figure 39 Deflected shape taken from FEM analysis.

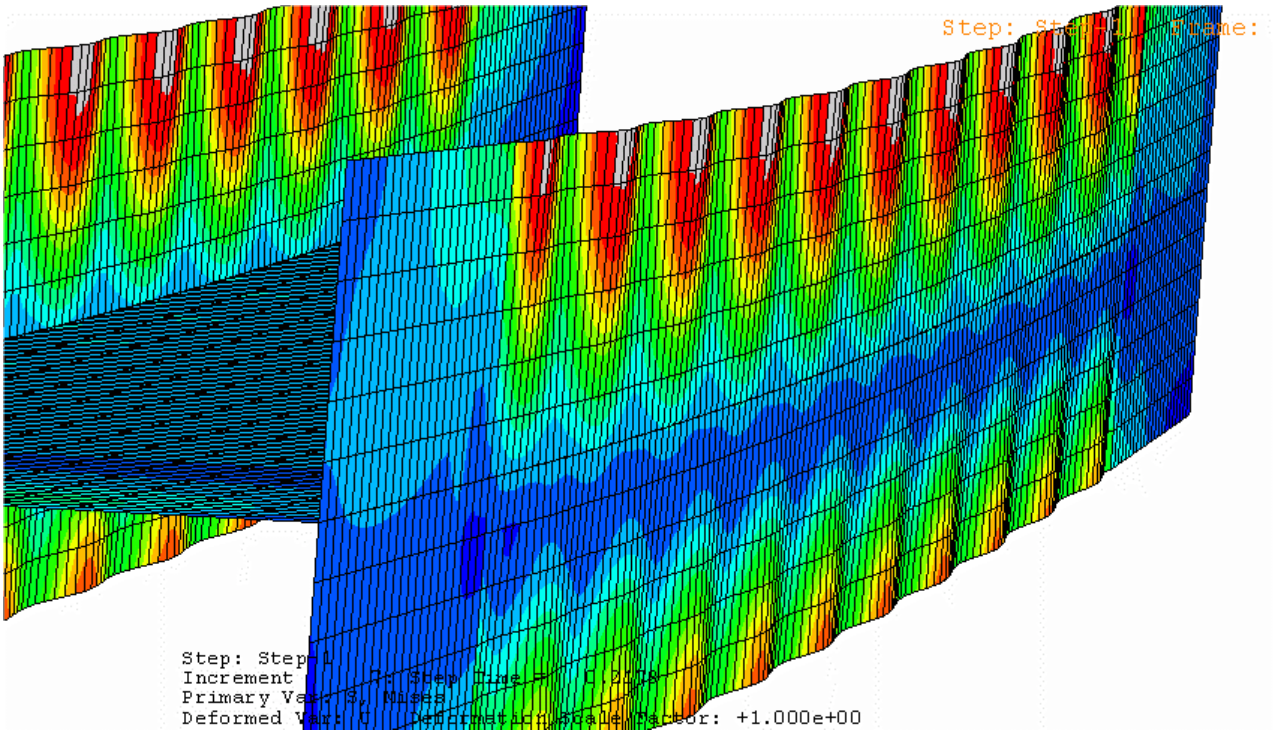

Figure 40 von-Mises stress plot for beam under both minor axis bending and axial force

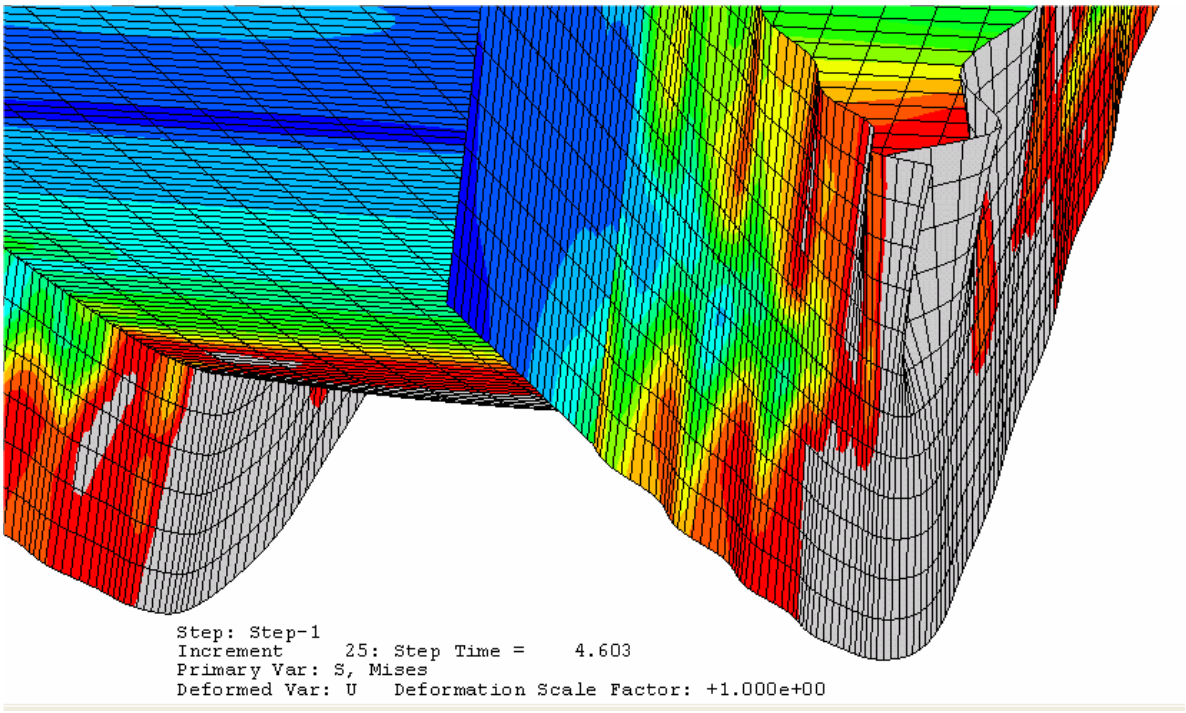

Figure 41 von-Mises stress plot for beam under both minor axis bending and axial force

5.3 THE AISC-LRFD BEAM-COLUMN INTERACTION EQUATIONS.

In LRFD Chapter H, the interaction equation for doubly and singly symmetric members subject to bending and axial force is given by H1-1a and H1-1b as below;

For $\frac{P_u}{\phi P_n} \geq 0.2$

$$\frac{P_u}{\phi P_n} + \frac{8}{9}\left(\frac{M_{ux}}{\phi_b M_{nx}} + \frac{M_{uy}}{\phi_b M_{ny}}\right) \leq 1.0 \qquad (41)$$

For $\frac{P_u}{\phi P_n} < 0.2$

$$\frac{P_u}{2\phi P_n}+\left(\frac{M_{ux}}{\phi_b M_{nx}}+\frac{M_{uy}}{\phi_b M_{ny}}\right)\le 1.0 \tag{42}$$

Wherein, ϕP_n, is the design compression strength for flexural buckling, as calculated according to LRFD section E2.

$$P_n = A_g F_{cr} \quad \phi = 0.85 \tag{43}$$

For $\lambda_c \le 1.5$

$$F_{cr} = \left(0.658^{\lambda_c^2}\right) F_y \tag{44}$$

For $\lambda_c > 1.5$

$$F_{cr} = \left(\frac{0.877}{\lambda_c^2}\right) F_y \tag{45}$$

where the column slenderness parameter, λ_c, is defines as;

$$\lambda_c = \frac{KL}{r\pi}\sqrt{\frac{F_y}{E}} \tag{46}$$

In addition, ϕM_{ny}, the flexural design strength of the beam, is determined by the limit state of yielding according to LRFD (F1-1):

$$M_n = M_p \quad \phi = 0.9 \tag{47}$$

$$M_p = F_y Z_y \le 1.5 \times M_y \quad M_y = F_y S_y \tag{48}$$

And the Elastic Euler buckling load for the y-axis, $P_{e,y} = \frac{\pi^2 EI_y}{L_b^2}$, is calculated and tabulated with the calculated P_n and M_n in table 26.

Table 26 Cross-sectional properties

Cross-section	L_b/r_y	L_b	P_n	$P_{e,y}$	M_n
W12x72	40	121.60	938.52	3774.55	2430.00
	50	152.00	878.75	2415.71	2430.00
	100	304.00	507.82	603.93	2430.00
W12x96	40	123.60	1254.33	5058.53	3330.00
	50	154.50	1174.45	3237.46	3330.00
	100	309.00	678.70	809.37	3330.00
W14x132	40	150.40	1725.82	6933.98	5587.50
	50	188.00	1615.90	4437.75	5587.50
	100	376.00	933.81	1109.44	5587.50

Since the major axis bending is not at issue in this research, M_{ux} is taken zero. In the development of the interaction curves, all the resistance factors are taken as one so as to achieve nominal resistances, or design strengths. The current interaction equation from Chapter H of the LRFD specification (AISC 1999) is developed by solving M_u for a given P_u.

For

$$\frac{P_u}{P_n} \geq 0.2 \qquad M_u = M_n \times \frac{9}{8} \times \left(1 - \frac{P_u}{P_n}\right) \tag{49}$$

For

$$\frac{P_u}{P_n} < 0.2 \qquad M_u = M_n \times \left(1 - \frac{P_u}{2P_n}\right) \tag{50}$$

5.4 DISCUSSION OF RESULTS

More than 120 discrete parametric data points are obtained from the analysis space. Interaction curves are gleaned from the data sets associated with the nonlinear finite element modeling of the three cross-sections identified in table 25; for each of the three unbraced lengths $L_b / r_y = 40$, 50 and 100. Figures 42 through 50 display the results of this effort, as well as the accompanying predictions associated with the provisions contained in Chapter H of the AISC specification (1999).

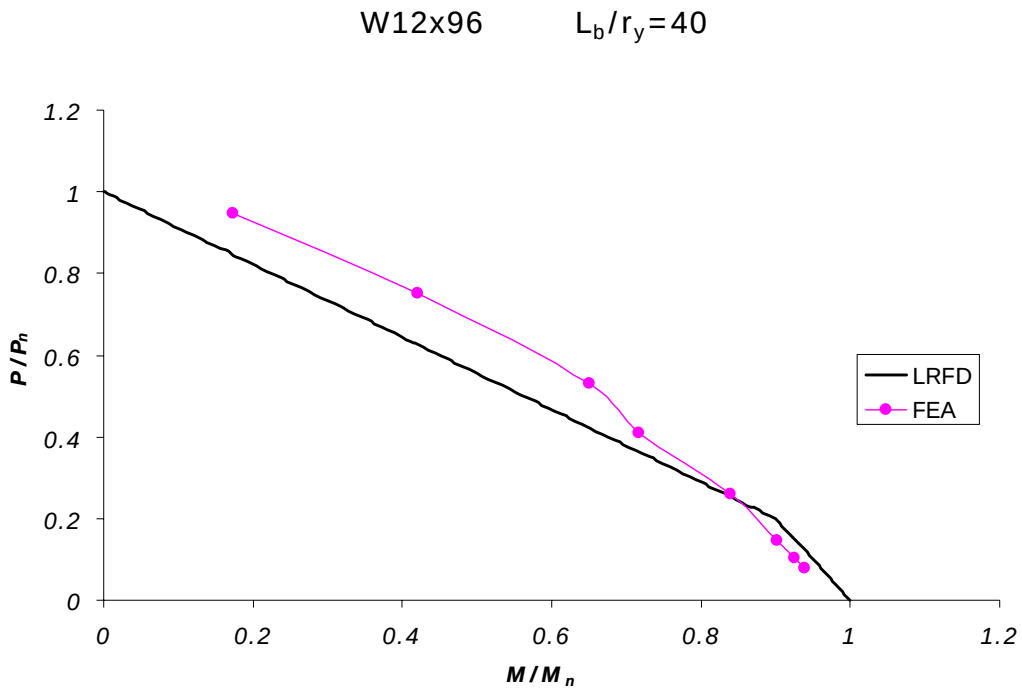

Figure 42 Comparison of FE interaction results with AISC

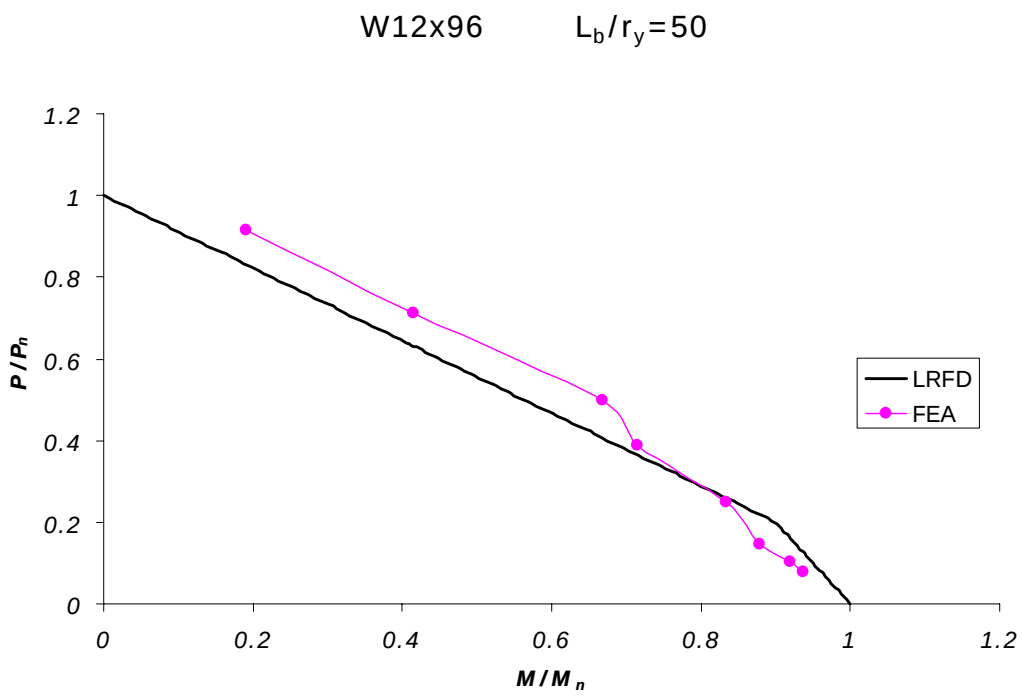

Figure 43 Comparison of FE interaction results with AISC

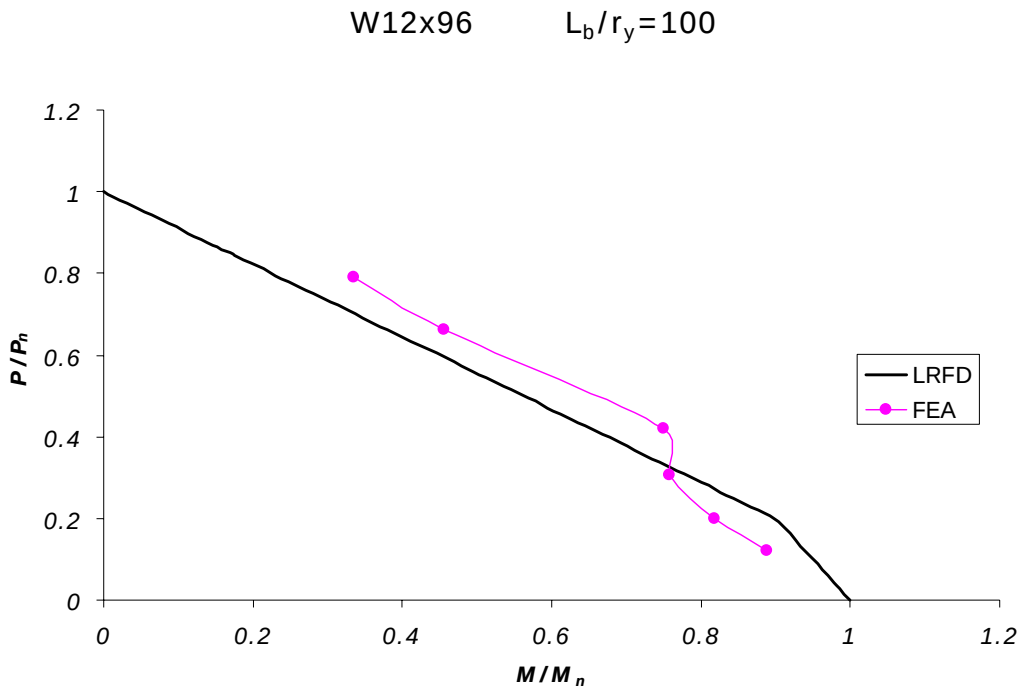

Figure 44 Comparison of FE interaction results with AISC

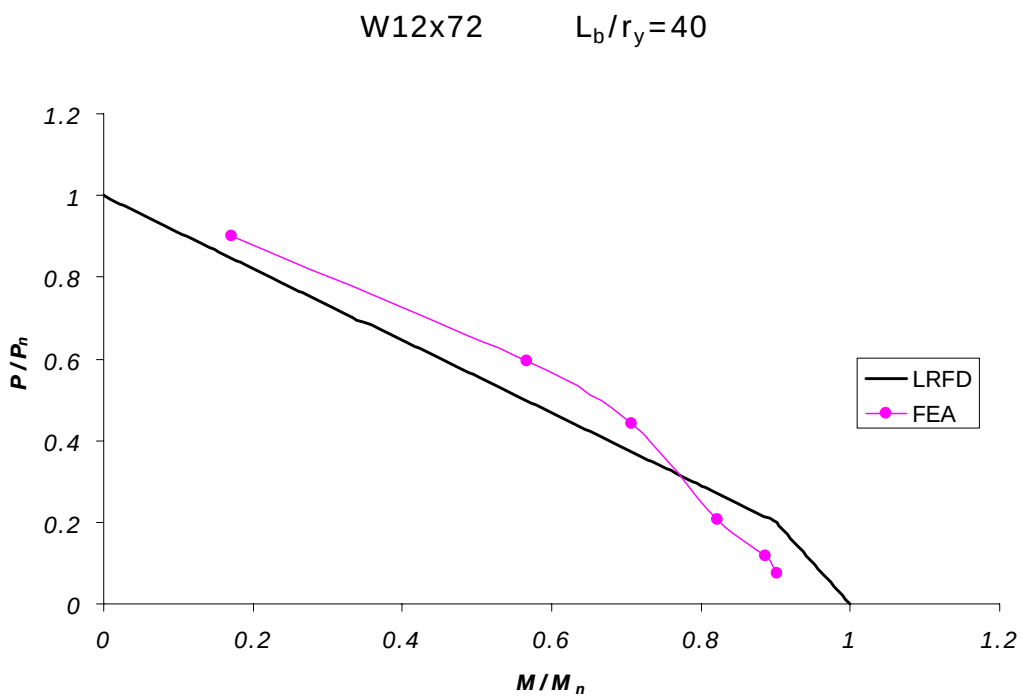

Figure 45 Comparison of FE interaction results with AISC

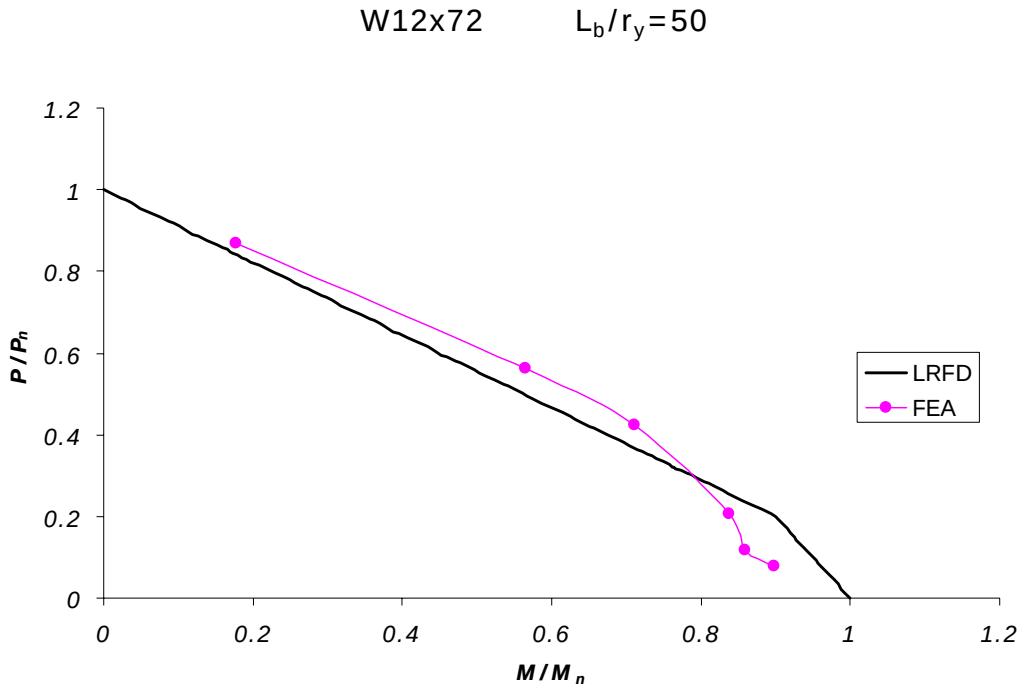

Figure 46 Comparison of FE interaction results with AISC

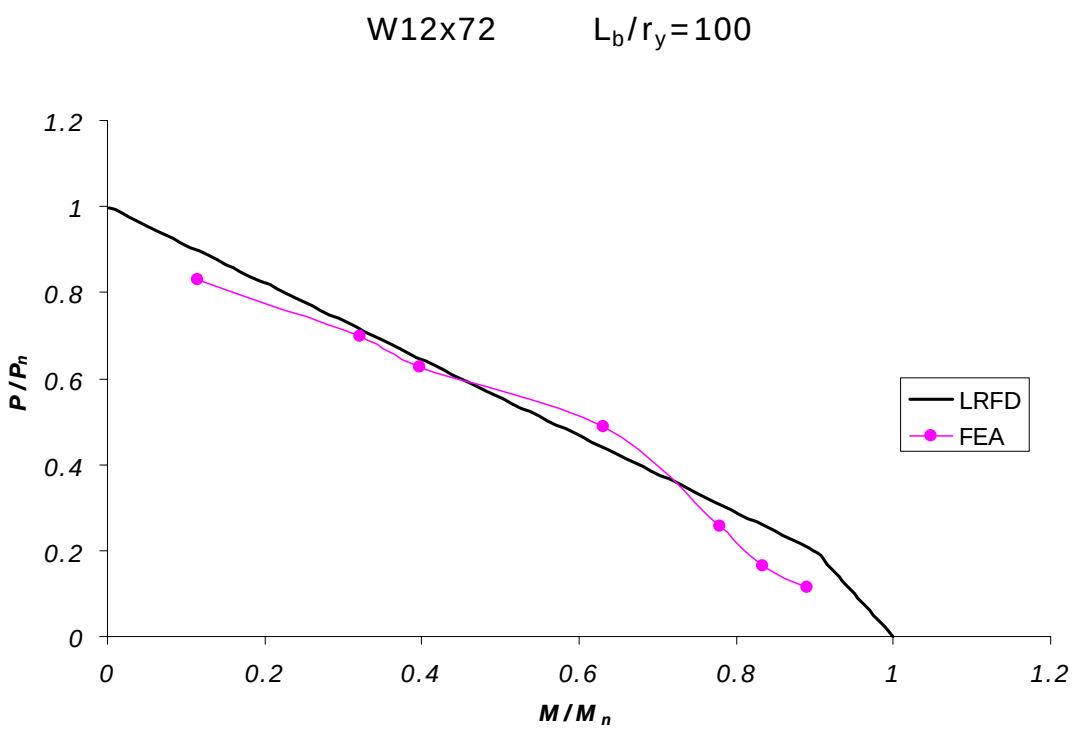

Figure 47 Comparison of FE interaction results with AISC

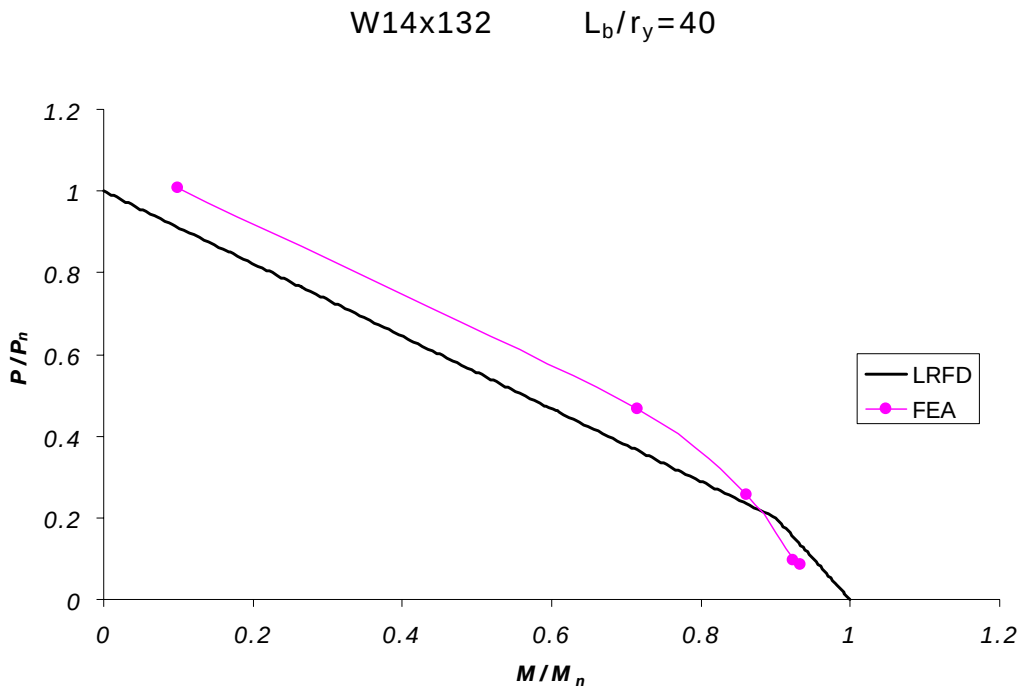

Figure 48 Comparison of FE interaction results with AISC

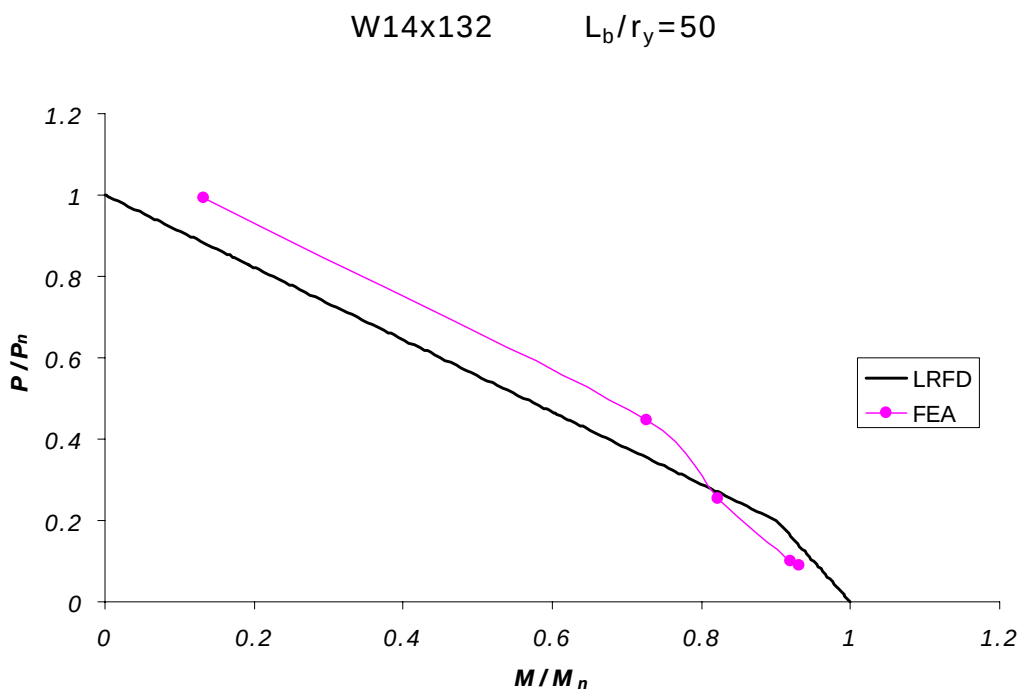

Figure 49 Comparison of FE interaction results with AISC

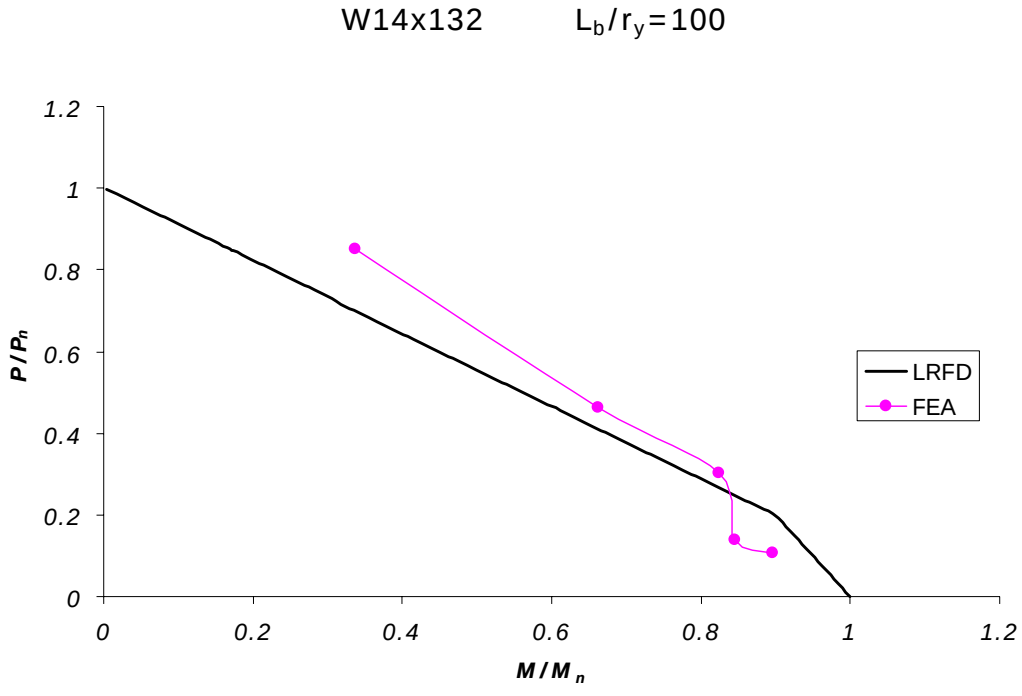

Figure 50 Comparison of FE interaction results with AISC

5.5 RECOMMENDED INTERACTION EQUATIONS

Based on plots presented above (figure 42-figure50), it is noted that the current AISC interaction expressions tend to be somewhat conservative in their capacity predictions for I-shaped beam-columns bent about the weak axis when the applied moment ratio, M/M_n is less than approximately 0.7 and unconservative at moment ratios greater than this. This finding is not surprising since, as was pointed out in the introduction, the AISC interaction equations were developed based on the behavior of I-shaped beam-columns bent about their strong axis (major principal centroidal axis).

The current research proposes amending the existing AISC interaction equations (equations 41 and 42 above), by specifying substantive changes to address the important observed behavioral differences for the case of I-shaped beam-columns bent about the weak axis (minor principal centroidal axis). The form of the new equations are given as:

for $\frac{P_u}{P_n} \geq 0.5$:

$$\frac{P_u}{P_n} + \frac{7}{9}\frac{M_u}{M_n} \leq 1.0 \tag{51}$$

and for $\frac{P_u}{P_n} < 0.5$:

$$\frac{7}{10}\frac{P_u}{P_n} + \frac{M_u}{M_n} \leq 1.0 \tag{52}$$

Figures 51 through 59 show a comparison between the results of the nonlinear finite element beam-column analyses, the current AISC interaction predictions, and the predictions obtained using the proposed equations 51 and 52.

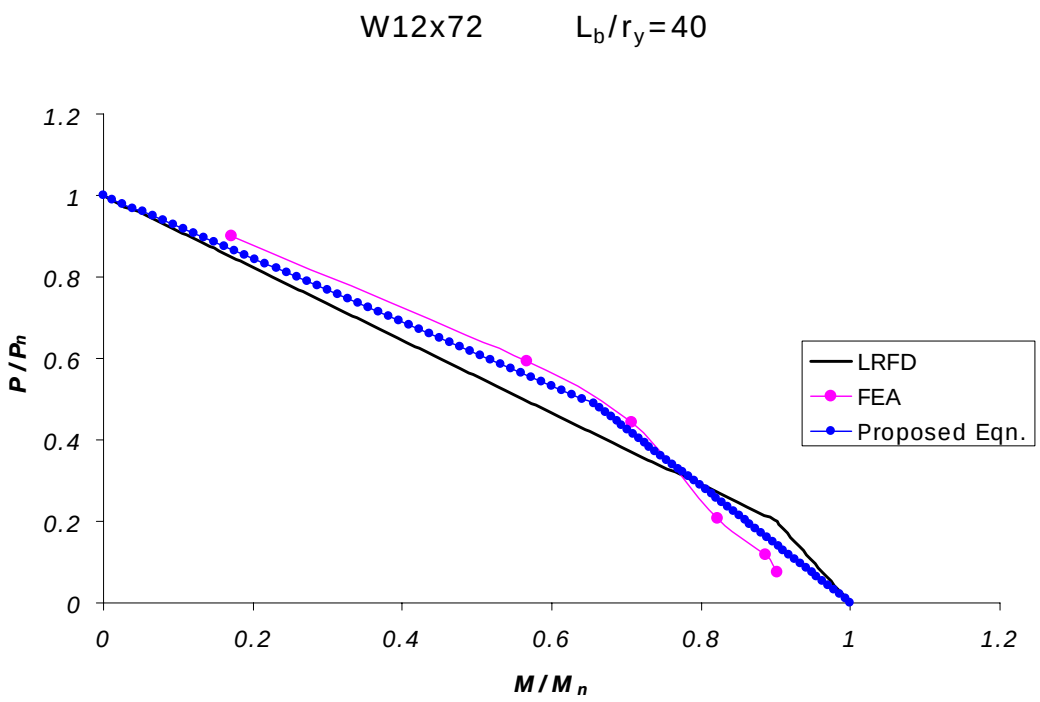

Figure 51 Comparison of FE interaction results with AISC and proposed equation.

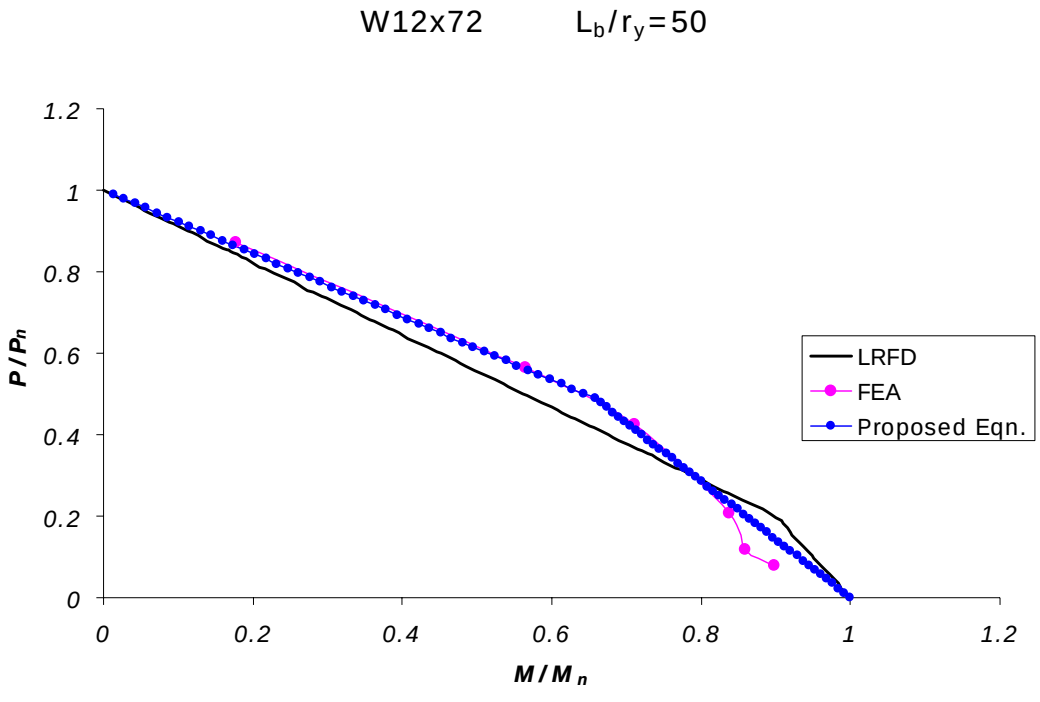

Figure 52 Comparison of FE interaction results with AISC and proposed equation.

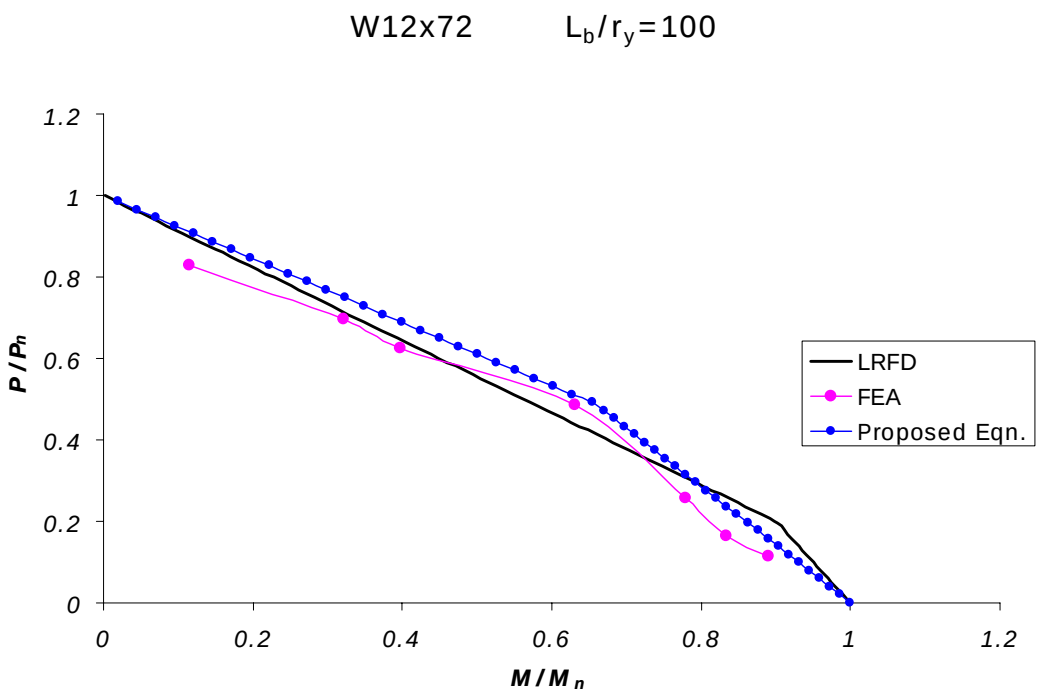

Figure 53 Comparison of FE interaction results with AISC and proposed equation.

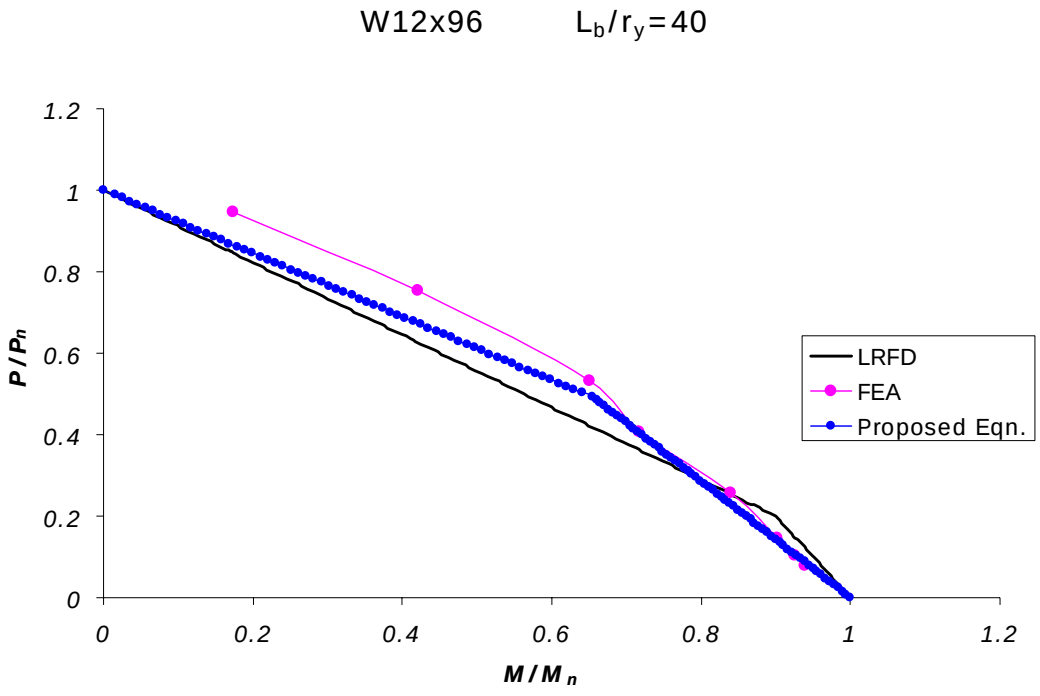

Figure 54 Comparison of FE interaction results with AISC and proposed equation.

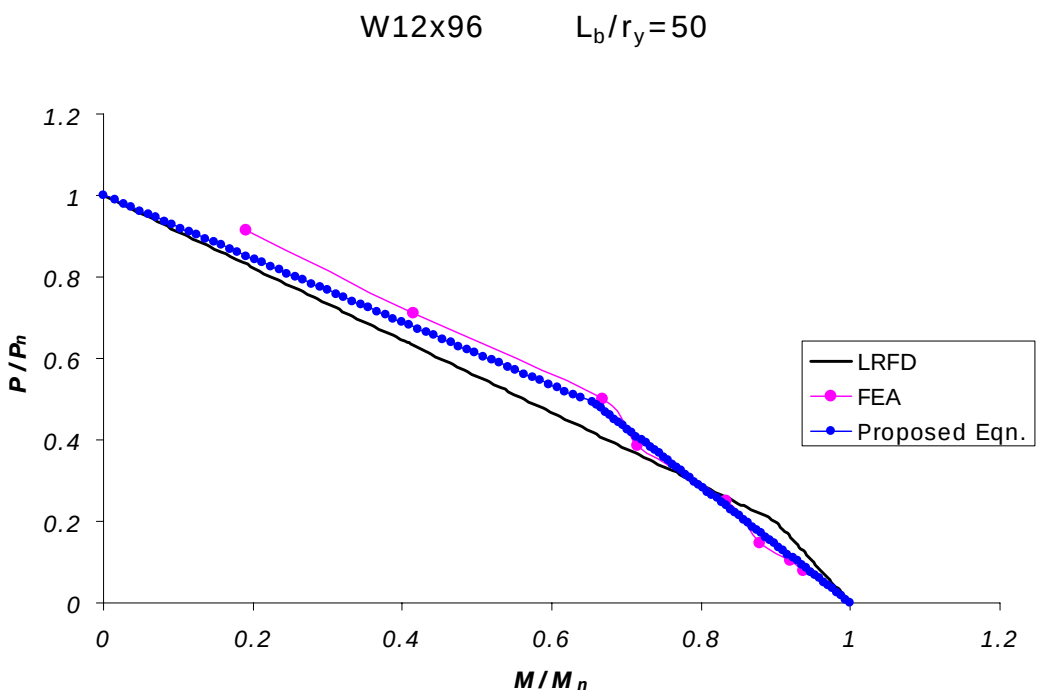

Figure 55 Comparison of FE interaction results with AISC and proposed equation.

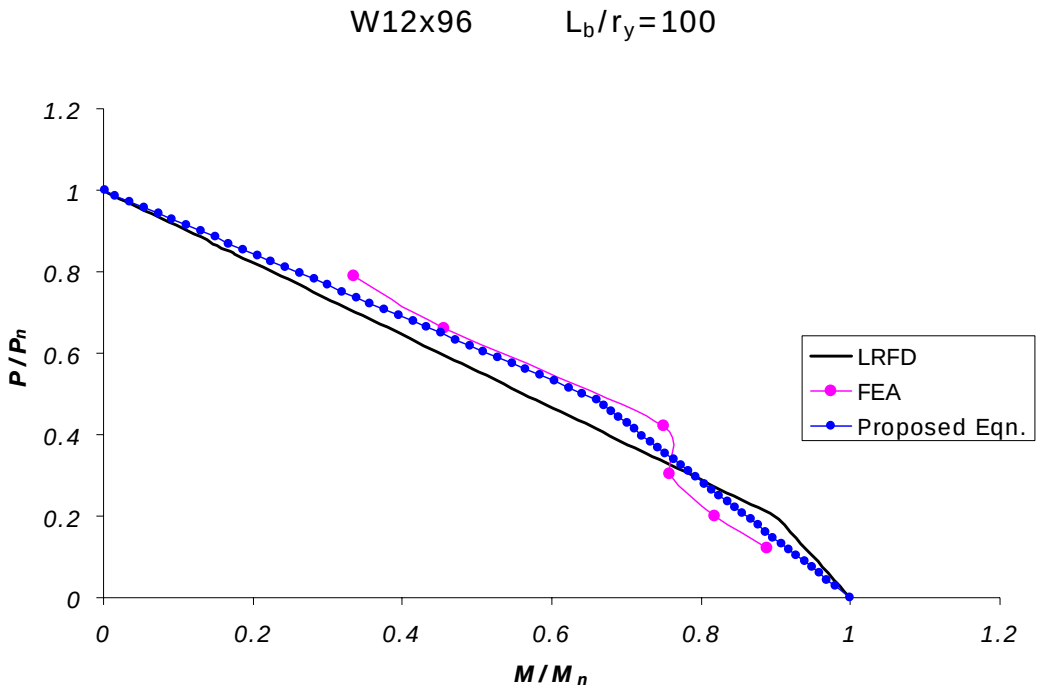

Figure 56 Comparison of FE interaction results with AISC and proposed equation.

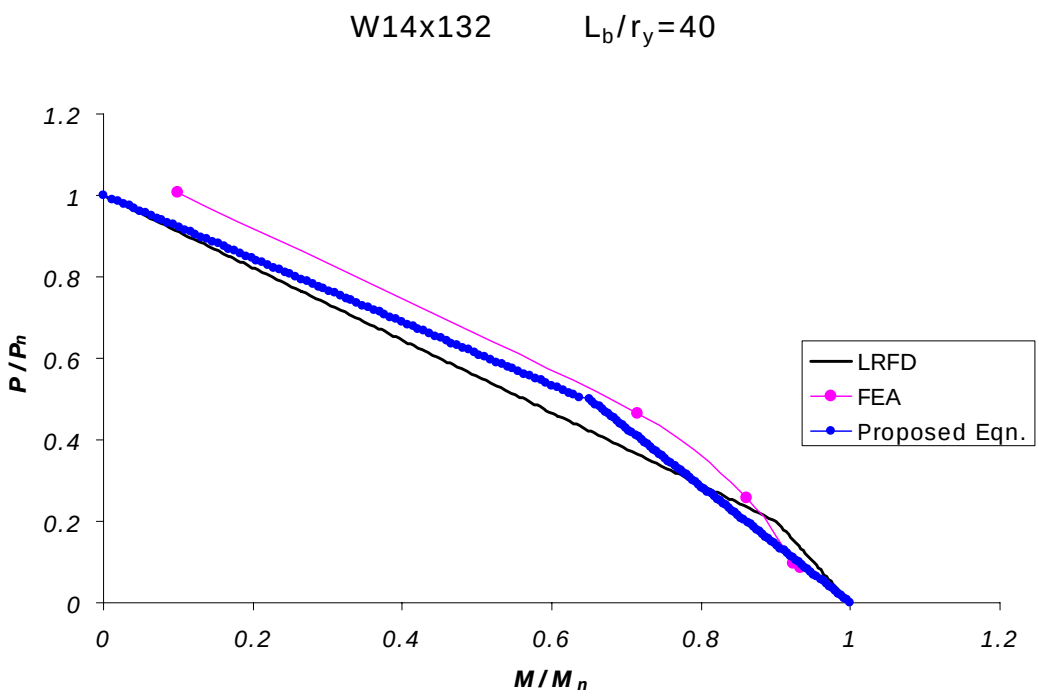

Figure 57 Comparison of FE interaction results with AISC and proposed equation.

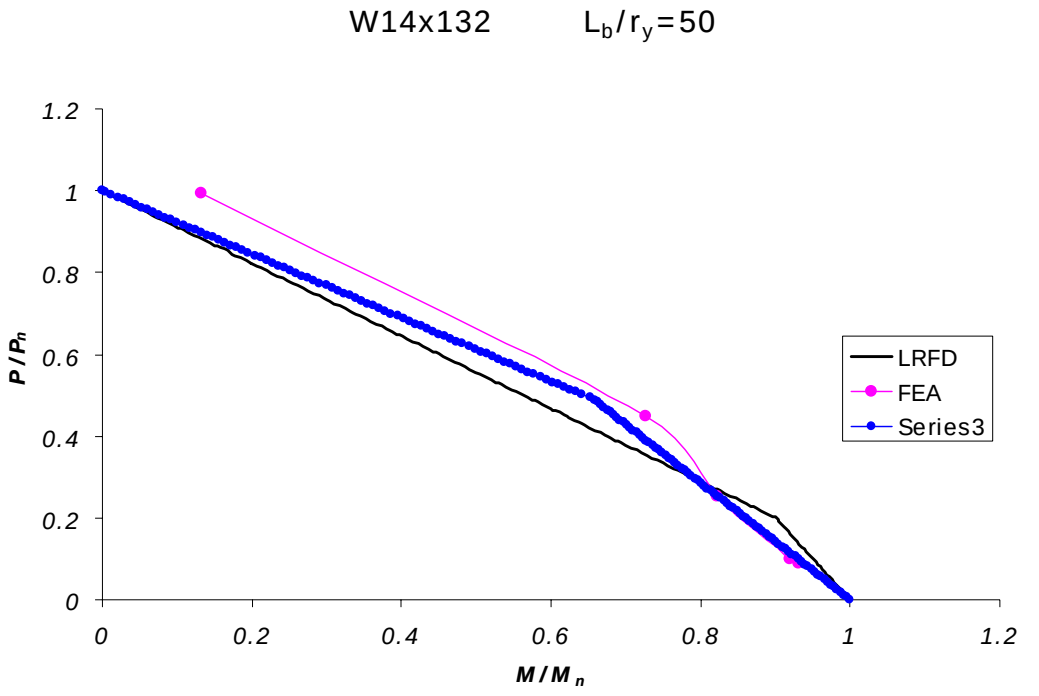

Figure 58 Comparison of FE interaction results with AISC and proposed equation.

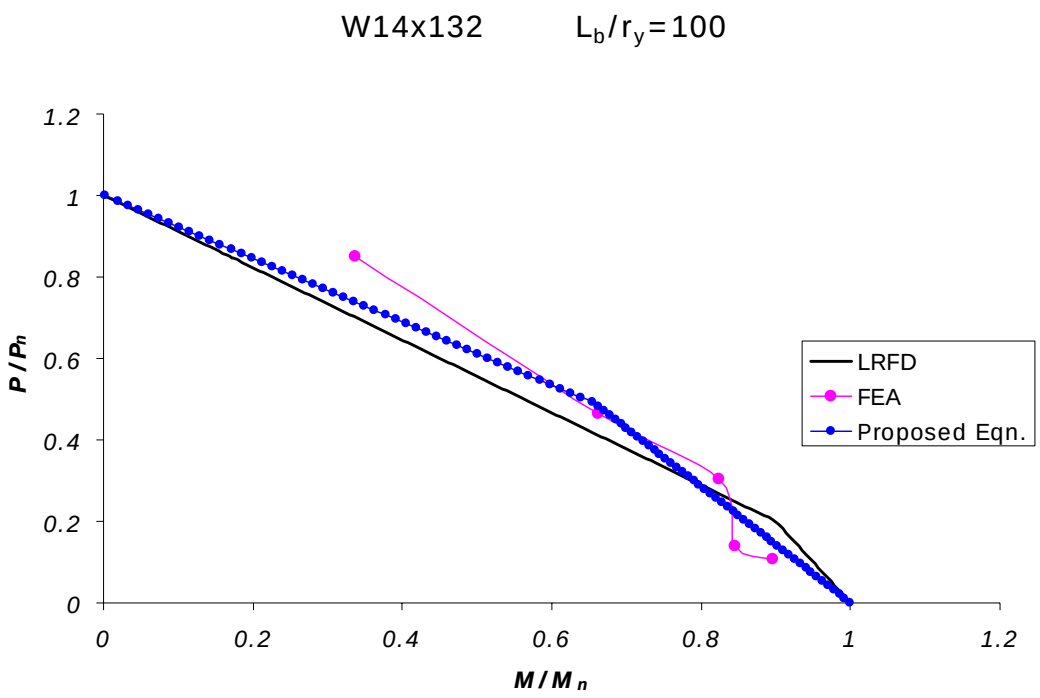

Figure 59 Comparison of FE interaction results with AISC and proposed equation.

6.0 CONCLUSION

6.1 COMPACTNESS

Employing the verified nonlinear finite element modeling techniques, I-shaped beams bent about the minor principal centroidal axis are studied. It appears to be unconservative to apply limiting plate slenderness ratios for the major principal axis flexural case when significant structural ductility is sought. Indeed, proper consideration of reserve capacity during inelastic buckling of constituent plate buckling elements used in the flanges must properly consider the important effects of rotational edge restraint afforded by the web along the flange-web junction.

As a crude but useful measure, one may deny the importance of this edge restraint and rely on a simple, but conservative plate slenderness limit that is not too philosophically different from the equations employed in the major axis flexural case and thus easily incorporated into existing specification formats.

6.2 INTERACTION EQUATIONS

Through the use of experimentally verified nonlinear finite element modeling techniques, the case of an I-shaped beam-column, subjected to bending about the minor principal centroidal axis, is treated. Based on these efforts, it is noted that the current AISC interaction expressions tend to be somewhat conservative in their capacity predictions for I-shaped beam-columns bent about the weak axis when the applied moment ratio, M / M_n, is less than approximately 0.7; and unconservative at moment ratios greater than this. This finding is not surprising since the AISC interaction equations were developed based on the behavior of I-shaped beam-columns bent about the strong axis (major principal centroidal axis).

As a means for mitigating the observed lack of agreement between the existing interaction equation predictions for this case, as compare with the nonlinear finite element modeling results, a modification of the form of the existing AISC interaction equations (AISC 1999) is proposed. The result of this effort is a set of two equations, following directly after the current equation format in Chapter H of the AISC specification (1999), that exhibit a better agreement with the observed minor axis beam-column modeling results as compared with the current form of the equations.

APPENDIX

ABAQUS INPUT FILE FOR I-SHAPED BEAMS UNDER MINOR AXIS BENDING

```
*HEADING
**Num. of ele in L/3 (m)=30
**Num of ele in bf/2 (n)=4
**Num of ele in d (k)=25
**
**Fy=50ksi & Est=2.9E4ksi & Iso.Hard
** d=25
** tf=0.417
** bf=7.5
** tw=0.278
** bf/d=0.3
** bf/2tf=9
** imp_size=0.075
** lw=3.75
** del_y=1
** P=-11.024
*NODE
**Left side of the Left Flange
1,0,0,0
365,0,0,3.75
729,0,0,7.5
**Right side of the Left Flange
91,0,90,0
455,0,90,3.75
819,0,90,7.5
**Left side of the Right Flange
820,24.583,0,0
1184,24.583,0,3.75
1548,24.583,0,7.5
**Right side of the Right Flange
910,24.583,90,0
1274,24.583,90,3.75
1638,24.583,90,7.5
**Web
1639,0.2085,0,3.75
1669,0.2085,30,3.75
1699,0.2085,60,3.75
1729,0.2085,90,3.75
3914,24.3745,0,3.75
3944,24.3745,30,3.75
3974,24.3745,60,3.75
4004,24.3745,90,3.75
**Middle of lflange
395,0,30,3.75
425,0,60,3.75
**Middle of rflange
1214,24.583,30,3.75
1244,24.583,60,3.75
**Constant Moment Region
```

****
**Left flange Bottom
31,0,30,0
32,0.0557527809112509,31,0
33,0.0745838381863687,32,0
34,0.0440224917781132,33,0
35,-0.0156923111687995,34,0
36,-0.0650150374028232,35,0
37,-0.0712822029285651,36,0
38,-0.0303434398228237,37,0
39,0.030689963962659,38,0
40,0.0713992449095712,39,0
41,0.0648250873392884,40,0
42,0.0153211615976319,41,0
43,-0.0443290507515532,42,0
44,-0.074622790936483,43,0
45,-0.0554983313674026,44,0
46,0.000379345162739933,45,0
47,0.0560058041386644,46,0
48,0.074542977367232,47,0
49,0.0437148065827612,48,0
50,-0.0160630592855293,49,0
51,-0.0652033241947715,50,0
52,-0.0711633373438593,51,0
53,-0.029996139410555,52,0
54,0.031035702964977,53,0
55,0.0715144602926071,54,0
56,0.0646334788636361,55,0
57,0.0149496200670996,56,0
58,-0.0446344756604212,57,0
59,-0.0746598346210515,58,0
60,-0.0552424620166707,59,0
61,0,60,0
**Left Flange Top
759,0,30,7.5
760,0.0557527809112509,31,7.5
761,0.0745838381863687,32,7.5
762,0.0440224917781132,33,7.5
763,-0.0156923111687995,34,7.5
764,-0.0650150374028232,35,7.5
765,-0.0712822029285651,36,7.5
766,-0.0303434398228237,37,7.5
767,0.030689963962659,38,7.5
768,0.0713992449095712,39,7.5
769,0.0648250873392884,40,7.5
770,0.0153211615976319,41,7.5
771,-0.0443290507515532,42,7.5
772,-0.074622790936483,43,7.5
773,-0.0554983313674026,44,7.5
774,0.000379345162739933,45,7.5
775,0.0560058041386644,46,7.5
776,0.074542977367232,47,7.5
777,0.0437148065827612,48,7.5
778,-0.0160630592855293,49,7.5
779,-0.0652033241947715,50,7.5
780,-0.0711633373438593,51,7.5
781,-0.029996139410555,52,7.5
782,0.031035702964977,53,7.5
783,0.0715144602926071,54,7.5
784,0.0646334788636361,55,7.5
785,0.0149496200670996,56,7.5
786,-0.0446344756604212,57,7.5
787,-0.0746598346210515,58,7.5
788,-0.0552424620166707,59,7.5
789,0,60,7.5
**Right Flange Bottom
850,24.583,30,0
851,24.5272472190887,31,0
852,24.5084161618136,32,0
853,24.5389775082219,33,0

854,24.5986923111688,34,0
855,24.6480150374028,35,0
856,24.6542822029286,36,0
857,24.6133434398228,37,0
858,24.5523100360373,38,0
859,24.5116007550904,39,0
860,24.5181749126607,40,0
861,24.5676788384024,41,0
862,24.6273290507516,42,0
863,24.6576227909365,43,0
864,24.6384983313674,44,0
865,24.5826206548373,45,0
866,24.5269941958613,46,0
867,24.5084570226328,47,0
868,24.5392851934172,48,0
869,24.5990630592855,49,0
870,24.6482033241948,50,0
871,24.6541633373439,51,0
872,24.6129961394106,52,0
873,24.551964297035,53,0
874,24.5114855397074,54,0
875,24.5183665211364,55,0
876,24.5680503799329,56,0
877,24.6276344756604,57,0
878,24.6576598346211,58,0
879,24.6382424620167,59,0
880,24.583,60,0
**Right Flange Top
1578,24.583,30,7.5
1579,24.5272472190887,31,7.5
1580,24.5084161618136,32,7.5
1581,24.5389775082219,33,7.5
1582,24.5986923111688,34,7.5
1583,24.6480150374028,35,7.5
1584,24.6542822029286,36,7.5
1585,24.6133434398228,37,7.5
1586,24.5523100360373,38,7.5
1587,24.5116007550904,39,7.5
1588,24.5181749126607,40,7.5
1589,24.5676788384024,41,7.5
1590,24.6273290507516,42,7.5
1591,24.6576227909365,43,7.5
1592,24.6384983313674,44,7.5
1593,24.5826206548373,45,7.5
1594,24.5269941958613,46,7.5
1595,24.5084570226328,47,7.5
1596,24.5392851934172,48,7.5
1597,24.5990630592855,49,7.5
1598,24.6482033241948,50,7.5
1599,24.6541633373439,51,7.5
1600,24.6129961394106,52,7.5
1601,24.551964297035,53,7.5
1602,24.5114855397074,54,7.5
1603,24.5183665211364,55,7.5
1604,24.5680503799329,56,7.5
1605,24.6276344756604,57,7.5
1606,24.6576598346211,58,7.5
1607,24.6382424620167,59,7.5
1608,24.583,60,7.5
**Left of the left flange
*NGEN,NSET=LLB
1,31,1
*NGEN,NSET=LLM
365,395,1
*NGEN,NSET=LLT
729,759,1
*NFILL,NSET=LEFTLF1
LLB,LLM,4,91
*NFILL,NSET=LEFTLF2
LLM,LLT,4,91

```
**Right of the left flange
*NGEN,NSET=LRB
61,91,1
*NGEN,NSET=LRM
425,455,1
*NGEN,NSET=LRT
789,819,1
*NFILL,NSET=RIGHTLF1
LRB,LRM,4,91
*NFILL,NSET=RIGHTLF2
LRM,LRT,4,91
**Middle of the left flange
*NSET,NSET=LMB,GENERATE
31,61,1
*NGEN,NSET=LMM
395,425,1
*NSET,NSET=LMT,GENERATE
759,789,1
*NFILL,NSET=MIDLF1
LMB,LMM,4,91
*NFILL,NSET=MIDLF2
LMM,LMT,4,91
**Left of the right flange
*NGEN,NSET=RLB
820,850,1
*NGEN,NSET=RLM
1184,1214,1
*NGEN,NSET=RLT
1548,1578,1
*NFILL,NSET=LEFTRF1
RLB,RLM,4,91
*NFILL,NSET=LEFTRF2
RLM,RLT,4,91
**Right of the right flange
*NGEN,NSET=RRB
880,910,1
*NGEN,NSET=RRM
1244,1274,1
*NGEN,NSET=RRT
1608,1638,1
*NFILL,NSET=RIGHTRF1
RRB,RRM,4,91
*NFILL,NSET=RIGHTRF2
RRM,RRT,4,91
**Middle of the right flange
*NSET,NSET=RMB,GENERATE
850,880,1
*NGEN,NSET=RMM
1214,1244,1
*NSET,NSET=RMT,GENERATE
1578,1608,1
*NFILL,NSET=MIDRF1
RMB,RMM,4,91
*NFILL,NSET=MIDRF2
RMM,RMT,4,91
**
**WEB NODES
**
*NGEN,NSET=WLT
1639,1669,1
*NGEN,NSET=WMT
1669,1699,1
*NGEN,NSET=WRT
1699,1729,1
*NGEN,NSET=WLB
3914,3944,1
*NGEN,NSET=WMB
3944,3974,1
*NGEN,NSET=WRB
3974,4004,1
```

```
*NFILL,NSET=WL
WLT,WLB,25,91
*NFILL,NSET=WM
WMT,WMB,25,91
*NFILL,NSET=WR
WRT,WRB,25,91
**NSET FOR BOUNDARY CONDITION
*NSET,NSET=PINNED,GENERATE
1639,3914,91
365,1184,819
*NSET,NSET=ROLLER,GENERATE
1729,4004,91
455,1274,819
**
**ELEMENT DEFINITIONS
**
**
**LEFT FLANGE
*ELEMENT,TYPE=S4R
1,1,2,93,92
*ELGEN,ELSET=LFL1
1,30,1,1,4,91,90
*ELEMENT,TYPE=S4R
361,365,366,457,456
*ELGEN,ELSET=LFL2
361,30,1,1,4,91,90
*ELEMENT,TYPE=S4R
31,31,32,123,122
*ELGEN,ELSET=LFM1
31,30,1,1,4,91,90
*ELEMENT,TYPE=S4R
391,395,396,487,486
*ELGEN,ELSET=LFM2
391,30,1,1,4,91,90
*ELEMENT,TYPE=S4R
61,61,62,153,152
*ELGEN,ELSET=LFR1
61,30,1,1,4,91,90
*ELEMENT,TYPE=S4R
421,425,426,517,516
*ELGEN,ELSET=LFR2
421,30,1,1,4,91,90
**RIGHT FLANGE
*ELEMENT,TYPE=S4R
721,820,821,912,911
*ELGEN,ELSET=RFL1
721,30,1,1,4,91,90
*ELEMENT,TYPE=S4R
1081,1184,1185,1276,1275
*ELGEN,ELSET=RFL2
1081,30,1,1,4,91,90
*ELEMENT,TYPE=S4R
751,850,851,942,941
*ELGEN,ELSET=RFM1
751,30,1,1,4,91,90
*ELEMENT,TYPE=S4R
1111,1214,1215,1306,1305
*ELGEN,ELSET=RFM2
1111,30,1,1,4,91,90
*ELEMENT,TYPE=S4R
781,880,881,972,971
*ELGEN,ELSET=RFR1
781,30,1,1,4,91,90
*ELEMENT,TYPE=S4R
1141,1244,1245,1336,1335
*ELGEN,ELSET=RFR2
1141,30,1,1,4,91,90
**TOP STITCH
*ELEMENT,TYPE=S4R
1441,365,366,1640,1639
```

```
*ELGEN,ELSET=TSL
1441,30,1,1,1
*ELEMENT,TYPE=S4R
1471,395,396,1670,1669
*ELGEN,ELSET=TSM
1471,30,1,1,1
*ELEMENT,TYPE=S4R
1501,425,426,1700,1699
*ELGEN,ELSET=TSR
1501,30,1,1,1
**BOTTOM STITCH
*ELEMENT,TYPE=S4R
3781,3914,3915,1185,1184
*ELGEN,ELSET=BSL
3781,30,1,1,1
*ELEMENT,TYPE=S4R
3811,3944,3945,1215,1214
*ELGEN,ELSET=BSM
3811,30,1,1,1
*ELEMENT,TYPE=S4R
3841,3974,3975,1245,1244
*ELGEN,ELSET=BSR
3841,30,1,1,1
**WEB ELEMENTS
*ELEMENT,TYPE=S4R
1531,1639,1640,1731,1730
*ELGEN,ELSET=WEBL
1531,30,1,1,25,91,90
*ELEMENT,TYPE=S4R
1561,1669,1670,1761,1760
*ELGEN,ELSET=WEBM
1561,30,1,1,25,91,90
*ELEMENT,TYPE=S4R
1591,1699,1700,1791,1790
*ELGEN,ELSET=WEBR
1591,30,1,1,25,91,90
**GROUPING ELEMENTS
*ELSET,ELSET=LFLANGELEFT
LFL1,LFL2
*ELSET,ELSET=LFLANGEMIDDLE
LFM1,LFM2
*ELSET,ELSET=LFLANGERIGHT
LFR1,LFR2
*ELSET,ELSET=RFLANGELEFT
RFL1,RFL2
*ELSET,ELSET=RFLANGEMIDDLE
RFM1,RFM2
*ELSET,ELSET=RFLANGERIGHT
RFR1,RFR2
*ELSET,ELSET=LFLANGE
LFLANGELEFT,LFLANGEMIDDLE,LFLANGERIGHT
*ELSET,ELSET=RFLANGE
RFLANGELEFT,RFLANGEMIDDLE,RFLANGERIGHT
*ELSET,ELSET=WEBLEFT
TSL,BSL,WEBL
*ELSET,ELSET=WEBMIDDLE
TSM,BSM,WEBM
*ELSET,ELSET=WEBRIGHT
TSR,BSR,WEBR
*ELSET,ELSET=WEB
WEBLEFT,WEBMIDDLE,WEBRIGHT
*ELSET,ELSET=TOPSTC
TSL,TSM,TSR
*ELSET,ELSET=BOTTOMSTC
BSL,BSM,BSR
*ELSET,ELSET=BEAMRIGHT
LFLANGERIGHT,RFLANGERIGHT,WEBRIGHT
*ELSET,ELSET=BEAMMIDDLE
LFLANGEMIDDLE,RFLANGEMIDDLE,WEBMIDDLE
*ELSET,ELSET=BEAMLEFT
```

```
LFLANGELEFT,RFLANGELEFT,WEBLEFT
*ELSET,ELSET=FLANGERIGID
LFL1,LFL2,RFL1,RFL2,LFR2,LFR1,RFR2,RFR1
*ELSET,ELSET=FLANGEFLEX
LFM2,LFM1,RFM2,RFM1
*ELSET,ELSET=WEBRIGID
TSL,WEBL,BSL,TSR,WEBR,BSR
*SHELL SECTION,MATERIAL=FLEX,ELSET=FLANGEFLEX
0.417
*SHELL SECTION,MATERIAL=FLEX,ELSET=WEBMIDDLE
0.278
*SHELL SECTION,MATERIAL=RIGID,ELSET=FLANGERIGID
0.417
*SHELL SECTION,MATERIAL=RIGID,ELSET=WEBRIGID
0.278
*MATERIAL,NAME=RIGID
*ELASTIC
290000,0.3
*MATERIAL,NAME=FLEX
*ELASTIC
29000,0.3
*PLASTIC
50,0
51.345,0.00922948
75,0.0557238
80,0.090034
*BOUNDARY
PINNED,1,3
ROLLER,1
ROLLER,3
395,1
759,1
31,1
789,1
425,1
61,1
1578,1
1608,1
1214,1
1244,1
850,1
880,1
*STEP,NLGEOM,INC=70
*STATIC,RIKS
0.01,1,0.0000000001
*CONTROLS,ANALYSIS=DISCONTINUOUS
*CLOAD
395,3,-10.154
1214,3,-10.154
425,3,-10.154
1244,3,-10.154
*RESTART,WRITE,FREQUENCY=1
*ELPRINT,FREQUENCY=0
*NODE PRINT,FREQUENCY=1
CF
*END STEP
```

ABAQUS INPUT FILE FOR I-SHAPED BEAMS UNDER MINOR AXIS MOMENT – THRUST

```
*HEADING
**                          b=8     Lb=8
**                          j=14     Lj=14
**                          k=10     d=10.33
**                          n=6     bf=5.77
**                          a=0     La=0
**                          m=54     Lf=54.4
**                          tf=0.44     tw=0.26
**                    impsize=0.0577     lw=2.885
**                    camber=0     dely=1.00740740740741
**                      Ntotal=338     P=304.2
**                   totalaxial=23
**                          E=
**j     14
**j+a     14
**j+a+b     22
**j+a+b+m     76
**j+a+2*b+m     84
**j+2*a+2*b+m     84
**2*j+2*a+2*b+m     98
**
*NODE
**Bottom1
1,0,0,0
15,0,14,0
23,0,22,0
77,0,76.4,0
85,0,84.4,0
99,0,98.4,0
**Middle1
298,0,0,2.885
312,0,14,2.885
320,0,22,2.885
374,0,76.4,2.885
382,0,84.4,2.885
396,0,98.4,2.885
**Top1
595,0,0,5.77
609,0,14,5.77
617,0,22,5.77
671,0,76.4,5.77
679,0,84.4,5.77
693,0,98.4,5.77
**Bottom2
694,10.77,0,0
708,10.77,14,0
716,10.77,22,0
770,10.77,76.4,0
778,10.77,84.4,0
792,10.77,98.4,0
**Middle2
991,10.77,0,2.885
1005,10.77,14,2.885
1013,10.77,22,2.885
1067,10.77,76.4,2.885
1075,10.77,84.4,2.885
1089,10.77,98.4,2.885
**Top2
1288,10.77,0,5.77
1302,10.77,14,5.77
1310,10.77,22,5.77
1364,10.77,76.4,5.77
```

1372,10.77,84.4,5.77
1386,10.77,98.4,5.77
**Web Top
1387,1.077,0,2.885
1401,1.077,14,2.885
1409,1.077,22,2.885
1463,1.077,76.4,2.885
1471,1.077,84.4,2.885
1485,1.077,98.4,2.885
**Web Bottom
2179,9.693,0,2.885
2193,9.693,14,2.885
2201,9.693,22,2.885
2255,9.693,76.4,2.885
2263,9.693,84.4,2.885
2277,9.693,98.4,2.885
**Constant Moment Region
****
**Left flange Bottom
23,0,22,0
24,0.0513557058728689,23.0074074074074,0
25,0.046822946147168,24.0148148148148,0
26,-0.00866544879943186,25.0222222222222,0
27,-0.0547235646973492,26.0296296296296,0
28,-0.0412281020583456,27.037037037037,0
29,0.017134339320784,28.0444444444444,0
30,0.0568501295166074,29.0518518518519,0
31,0.0346980813922161,30.0592592592593,0
32,-0.0252145718151973,31.0666666666667,0
33,-0.0576871634846619,32.0740740740741,0
34,-0.0273810045344245,33.0814814814815,0
35,0.0327228624594854,34.0888888888889,0
36,0.0572156801693888,35.0962962962963,0
37,0.0194428446573978,36.1037037037037,0
38,-0.0394889007810437,37.1111111111111,0
39,-0.0554463742215485,38.1185185185185,0
40,-0.011063662952733,39.1259259259259,0
41,0.0453592128083917,40.1333333333333,0
42,0.0524193787881428,41.1407407407407,0
43,0.00243352430520481,42.1481481481481,0
44,-0.0502006423195506,43.1555555555556,0
45,-0.0482033551726907,44.162962962963,0
46,0.00625181394688691,45.1703703703704,0
47,0.0539033712231341,46.1777777777778,0
48,0.0428939353916493,47.1851851851852,0
49,-0.0147953423732309,48.1925925925926,0
50,-0.0563834105608863,49.2,0
51,-0.036611552954456,50.2074074074074,0
52,0.0230032682142046,51.2148148148148,0
53,0.0575845056282812,52.2222222222222,0
54,0.0294987110715816,53.2296296296296,0
55,-0.0306894111798719,54.237037037037,0
56,-0.0574794119993549,55.2444444444444,0
57,-0.0217167502558045,56.2518518518518,0
58,0.0376794265754137,57.2592592592593,0
59,0.0560705135117159,58.2666666666667,0
60,0.0134421886371641,59.2740740740741,0
61,-0.0438147599598885,60.2814814814815,0
62,-0.0533897681939817,61.2888888888889,0
63,-0.00486271800419616,62.2962962962963,0
64,0.0489562436348416,63.3037037037037,0
65,0.0494979833621752,64.3111111111111,0
66,-0.00382705360680747,65.3185185185185,0
67,-0.0529872533836495,66.3259259259259,0
68,-0.0444834363280547,67.3333333333333,0
69,0.0124300162037034,68.3407407407407,0
70,0.0558163538573204,69.3481481481481,0
71,0.0384598720058418,70.3555555555556,0
72,-0.0207510288822458,71.362962962963,0
73,-0.0573793726014906,72.3703703703704,0

74,-0.0315639228376029,73.3777777777778,0
75,0.0286013462050269,74.3851851851852,0
76,0.0576408556794895,75.3925925925926,0
77,0,76.4,0
**Left Flange Top
617,0,22,5.77
618,-0.0513557058728689,23.0074074074074,5.77
619,-0.046822946147168,24.0148148148148,5.77
620,0.0086654879943186,25.0222222222222,5.77
621,0.0547235646973492,26.0296296296296,5.77
622,0.0412281020583456,27.037037037037,5.77
623,-0.017134339320784,28.0444444444444,5.77
624,-0.0568501295166074,29.0518518518519,5.77
625,-0.0346980813922161,30.0592592592593,5.77
626,0.0252145718151973,31.0666666666667,5.77
627,0.0576871634846619,32.0740740740741,5.77
628,0.0273810045344245,33.0814814814815,5.77
629,-0.0327228624594854,34.0888888888889,5.77
630,-0.0572156801693888,35.0962962962963,5.77
631,-0.0194428446573978,36.1037037037037,5.77
632,0.0394889007810437,37.1111111111111,5.77
633,0.0554463742215485,38.1185185185185,5.77
634,0.011063662952733,39.1259259259259,5.77
635,-0.0453592128083917,40.1333333333333,5.77
636,-0.0524193787881428,41.1407407407407,5.77
637,-0.00243352430520481,42.1481481481481,5.77
638,0.0502006423195506,43.1555555555556,5.77
639,0.0482033551726907,44.162962962963,5.77
640,-0.00625181394688691,45.1703703703704,5.77
641,-0.0539033712231341,46.1777777777778,5.77
642,-0.0428939353916493,47.1851851851852,5.77
643,0.0147953423732309,48.1925925925926,5.77
644,0.0563834105608863,49.2,5.77
645,0.036611552954456,50.2074074074074,5.77
646,-0.0230032682142046,51.2148148148148,5.77
647,-0.0575845056282812,52.2222222222222,5.77
648,-0.0294987110715816,53.2296296296296,5.77
649,0.0306894111798719,54.237037037037,5.77
650,0.0574794119993549,55.2444444444444,5.77
651,0.0217167502558045,56.2518518518518,5.77
652,-0.0376794265754137,57.2592592592593,5.77
653,-0.0560705135117159,58.2666666666667,5.77
654,-0.0134421886371641,59.2740740740741,5.77
655,0.0438147599598885,60.2814814814815,5.77
656,0.0533897681939817,61.2888888888889,5.77
657,0.00486271800419616,62.2962962962963,5.77
658,-0.0489562436348416,63.3037037037037,5.77
659,-0.0494979833621752,64.3111111111111,5.77
660,0.00382705360680747,65.3185185185185,5.77
661,0.0529872533836495,66.3259259259259,5.77
662,0.0444834363280547,67.3333333333333,5.77
663,-0.0124300162037034,68.3407407407407,5.77
664,-0.0558163538573204,69.3481481481481,5.77
665,-0.0384598720058418,70.3555555555556,5.77
666,0.0207510288822458,71.362962962963,5.77
667,0.0573793726014906,72.3703703703704,5.77
668,0.0315639228376029,73.3777777777778,5.77
669,-0.0286013462050269,74.3851851851852,5.77
670,-0.0576408556794895,75.3925925925926,5.77
671,0,76.4,5.77
**Right Flange Bottom
716,10.77,22,0
717,10.7186442941271,23.0074074074074,0
718,10.7231770538528,24.0148148148148,0
719,10.7786654487994,25.0222222222222,0
720,10.8247235646973,26.0296296296296,0
721,10.8112281020583,27.037037037037,0
722,10.7528656606792,28.0444444444444,0
723,10.7131498704834,29.0518518518519,0
724,10.7353019186078,30.0592592592593,0

725,10.7952145718152,31.0666666666667,0
726,10.8276871634847,32.0740740740741,0
727,10.7973810045344,33.0814814814815,0
728,10.7372771375405,34.0888888888889,0
729,10.7127843198306,35.0962962962963,0
730,10.7505571553426,36.1037037037037,0
731,10.809488900781,37.1111111111111,0
732,10.8254463742215,38.1185185185185,0
733,10.7810636629527,39.1259259259259,0
734,10.7246407871916,40.1333333333333,0
735,10.7175806212119,41.1407407407407,0
736,10.7675664756948,42.1481481481481,0
737,10.8202006423196,43.1555555555556,0
738,10.8182033551727,44.162962962963,0
739,10.7637481860531,45.1703703703704,0
740,10.7160966287769,46.1777777777778,0
741,10.7271060646083,47.1851851851852,0
742,10.7847953423732,48.1925925925926,0
743,10.8263834105609,49.2,0
744,10.8066115529545,50.2074074074074,0
745,10.7469967317858,51.2148148148148,0
746,10.7124154943717,52.2222222222222,0
747,10.7405012889284,53.2296296296296,0
748,10.8006894111799,54.237037037037,0
749,10.8274794119994,55.2444444444444,0
750,10.7917167502558,56.2518518518518,0
751,10.7323205734246,57.2592592592593,0
752,10.7139294864883,58.2666666666667,0
753,10.7565578113628,59.2740740740741,0
754,10.8138147599599,60.2814814814815,0
755,10.823389768194,61.2888888888889,0
756,10.7748627180042,62.2962962962963,0
757,10.7210437563652,63.3037037037037,0
758,10.7205020166378,64.3111111111111,0
759,10.7738270536068,65.3185185185185,0
760,10.8229872533836,66.3259259259259,0
761,10.8144834363281,67.3333333333333,0
762,10.7575699837963,68.3407407407407,0
763,10.7141836461427,69.3481481481481,0
764,10.7315401279942,70.3555555555556,0
765,10.7907510288822,71.362962962963,0
766,10.8273793726015,72.3703703703704,0
767,10.8015639228376,73.3777777777778,0
768,10.741398653795,74.3851851851852,0
769,10.7123591443205,75.3925925925926,0
770,10.77,76.4,0
**Right Flange Top
1310,10.77,22,5.77
1311,10.8213557058729,23.0074074074074,5.77
1312,10.8168229461472,24.0148148148148,5.77
1313,10.7613345512006,25.0222222222222,5.77
1314,10.7152764353027,26.0296296296296,5.77
1315,10.7287718979417,27.037037037037,5.77
1316,10.7871343393208,28.0444444444444,5.77
1317,10.8268501295166,29.0518518518519,5.77
1318,10.8046980813922,30.0592592592593,5.77
1319,10.7447854281848,31.0666666666667,5.77
1320,10.7123128365153,32.0740740740741,5.77
1321,10.7426189954656,33.0814814814815,5.77
1322,10.8027228624595,34.0888888888889,5.77
1323,10.8272156801694,35.0962962962963,5.77
1324,10.7894428446574,36.1037037037037,5.77
1325,10.730511099219,37.1111111111111,5.77
1326,10.7145536257785,38.1185185185185,5.77
1327,10.7589363370473,39.1259259259259,5.77
1328,10.8153592128084,40.1333333333333,5.77
1329,10.8224193787881,41.1407407407407,5.77
1330,10.7724335243052,42.1481481481481,5.77
1331,10.7197993576804,43.1555555555556,5.77
1332,10.7217966448273,44.162962962963,5.77

1333,10.7762518139469,45.1703703703704,5.77
1334,10.8239033712231,46.1777777777778,5.77
1335,10.8128939353916,47.1851851851852,5.77
1336,10.7552046576268,48.1925925925926,5.77
1337,10.7136165894391,49.2,5.77
1338,10.7333884470455,50.2074074074074,5.77
1339,10.7930032682142,51.2148148148148,5.77
1340,10.8275845056283,52.2222222222222,5.77
1341,10.7994987110716,53.2296296296296,5.77
1342,10.7393105888201,54.237037037037,5.77
1343,10.7125205880006,55.2444444444444,5.77
1344,10.7482832497442,56.2518518518518,5.77
1345,10.8076794265754,57.2592592592593,5.77
1346,10.8260705135117,58.2666666666667,5.77
1347,10.7834421886372,59.2740740740741,5.77
1348,10.7261852400401,60.2814814814815,5.77
1349,10.716610231806,61.2888888888889,5.77
1350,10.7651372819958,62.2962962962963,5.77
1351,10.8189562436348,63.3037037037037,5.77
1352,10.8194979833622,64.3111111111111,5.77
1353,10.7661729463932,65.3185185185185,5.77
1354,10.7170127466163,66.3259259259259,5.77
1355,10.7255165636719,67.3333333333333,5.77
1356,10.7824300162037,68.3407407407407,5.77
1357,10.8258163538573,69.3481481481481,5.77
1358,10.8084598720058,70.3555555555556,5.77
1359,10.7492489711178,71.362962962963,5.77
1360,10.7126206273985,72.3703703703704,5.77
1361,10.7384360771624,73.3777777777778,5.77
1362,10.798601346205,74.3851851851852,5.77
1363,10.8276408556795,75.3925925925926,5.77
1364,10.77,76.4,5.77
**Flange1
*NGEN,NSET=a1
1,15,1
*NGEN,NSET=a3
15,23,1
*NSET,NSET=a4,GENERATE
23,77,1
*NGEN,NSET=a5
77,85,1
*NGEN,NSET=a6
85,99,1
*NGEN,NSET=b1
298,312,1
*NGEN,NSET=b3
312,320,1
*NGEN,NSET=b4
320,374,1
*NGEN,NSET=b5
374,382,1
*NGEN,NSET=b6
382,396,1
*NGEN,NSET=c1
595,609,1
*NGEN,NSET=c3
609,617,1
*NSET,NSET=c4,GENERATE
617,671,1
*NGEN,NSET=c5
671,679,1
*NGEN,NSET=c6
679,693,1
**Flange 2
*NGEN,NSET=d1
694,708,1
*NGEN,NSET=d3
708,716,1
*NSET,NSET=d4,GENERATE
716,770,1

```
*NGEN,NSET=d5
770,778,1
*NGEN,NSET=d6
778,792,1
*NGEN,NSET=e1
991,1005,1
*NGEN,NSET=e3
1005,1013,1
*NGEN,NSET=e4
1013,1067,1
*NGEN,NSET=e5
1067,1075,1
*NGEN,NSET=e6
1075,1089,1
*NGEN,NSET=f1
1288,1302,1
*NGEN,NSET=f3
1302,1310,1
*NSET,NSET=f4,GENERATE
1310,1364,1
*NGEN,NSET=f5
1364,1372,1
*NGEN,NSET=f6
1372,1386,1
**Web
*NGEN,NSET=g1
1387,1401,1
*NGEN,NSET=g3
1401,1409,1
*NGEN,NSET=g4
1409,1463,1
*NGEN,NSET=g5
1463,1471,1
*NGEN,NSET=g6
1471,1485,1
*NGEN,NSET=h1
2179,2193,1
*NGEN,NSET=h3
2193,2201,1
*NGEN,NSET=h4
2201,2255,1
*NGEN,NSET=h5
2255,2263,1
*NGEN,NSET=h6
2263,2277,1
**Flange1
*NFILL,NSET=z1
a1,b1,3,99
*NFILL,NSET=z3
a3,b3,3,99
*NFILL,NSET=z4
a4,b4,3,99
*NFILL,NSET=z5
a5,b5,3,99
*NFILL,NSET=z6
a6,b6,3,99
*NFILL,NSET=z8
b1,c1,3,99
*NFILL,NSET=z10
b3,c3,3,99
*NFILL,NSET=z11
b4,c4,3,99
*NFILL,NSET=z12
b5,c5,3,99
*NFILL,NSET=z13
b6,c6,3,99
**Flange2
*NFILL,NSET=z15
d1,e1,3,99
*NFILL,NSET=z17
```

```
d3,e3,3,99
*NFILL,NSET=z18
d4,e4,3,99
*NFILL,NSET=z19
d5,e5,3,99
*NFILL,NSET=z20
d6,e6,3,99
*NFILL,NSET=z22
e1,f1,3,99
*NFILL,NSET=z24
e3,f3,3,99
*NFILL,NSET=z25
e4,f4,3,99
*NFILL,NSET=z26
e5,f5,3,99
*NFILL,NSET=z27
e6,f6,3,99
**Web
*NFILL,NSET=z29
g1,h1,8,99
*NFILL,NSET=z31
g3,h3,8,99
*NFILL,NSET=z32
g4,h4,8,99
*NFILL,NSET=z33
g5,h5,8,99
*NFILL,NSET=z34
g6,h6,8,99
**NSET FOR AXIAL LOAD
*NSET,NSET=AXIALLOAD,GENERATE
99,693,99
792,1386,99
1485,2277,99
**
**Element definitions
**
**Flange1
*ELEMENT,TYPE=S4R
1,1,2,101,100
*ELGEN,ELSET=el1
1,14,1,1,6,99,98
*ELEMENT,TYPE=S4R
15,15,16,115,114
*ELGEN,ELSET=el3
15,8,1,1,6,99,98
*ELEMENT,TYPE=S4R
23,23,24,123,122
*ELGEN,ELSET=el4
23,54,1,1,6,99,98
*ELEMENT,TYPE=S4R
77,77,78,177,176
*ELGEN,ELSET=el5
77,8,1,1,6,99,98
*ELEMENT,TYPE=S4R
85,85,86,185,184
*ELGEN,ELSET=el6
85,14,1,1,6,99,98
**Flange2
*ELEMENT,TYPE=S4R
589,694,695,794,793
*ELGEN,ELSET=el8
589,14,1,1,6,99,98
*ELEMENT,TYPE=S4R
603,708,709,808,807
*ELGEN,ELSET=el10
603,8,1,1,6,99,98
*ELEMENT,TYPE=S4R
611,716,717,816,815
*ELGEN,ELSET=el11
611,54,1,1,6,99,98
```

```
*ELEMENT,TYPE=S4R
665,770,771,870,869
*ELGEN,ELSET=el12
665,8,1,1,6,99,98
*ELEMENT,TYPE=S4R
673,778,779,878,877
*ELGEN,ELSET=el13
673,14,1,1,6,99,98
**Web
*ELEMENT,TYPE=S4R
1177,298,299,1388,1387
*ELGEN,ELSET=el15
1177,14,1,1,1,99,98
*ELEMENT,TYPE=S4R
1191,312,313,1402,1401
*ELGEN,ELSET=el17
1191,8,1,1,1,99,98
*ELEMENT,TYPE=S4R
1199,320,321,1410,1409
*ELGEN,ELSET=el18
1199,54,1,1,1,99,98
*ELEMENT,TYPE=S4R
1253,374,375,1464,1463
*ELGEN,ELSET=el19
1253,8,1,1,1,99,98
*ELEMENT,TYPE=S4R
1261,382,383,1472,1471
*ELGEN,ELSET=el20
1261,14,1,1,1,99,98
*ELEMENT,TYPE=S4R
1275,1387,1388,1487,1486
*ELGEN,ELSET=el22
1275,14,1,1,8,99,98
*ELEMENT,TYPE=S4R
1289,1401,1402,1501,1500
*ELGEN,ELSET=el24
1289,8,1,1,8,99,98
*ELEMENT,TYPE=S4R
1297,1409,1410,1509,1508
*ELGEN,ELSET=el25
1297,54,1,1,8,99,98
*ELEMENT,TYPE=S4R
1351,1463,1464,1563,1562
*ELGEN,ELSET=el26
1351,8,1,1,8,99,98
*ELEMENT,TYPE=S4R
1359,1471,1472,1571,1570
*ELGEN,ELSET=el27
1359,14,1,1,8,99,98
*ELEMENT,TYPE=S4R
2059,2179,2180,992,991
*ELGEN,ELSET=el29
2059,14,1,1,1,99,98
*ELEMENT,TYPE=S4R
2073,2193,2194,1006,1005
*ELGEN,ELSET=el31
2073,8,1,1,1,99,98
*ELEMENT,TYPE=S4R
2081,2201,2202,1014,1013
*ELGEN,ELSET=el32
2081,54,1,1,1,99,98
*ELEMENT,TYPE=S4R
2135,2255,2256,1068,1067
*ELGEN,ELSET=el33
2135,8,1,1,1,99,98
*ELEMENT,TYPE=S4R
2143,2263,2264,1076,1075
*ELGEN,ELSET=el34
2143,14,1,1,1,99,98
*ELEMENT,TYPE=B31
```

```
2157,1,100
*ELGEN,ELSET=F1
2157,6,99
*ELEMENT,TYPE=B31
2163,99,198
*ELGEN,ELSET=F2
2163,6,99
*ELEMENT,TYPE=B31
2169,694,793
*ELGEN,ELSET=F3
2169,6,99
*ELEMENT,TYPE=B31
2175,792,891
*ELGEN,ELSET=F4
2175,6,99
*ELEMENT,TYPE=B31
2181,298,1387
*ELEMENT,TYPE=B31
2182,1387,1486
*ELGEN,ELSET=W1
2182,8,99
*ELEMENT,TYPE=B31
2190,2179,991
*ELEMENT,TYPE=B31
2191,396,1485
*ELEMENT,TYPE=B31
2192,1485,1584
*ELGEN,ELSET=W2
2192,8,99
*ELEMENT,TYPE=B31
2200,2277,1089
*ELSET,ELSET=BEAM
F1,F2,F3,F4,W1,W2,2181,2190,2191,2200
**GROUPING ELEMENTS
*ELSET,ELSET=web_rigid
el15,el22,el29,el20,el27,el34,el17,el24,el31,el19,el26,el33
*ELSET,ELSET=web_flex
el18,el25,el32
*ELSET,ELSET=flange_thick
el3,el5,el10,el12
*ELSET,ELSET=flange_rigid
el1,el6,el8,el13
*ELSET,ELSET=flange_flex
el4,el11
*ELSET,ELSET=rigidbeam
flange_rigid,web_rigid
*ELSET,ELSET=flexbeam
el3,el4,el5,el10,el11,el12,web_flex
*ELSET,ELSET=one_flange
el1,el3,el4,el5,el6
*ELSET,ELSET=two_flange
el8,el10,el11,el12,el13
*ELSET,ELSET=web
web_rigid,web_flex
*SHELL SECTION,MATERIAL=RIGID,ELSET=flange_rigid
2
*SHELL SECTION,MATERIAL=RIGID,ELSET=web_rigid
2
*SHELL SECTION,MATERIAL=FLEX,ELSET=web_flex
0.26
*SHELL SECTION,MATERIAL=FLEX,ELSET=flange_flex
0.44
*SHELL SECTION,MATERIAL=RIGID,ELSET=flange_thick
2
*BEAM SECTION,SECTION=CIRC,ELSET=BEAM,MATERIAL=BEAM
2
0,-1,0
*MATERIAL,NAME=BEAM
*ELASTIC
290000,0.3
```

```
*MATERIAL,NAME=RIGID
*ELASTIC
290000,0.3
*MATERIAL,NAME=FLEX
*ELASTIC
29000,0.3
*PLASTIC
50,0
51.345,0.00922948
75,0.0557238
80,0.090034
*BOUNDARY
1783,1,3
1881,1
1881,3
1783,5
1881,5
613,5
675,5
1306,5
1368,5
19,5
81,5
712,5
774,5
*STEP,NLGEOM,INC=30
*STATIC,RIKS
0.01,1,0.0000000001
*CONTROLS,ANALYSIS=DISCONTINUOUS
*CLOAD
316,3,-304.2
378,3,-304.2
1009,3,-304.2
1071,3,-304.2
AXIALLOAD,2,-14.695652173913
*RESTART,WRITE,FREQUENCY=1
*ELPRINT,FREQUENCY=0
*NODE PRINT,FREQUENCY=1
CF
*END STEP
```

BIBLIOGRAPHY

ABAQUS, (2001). "Users Manual," Version 6.2, Hibbitt, Karlsson & Sorenson, Inc., Pawtucket, Rhode Island, USA.

ABAQUS, (2003). "ABAQUS Theory Manual," Hibbitt, Karlsson & Sorensen, Inc., Pawtucket, Rhode Island, USA.

AISC, (1999). Load *and Resistance Factor Design Specification for Structural Steel Buildings,* 3rd Ed., American Institute of Steel Construction Inc., Chicago, Illinois.

Alduri, S.M.R., and Madugula, M.K.S. (1992) "Eccentrically Loaded Steel Angle Structs," *Engineering Journal, 31(3),* American Institute of Steel Construction, Chicago, Illinois, USA, pp. 59-66.

ASCE, (1971) *Plastic Design in Steel, A Guide and Commentary,* American Society of Civil Engineers, New York, New York, p. 80.

AWS D1.1, (2000). *American Welding Society-Structural Welding Code*, USA

Bathe, K.J., (1982). *Finite Element Procedures in Engineering Analysis*, Prentice Hall, Inc., New Jersey.

Boresi, A.P., Schmidt, R.J., (2002). *Advanced Mechanics of Materials*, 6th edition, John Wiley & Sons, Inc., USA.

Chacrabarty, J., (1987). *Theory of Plasticity*, McGraw-Hill Book Company.

Chen, W.F., Lui, E.M. ,(1987) *Structural Stability: Theory and Implementation,* Prentice Hall, Englewood Cliffs, New Jersey, USA.

Cook, R.D., Malkus, D.S. Plesha, M.E., (1989). *Concepts and Application of Finite Element Analysis*, 3rd edition, John Wiley & Sons, Inc., USA.

Crisfield, M.A.,(1981). "A fast incremental/iteration solution Procedure that Handles Snap-Through," *Computers and Structures*, Vol. 13, pp. 55-62.

CSA (2002) *Limit States Design of Steel Structures,* CAN/CSA-S16-01 6th Edition, Canadian Standards Association, Rexdale, Ontario, CANADA.

Deierlein, G., Hajjar, J.F., Kavinde, A. ,(2001). "Material Nonlinear Analysis of Structures: A Concentrated Plasticity Approach", *University of Minnesota,* Minnesota,USA.

ECS (2002). *Eurocode 3: Design of Steel Structures,* European Committee for Standardization, Brussels, BELGIUM.

Galambos, T. V., (1998) *Guide to Stability Design Criteria for Metal Structures, Fifth Edition*, John Wiley & Sons, Inc., New York, New York.

Galambos, T.V. (2001) "Strength of Singly Symmetric I-Shaped Beam-Columns," *Engineering Journal, Second Quarter*, American Institute of Steel Construction, Chicago, Illinois, USA. pp. 65-77.

Galambos, T. V., Ravindra, M. K. (1978). "Properties of Steel for Use in LRFD," *Journal of the Structural Division*, Vol. 104 , No. ST9, pp.1459-1468.

Greco, N., Earls, C.J., (2003). "Structural Ductility in Hybrid High Performance Steel Beams," *Journal of Structural Engineering*, Vol. 129, No. 12, American Society of Civil Engineers, Reston, Virginia, pp.1584-1595.

Haaijer, G., Thurlimann, B., (1958). "On Inelastic Buckling in Steel", *Journal of the Engineering Mechanics Division,* Proceedings of the American Society of Civil Engineers, Paper 1581, EM 2, April, pp. 1581-1 to 1581-48.

Hajjar, J.F. (2003). "Evolution of Stress-resultant loading and ultimate strength surfaces in cyclic plasticity of steel wide-flange cross-sections," *Journal of Constructional Steel Research*, Volume 59, Elsevier Science Ltd., ENGLAND, pp. 713-750.

Johnston, B.G. (1976). *Guide to Stability Design Criteria for Metal Structures*, 3rd edition, Wiley, New York.

Kanchanalai, T. (1977). "The Design and Behavior of Beam-Columns in Unbraced Steel Frames," *AISI Project No. 189, Report No. 2,* Civil Engineering / Structures Research Lab, University of Texas at Austin, Texas, USA.

Kemp, A.R. (1985). "Interaction of Plastic Local and Lateral Buckling," *Journal of Structural Engineering*, Vol. 111, No. 10, pp.2181-2196.

Lay, M.G. and Galambos, T.V. (1965). "Inelastic Steel Beams under Uniform Moment," *Journal of the Structural Division*, ASCE, Vol. 92, No. ST2, pp.207-228.

Liew, J.Y.R., White, D.W., Chen, W.F. (1991) "Beam-Column Design in Steel Frameworks – Insights on Current Methods and Trends," *Journal of Constructional Steel Research*, Volume 18, Elsevier Science Publishers, ENGLAND, pp. 269-308

MacNeal, R.H., (1978) "A Simple Quadrilateral Shell Element," *Computers and Structures,* Pergamon Press Ltd., Great Britain, Vol. 8 pp. 175-183.

Ramm, E. Stegmuller, H., (1982). "Buckling of Shells", *Proceeding of a State of the Art Colloqium*

Rasmussen, K.J.R. and Chick, C.G. (1995). "Tests of thin walled I-section in combined compression and minor axis bending- Part II-Proportional Loading Tests," *The University of Sydney – School of Civil and Mining Engineering Research Report No.R717*.

Riks, E., (1972). "The application of Newton's Method to the problem of Elastic Stability," *Journal Applied Mechanics*, Vol. 39, No. 4, pp. 1060-1066.

Riks, E., (1979). "An incremental approach to the solution of snapping and buckling problems." *International Journal of Solids and Structures*, 15, pp.529-551

Roik, K. and Kuhlmann, U. (1987). "Experimentalle Ermittlung der Rotations kapazitat biegebean spruchler I-profile." *Stahlbau*, 56, pp.321-327.

Salmon, C.G., Johnson, J.E. (1996) *Steel Structures: Design and Behavior, 4th Edition*, HarperCollins Publishers, Inc. New York, New York, USA.

Segui, W.T., (2003). *LRFD Steel Design*, 3rd edition, Thomson Brooks/Cole, Inc.,CA,USA.

Thomas, S., Earls, C.J., (2003a) "Cross-sectional Compactness and Bracing Requirements for HPS483W Girders," *Journal of Structural Engineering,* Vol. 129, No. 12 American Society of Civil Engineers, Reston, Virginia, pp. 1569-1583

Yura, J.A., Galambos, T.V. , and Ravindra, M.K. (1978). "The Bending Resistance of Steel Beams," *Journal of the Structural Division*, ASCE, Vol. 104, ST9, pp.1355-1370.